Modeling and predicting response to ankle exoskeletons

Michael C. Rosenberg

A dissertation

submitted in partial fulfillment of the

requirements for the degree of

Doctor of Philosophy

University of Washington

2021

Reading Committee:

Katherine M. Steele, Chair

I.Y. Shen

Samuel A. Burden

Program Authorized to Offer Degree:

Mechanical Engineering

University of Washington

Abstract

Modeling and predicting response to ankle exoskeletons

Michael C. Rosenberg

Chair of the Supervisory Committee:
Katherine M. Steele
Department of Mechanical Engineering

Ankle exoskeletons are designed and personalized to enhance mobility in unimpaired adults and improve gait in individuals with motor impairments. Ankle exoskeletons are challenging to prescribe and optimize for an individual, resulting in inconsistent intervention outcomes. Quantifying and predicting changes in kinematics and muscle activity in response to varying exoskeleton properties may improve intervention outcomes, enhance mobility, and inform device design for individuals with diverse motor impairments. However, model-based approaches for understanding responses to ankle exoskeletons often rely on physiologically-detailed frameworks that require extensive experimental datasets to model heterogeneous physiology and motor control in individuals with motor impairments. To better understand responses to ankle exoskeletons across individuals with diverse physiology, the goal of this dissertation is to examine physiologically-detailed and non-physiological approaches to modeling and

understanding responses to ankle exoskeletons in individuals with motor impairments and unimpaired adults.

Cerebral palsy (CP) is one of the most common motor impairments among children and one of the largest groups who use ankle exoskeletons. Optimized powered and passive ankle exoskeletons have been shown to reduce the energetic demands of walking in children with CP. However, CP represents a heterogeneous population, with widely varying gait patterns. Understanding how heterogeneous kinematics and kinetics in CP alter exoskeletons impact on the energetic demands of walking could inform device design. Using subject-specific musculoskeletal simulations of walking with ankle exoskeletons, we found that idealized powered ankle exoskeletons reduced muscle demand in children with CP more than passive exoskeletons and that reductions in ankle plantarflexor demand drove overall muscle demand. However, walking speed and knee flexion angle impacted reductions in muscle demand. Powered ankle exoskeletons may, therefore, benefit children with CP, but may not provide benefits over optimized passive exoskeletons for all individuals.

While musculoskeletal simulations provide a powerful platform to evaluate ‘what-if’ questions and probe complex systems, the underlying models often have normative assumptions about physiology and motor control that may limit their ability to accurately predict subject-specific responses to exoskeletons. Constructing dynamical models of walking with exoskeletons from data alone may enable exoskeleton responses to be predicted without detailed knowledge of an individual’s physiology. To test this theory, we built a passive ankle exoskeleton and collected extended treadmill walking data across four levels of dorsiflexion stiffness for 12 unimpaired

adults. We developed three data-driven phase-varying models of each individual's response to ankle exoskeleton torque and evaluated their predictive ability in unimpaired adults walking in bilateral ankle exoskeletons. We found that linear and nonlinear phase-varying models could accurately predict kinematic responses to torque but could not predict stride-to-stride variations in myoelectric responses. These models show promising potential to model responses to exoskeletons in individuals with motor impairments, though improving myoelectric predictions represents an exciting area of future research.

While exoskeleton impacts on gait mechanics and energetics have been investigated, if and how an individual modulates their center-of-mass (COM) dynamics changes with ankle exoskeletons remains unclear. Quantifying changes in the whole-limb mechanisms describing COM dynamics with exoskeletons may identify characteristic sub-classes of responses to exoskeletons. We developed and identified template signatures – low-dimensional, physics-based representations of COM dynamics – during walking with and without passive ankle exoskeletons in 12 unimpaired adults and one individual with post-stroke hemiparesis. We found that the template signatures were consistent across unimpaired adults and were robust to changes in exoskeleton dorsiflexion stiffness. Conversely, the template signatures post-stroke reflected the individual's increased paretic-limb stiffness and changed in response to exoskeletons. This work suggests that unimpaired COM dynamics do not change with passive ankle exoskeletons, but that COM dynamics in individuals post-stroke may adapt to ankle exoskeletons.

This dissertation contributed to our knowledge of how ankle exoskeleton properties impact muscle demand and COM dynamics during walking, and the potential of data-driven modeling

frameworks to quantify and predict responses to ankle exoskeletons. This knowledge may inform exoskeleton design and prescription, potentially improving exoskeleton efficacy for individuals with motor impairments. The research in this dissertation added to an existing open-source dataset for musculoskeletal simulations of walking in children with CP and created a novel, open-source dataset containing long time-series of walking with passive ankle exoskeletons in unimpaired adults. This research lays the foundation for future work aimed at identifying mechanisms driving heterogeneous responses to exoskeletons or other assistive devices in individuals with motor impairments.

ACKNOWLEDGMENTS

These acknowledgments will undoubtedly feel like an understatement upon completion and insufficient upon reflection years from now. Without support, mentorship, and opportunities provided by those around me, achieving a doctoral degree seems, to me, unlikely. I will try to give due credit to those who helped shape my path to a PhD.

Above all, I thank my parents, Edwin and Judith, without whom I may never have adopted the desires to explore and seek to understand the world. Their unwavering support and excitement to let me find my way through life's myriad opportunities have enabled me to arrive at a path that I find genuinely fulfilling. For that I am grateful. I also must thank my brother, Daniel, who accompanied me through many an experience and mistake, each of which has influenced who I am today.

I also must thank the many faculty members who have given me support and opportunities over the years. First and foremost, I thank my advisor, Dr. Kat Steele, for her patience, mentorship, and support during my PhD. I cannot imagine where I would be today without her guidance. I must also thank my collaborators and committee members, Drs. Bora Banjanin, Sam Burden, Josh Proctor, Steve Shen, and Brian Hafner for their contributions to my development as a researcher and the research itself. I also thank those who have given me opportunities to grow as a teacher, mentor, and researcher: Drs. Eric Chudler, Sara Morgan, Mike Schwartz, Nate Sniadecki, and Sue Spaulding. Finally, I want to thank Dr. Mohammed Zikry, who gave me my first research opportunity as an undergraduate student and the mentorship that enabled me to discover a love of discovery.

I am grateful to the many Steele Lab members with whom I have had enjoyed working so much. I first want to thank the cohort that welcomed me into the lab: Hwan Choi, Gaurav Mukherjee, Keshia Peters, and Ben Shuman, for the environment that they created and their mentorship during my budding years as a PhD student. I am also grateful to the many labmates who have supported my research and writing: Karley Benoff, Nick Biacoianu, Charlotte Caskey, Megan Ebers, Heather Feldner, Darrin Howell, Elijah Kuska, Naser Mehrabi, Lauren Sepp, Alyssa Spomer, Momona Yamagami, and Nicole Zaino. Their patience when reviewing my longest manuscripts, their ideas that brought my research a little closer to reality, and the wonderful lab environment that they maintained were invaluable. Finally, I want to thank my undergraduate mentees, from whom I learned just how challenging and fun it is to get someone to do research for you: Kalle Chastain, Julia Costacurta, Makoto Eyre, Ava Lakmazaheri, Wing-Sum Law, Madelyn Lew, Noah Lukosky, Brett Musolf, and Leif Wesche.

My dissertation was supported by the University of Washington (UW) College of Engineering Fellowship, a National Science Foundation (NSF) Graduate Research Fellowship (grant No. DGE-1762114), NSF grant No. CBET-1452646, the AMP Center Strategic Research Initiative of the University of Washington College of Engineering, and the Institute for Translational Health Sciences (grant No. TL1TR000422), and a Gatzert Child Welfare Fellowship.

Pursuing a PhD would have been less feasible and far less enjoyable without the support of those mentioned above and of the faculty, staff, and students in the UW Mechanical Engineering Department. I feel incredibly fortunate to have found the UW and the Steele Lab, and will try to extend their culture of support and comradery wherever I end up. I am confident that I have failed to comprehensively express my gratitude to those who supported me. Thank you all.

TABLE OF CONTENTS

LIST OF FIGURES

LIST OF TABLES

Chapter 1. INTRODUCTION

Walking is a ubiquitous and efficient way for humans to interact with their physical and social environments. Augmenting walking capacity, therefore, improves our ability to interact with the world around us. While devices to assist walking function have existed for centuries [1], only in the last two decades has the vision of augmenting human walking capacity through wearable robots begun to be realized [2]. In particular, *ankle exoskeletons* have promising potential to augment unimpaired locomotion, as well as to assist and improve gait kinematics, and restore walking function following neurological injury [3, 4].

Since the 1960s, exoskeletons have been used in military and civilian applications, such as soldier augmentation, assisting manufacturing processes, or assisting locomotion and rehabilitation for individuals with motor impairments [3, 5-8]. While ankle exoskeletons have been used for decades to assist and improve walking in individuals with motor impairments (*e.g.* approximately 50% of children with cerebral palsy (CP) and stroke survivors) they have only recently received increased research attention for their ability to reduce the energetic demands of walking for unimpaired individuals and their potential as rehabilitative tools [3, 4, 9-19]. However, personalizing exoskeletons for individuals with motor impairments remains challenging.

Our understanding of how ankle exoskeleton properties impact gait has exploded in the last decade. While much exoskeleton research to date focuses on reducing the energetic costs of walking, the next ten years will likely see the expansion of exoskeleton research beyond the laboratory and towards augmenting additional features of locomotion, such as stability and agility [2]. However, personalizing exoskeletons to assist walking or achieve clinical outcomes remains challenging.

This challenge is particularly apparent for individuals with motor impairments, who have unique physiology and motor control and exhibit variable responses to exoskeleton interventions [4, 20]. Advancing our understanding of ankle exoskeleton impacts on gait and developing methods to study exoskeleton impacts in heterogeneous populations will be critical to realizing the promise of these devices.

Data-driven modeling is an emerging area of research in the biomechanics of locomotion and has the potential to advance exoskeleton personalization through understanding diverse responses to exoskeletons [21, 22]. From popular musculoskeletal simulations to black-box machine learning algorithms, data-driven models enable an individual's dynamics, control, and sensing to be encoded from data. However, data-driven modeling is in its infancy in biomechanics. Drawing from research modeling a range of complex dynamical systems with similarities to human gait may enable a rich history of modeling work to provide novel insight into locomotion and the impacts of ankle exoskeletons on gait.

1.1 FOCUS OF THE DISSERTATION

This dissertation explores physiological, physics-based, and non-physiological modeling approaches to understanding and predicting changes in gait with ankle exoskeletons. Our premise was that data-driven models would provide insight into muscle, joint, and whole-body impacts of ankle exoskeletons during walking. To understand how gait mechanics altered ankle exoskeleton impacts on muscle demand, we created subject-specific musculoskeletal models of children with CP walking with passive and powered ankle exoskeletons (Chapter 3). We found powered ankle exoskeletons may reduce muscle demand more than passive exoskeletons in children with CP and

that knee flexion moments during walking were negatively associated with potential reductions in muscle demand with ankle exoskeletons. To determine if data-driven models grounded in dynamical systems theory could predict kinematic and myoelectric responses to ankle exoskeletons, we evaluated linear and nonlinear phase-varying models of response to exoskeleton torque Chapter 4. We found that linear phase-varying models could predict kinematic responses to torque but could not predict stride-to-stride variations in myoelectric responses, identifying an important area of future work. To understand if and how control of center-of-mass (COM) motion changes with ankle exoskeletons, we extended a novel data-driven modeling technique ([23]), to construct mechanistic walking models describing whole-leg contributions to COM motion (Chapter 5). We found that unimpaired control strategies were insensitive to exoskeletons, while one stroke survivor's control changed in response to both the exoskeleton frame and dorsiflexion stiffness. The model development and analyses conducted in this dissertation provide a foundation for data-driven exoskeleton personalization for individuals with motor impairments and novel analytical and predictive tools for researchers studying the biomechanics of locomotion.

1.2 SIGNIFICANCE

The research conducted in this dissertation contributes to the biomechanics and neuromechanics communities by advancing our understanding of, and ability to predict, responses to ankle exoskeletons. Beyond ankle exoskeletons, the methods developed in this dissertation may be used to study other assistive devices, interventions, and user groups. Understanding the diverse factors contributing to changes in gait in response to ankle exoskeletons may improve exoskeleton efficacy for individuals with motor impairments, enhancing mobility and moving towards data-driven exoskeleton prescription outside of the gait lab. Our ability to individualize ankle

exoskeletons has been limited by an inability to address uncertainty in physiology and motor control. The goal of this dissertation was to address this challenge by improving our understanding of responses to ankle exoskeletons using novel analytical and predictive tools. The primary contributions of this dissertation are:

Identifying factors predicting exoskeleton impacts on muscle demand in children with CP: The potential of state-of-the-art powered and passive ankle exoskeletons to assist locomotion had not been evaluated in children with CP. We developed subject-specific musculoskeletal simulations of children with CP to evaluate the impacts of optimized passive and powered ankle exoskeletons on muscle demand. Prior studies had developed subject-specific models of children with CP [24] and unimpaired adults with exoskeletons [25]. We extended these works by implementing both powered and passive exoskeletons in simulation. While ankle exoskeleton impacts on gait in children with CP were known to be affected by kinematics [26], we were the first to identify kinematic and kinetic features that predicted exoskeleton impacts on muscle demand. The musculoskeletal models developed for this research expanded an existing open-source dataset of children with CP and are freely available at https://simtk.org/projects/crouchgait.

Extending phase-varying data-driven models to quantify response to ankle exoskeletons: Predicting responses to exoskeletons without extensive knowledge of physiology and motor control may facilitate data-driven exoskeleton prescription for individuals with motor impairments, but such tools have not been extended to gait with ankle exoskeletons. Prior studies used phase-varying models to predict perturbation responses and quantify the stability properties of gait [27, 28]. We extended this approach to predict responses to ankle exoskeletons and showed

that linear phase-varying dynamics could encode responses to passive ankle exoskeletons in unimpaired adults. We made all data collected for the research in Chapter 4 freely available at https://simtk.org/projects/ankleexopred. These data constitute rare, long time-series datasets that include joint kinematics, muscle activity, and ground reaction force data from four-minute trials of four exoskeleton stiffness levels for 12 unimpaired adults and 1 adult stroke survivor. The repository additionally includes scaled musculoskeletal models for each participant. As these methods may extend to other exoskeletons devices or prostheses, we also made all code needed to generate and analyze phase-varying models available in this repository.

Quantifying the dynamical impacts of passive ankle exoskeletons: When studying and controlling ankle exoskeletons, understanding which phases of the gait cycle contain measurements that are useful for predicting responses to exoskeletons throughout the gait cycle may suggest control variables for state-based control of powered exoskeletons and inform studies of passive exoskeleton impacts on gait. Using phase-varying models, we showed that information from any initial posture improved predictions of kinematic responses to passive ankle exoskeletons only up to 20% of a stride in the future. While this threshold may vary with the device and population, our findings inform studies of the impacts of posture (*e.g.* joint angles at initial contact [29]) on responses to passive exoskeletons by providing a baseline threshold beyond which posture effects are unlikely to be identifiable. The code to conduct these analyses is also available at https://simtk.org/projects/ankleexopred.

Extending sparse regression for hybrid systems to study ankle exoskeleton impacts on whole-limb walking control: Developing subject-specific interpretable models of walking may identify

interindividual differences in strategies to achieve stable and efficient walking. This modeling approach is more flexible than existing approaches in biomechanics and may be extended to other assistive devices or interventions. While myriad interpretable, physics-based models of walking exist, only a single dynamical structure is typically selected to study gait [30-34]. We extended a physics-informed data-driven modeling algorithm, which automatically compares a large number of physics-based representations of system dynamics, to identify subject-specific walking dynamics with and without ankle exoskeletons [23].

Identifying the impacts of passive ankle exoskeletons on whole-limb control of walking: Understanding if and how strategies to control COM motion during walking change with ankle exoskeletons will guide investigation into neural and biomechanical mechanisms impacting responses to exoskeleton properties. We identified changes in physics-based representations of COM dynamics during walking with and without ankle exoskeletons in unimpaired adults and one stroke survivor. Prior work showed that ankle exoskeletons impacted gait mechanics and energetics ([9, 35]), as well as the changes in gait mechanics following neurological injury [36]. We extended this work by parameterizing changes in COM dynamics to determine if ankle exoskeletons altered the whole-limb mechanisms describing COM dynamics. We found that unimpaired adults maintain nearly invariant whole-limb control of COM motion in response to passive ankle exoskeletons, but that whole-limb control may be altered post-stroke and more sensitive to exoskeleton properties. These findings may explain observed changes in gait mechanics and motivate future investigation in a larger sample of individuals post-stroke.

1.3 DISSERTATION OVERVIEW

This dissertation focuses on three research studies aimed at understanding and predicting responses to ankle exoskeleton properties. The studies are presented as self-contained articles, each addressing a unique challenge in understanding gait with ankle exoskeletons. Chapter 2 provides an overview of relevant background information for the remaining chapters. Chapter 3 uses musculoskeletal simulation to examine the potential impacts of powered and passive ankle exoskeletons on gait in children with CP (Rosenberg, et al., *PLoS One*, 2017). Chapter 4 developed and evaluated phase-varying models to predict kinematic and myoelectric responses to ankle exoskeletons (Rosenberg, et al., *Journal of the Royal Society Interface*, 2020). Chapter 5 extends a physics-informed data-driven modeling framework to quantify changes in the whole-limb mechanisms used to accelerate the COM with ankle exoskeletons in unimpaired adults and one individual with post-stroke hemiparesis (Rosenberg, et al., *In preparation*). Chapter 6 summarizes our important findings and presents interesting directions for future research. Note that the pronoun "we" is used throughout the dissertation to recognize the collaborative efforts that contributed to this research. The individual contributors to each study are listed at the start of each chapter.

Chapter 2. BACKGROUND

2.1 ANKLE EXOSKELETONS DESIGN AND USER GROUPS

While the goals of ankle exoskeleton interventions are highly individualized, most devices alter gait by applying rhythmic mechanical perturbations to the user's ankle. Common ankle exoskeleton designs include a footplate, a hinged or solid ankle, and a cuff that surrounds the user's shank (Figure 2.1) [4, 9, 17-19, 37, 38]. During walking, ankle exoskeletons apply resistive or assistive torques about the ankle joint, typically in the ankle's flexion-extension plane. Altering the torque applied to the ankle is, therefore, the primary design objective for many ankle exoskeletons. In passive ankle exoskeletons, torque generation is a function of the user's ankle angle in the exoskeleton and the device's mechanical properties. Passive exoskeletons typically resist ankle dorsiflexion in early stance, assist ankle plantarflexion in mid- and late-stance, and resist ankle plantarflexion during swing [9, 39]. Exoskeleton stiffness influences the resistance to ankle flexion and is the most commonly-studied passive exoskeleton property, while the exoskeleton's equilibrium (*i.e.,* zero-torque) angle is also commonly tuned in clinical practice [9, 29, 39-44]. Understanding how exoskeleton design parameters impact walking function, mechanics, and energetics is an active area of research [4, 9, 19, 20, 25, 37, 45-47]. However, as discussed in the next section, exoskeletons can have diverse and unintuitive impacts on gait.

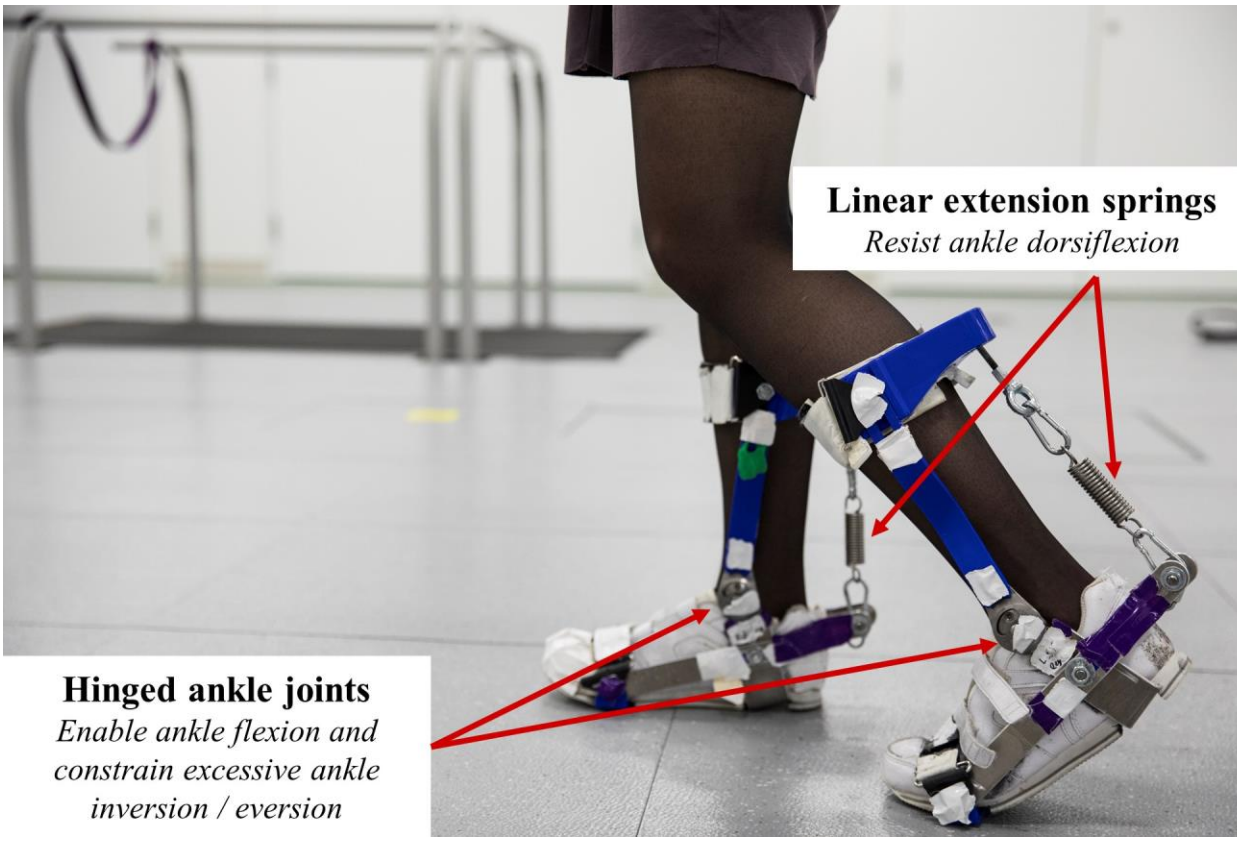

Figure 2.1. Depiction of experimental passive ankle exoskeleton with linear springs in parallel with the shank. This design is similar to passive exoskeletons studied to reduce the metabolic demand of walking. Photograph by the University of Washington.

Ankle-foot orthoses (AFOs) describe a type of exoskeleton used clinically to improve gait kinematics, spatiotemporal outcomes, and energetic efficiency during walking [4, 29, 48-51]. Mechanically, AFOs and exoskeletons are equivalent. Despite differences in some design features (*e.g.* AFOs are often a single piece of rigid thermoplastic), AFOs and ankle exoskeletons produce torques as described above. In this dissertation, we refer to all devices as 'ankle exoskeletons' (*e.g.* Chapter 4 & Chapter 5) unless specifically discussing devices with clinical implications, in which case, we use the term 'AFO' (*e.g.* Chapter 3). AFOs are often prescribed to individuals with motor impairments, such as those post-stroke or with CP. In CP alone, which affects 2-3 of every 1000

live births, over 50% of children are candidates for AFO prescription, often to reduce excessive knee flexion during stance or toe-walking, which are energetically expensive gait patterns and can lead to joint pain later in life [49, 52-54]. AFOs are typically prescribed based on an individual's physiology, nominal gait pattern, and personal goals [4, 26]. As will be discussed in Section 2.2.4, responses to AFO mechanical properties are highly variable and no gold-standard prescription protocol exists to personalize AFOs [4]. Much like the need for improved understanding of exoskeleton impacts on gait to advance state-of-the-art exoskeleton research and design, understanding why individuals with motor impairments exhibit heterogeneous responses to AFOs may improve AFO efficacy.

2.2 HETEROGENEOUS RESPONSES TO ANKLE EXOSKELETONS

Ankle exoskeletons impact many features of gait, including center-of-mass (COM) mechanics, joint mechanics, and muscle activity [9, 38, 55, 56]. Understanding exoskeleton impacts on these gait features is critical to informing exoskeleton design, as the features influence mobility, efficiency, and safety during walking. Particularly in individuals post-stroke or with CP, the impacts of ankle exoskeleton stiffness on gait are highly heterogeneous [4, 29]. In this section, we review normative ankle exoskeleton impacts on gait in unimpaired adults and heterogeneous impacts on gait in individuals with motor impairments.

2.2.1 *Center-of-mass mechanics*

The motion of the COM influences gait energetics and stability [57-61], making the control of COM motion fundamental to the task of walking. COM mechanics describe how gravity and the leg transfer energy to, and accelerate, the COM. Additionally, as will be discussed in Chapter 5,

COM mechanics are fundamental to simple models of locomotion. Understanding exoskeleton impacts on how each leg contributes to COM mechanics can provide insight into how stable and efficient walking is achieved.

Ankle exoskeletons generally have small impacts on COM mechanics. For example, in unimpaired adults, Collins and colleagues (2015) found that passive exoskeletons increased biological COM power during mid-stance, and decreased power in late stance [9]. However, the exoskeleton mechanical power mirrored these changes, such that total (biological + exoskeleton) COM power was insensitive to ankle exoskeleton stiffness. Mooney and colleagues (2016) corroborated this work for powered exoskeletons, finding that COM power was similar between walking with and without exoskeletons [18]. However, unilateral ankle exoskeletons, as may be used by individuals with hemiplegia, had larger effects on COM power. Jackson and colleagues (2015) found that increasing torque in unilateral powered ankle exoskeletons decreased late stance contributions to COM power of the leg with an exoskeleton [45]. Their results suggest that the asymmetric impacts of a unilateral exoskeleton may alter coordination such that altered COM motion is preferable.

COM mechanics appear more sensitive to ankle exoskeletons in individuals with motor impairments, compared to unimpaired adults. In individuals with unilateral impairments, Harper and colleagues (2014) showed that passive exoskeleton stiffness had small impacts on forward and mediolateral accelerations of the COM in both the exoskeleton-side limb and the no-exoskeleton limb [43]. Conversely, in individuals post-stroke, powered exoskeletons on the participants' paretic limb exhibited highly variable effects on paretic limb contributions to COM propulsion and power [20]. Many participants relied more heavily on their non-paretic limb when walking with

the exoskeleton; a possible compensation strategy for the inability to use the exoskeleton for propulsion. High interindividual variability in COM-level responses to exoskeletons indicates a need to understand the diverse mechanisms driving responses.

2.2.2 *Joint mechanics*

Joint mechanics describe an individual's biomechanical strategy to accelerate the COM and serve as outcomes for clinical exoskeleton interventions [4, 29, 39, 62]. While exoskeletons produce torques at the ankle, individuals may alter mechanics at the hip, knee, and ankle to achieve a desired walking pattern. Here, we describe exoskeleton impacts on joint kinematics, moments, and powers, all of which are impacted by ankle exoskeletons.

Passive ankle exoskeleton stiffness typically has small impacts on joint kinematics. Increasing exoskeleton stiffness decreases peak ankle dorsiflexion angle during stance and swing, but has only small effects on knee and hip flexion in unimpaired adults [9, 42]. Children with CP exhibit more variable responses to exoskeleton stiffness, though increasing stiffness has been found to decreases peak knee flexion during stance [29]. For powered ankle exoskeletons in unimpaired adults, impacts on ankle and knee kinematics are larger in magnitude but similar in direction to passive exoskeletons [35]. Conversely, Lerner and colleagues (2019) found that a small sample of children with CP walking in powered ankle exoskeletons exhibited variable changes in ankle, knee, and hip kinematics, despite similar exoskeleton torque profiles [55]. For example, some participants increased ankle dorsiflexion while others decreased dorsiflexion.

Joint moments exhibit larger responses to exoskeleton stiffness than do kinematics. Unsurprisingly, passive ankle exoskeletons were found to reduce the biological ankle moment during push-off in unimpaired adults [9]. Additionally, the total ankle moment increased in midstance and the knee flexion moment increased in late stance, suggesting that exoskeleton stiffness may impact the relative contributions of ankle and knee moments to overall joint motion. The impacts of ankle exoskeleton stiffness on individuals with motor impairments are variable. In children with CP, passive ankle exoskeleton stiffness did not alter ankle, knee, or hip moments [29]. However, in adults with calf muscle weakness, exoskeleton stiffness increased the total ankle moment and decreased knee moments in late stance, suggesting changes in joint contributions to propulsion [44, 62]. Changes in ankle moments with powered exoskeletons resemble those of passive exoskeletons in unimpaired adults, with the total ankle moment increasing in mid-stance, but not in late-stance [18]. Despite kinematic differences, Lerner and colleagues (2019) found that powered exoskeletons consistently decreased biological ankle moments, though changes in total ankle, knee, and hip moments varied between participants.

Joint power analysis provides particular insight into how joints are coordinated to achieve COM-level mechanics and how exoskeletons alter coordination. In unimpaired adults, Collins and colleagues (2015) showed that increasing passive exoskeleton stiffness decreased ankle power and increased knee power during late stance [9]. Since COM power was unaffected by exoskeleton stiffness in this study, changes in ankle and knee moments reflect changes in the relative contributions of the knee and ankle to COM power. In children with CP and adults with neuromuscular impairments, increasing ankle exoskeleton stiffness has been found to decrease peak ankle push-off power [29, 44]. Powered exoskeletons have been shown to increase positive

ankle power and decrease positive hip power in both unimpaired adults [18] and children with CP [55]. The redistribution of power in the leg joints suggests that ankle exoskeletons may alter the preferred coordination patterns to support and propel the body.

2.2.3 *Muscle activity*

Muscle activity patterns encode an individual's neuromuscular strategy to achieve joint moments and accelerate the COM during walking. Moreover, muscle activity is associated with both the energetic demands of walking and walking function in individuals with motor impairments [24, 63-66]. Therefore, understanding exoskeleton impacts on muscle activity may inform exoskeleton design for rehabilitation and assistance during walking.

In unimpaired adults, ankle exoskeleton properties have been found to primarily impact the ankle plantarflexor muscles. Collins and colleagues (2015) found that passive exoskeletons reduced soleus activity in early stance, and gastrocnemius activity in early and late stance [9]. For walking at a fixed speed, ankle exoskeletons reduced the biological ankle power required to maintain similar COM mechanics to walking without exoskeletons. Since COM power changes little with passive ankle exoskeletons, reductions in ankle plantarflexor activity are unsurprising [9]. Powered exoskeleton torque has similarly been found to reduced soleus activity in unimpaired adults, but to a greater degree than in passive exoskeletons [38, 45]. These studies showed that greater exoskeleton stiffness or torque tend to decrease soleus and gastrocnemius activity, though changes in activity may be highly individualized. In children with CP, Lerner and colleagues (2019) found that powered exoskeletons reduced gastrocnemius activity [55]. However, only five participants were evaluated and the magnitude and timing of reductions in gastrocnemius activity varied

between individuals. The connections between muscle activity, gait mechanics, and walking function make quantifying and predicting individualized changes in muscle activity with ankle exoskeletons critical to improving device efficacy for individuals with motor impairments.

2.2.4 *Heterogeneous responses to ankle exoskeletons*

Heterogeneous responses to exoskeletons make device personalization critical for using exoskeletons to assist and improve change in individuals with motor impairments and unimpaired adults. Exoskeleton personalization for individuals with motor impairments is particularly challenging due to the heterogeneity of responses to exoskeleton properties. For example, Ries and colleagues (2015) found that, while passive exoskeletons improved walking speed and step length in children with CP compared to barefoot walking, kinematic and spatiotemporal outcomes with exoskeletons were highly variable: ankle exoskeletons elicited clinically-meaningful improvements in joint kinematics in approximately 25% of the 378 children, while another 20% of children experienced clinically-meaningful degradations in kinematics [4]. Such heterogeneous responses highlight the importance of personalizing ankle exoskeleton properties for children with CP. Similarly, as noted in Section 2.2.2, individuals post-stroke and with CP also exhibit diverse responses to powered ankle exoskeletons at the COM, joint, and muscle levels [12, 20, 55]. Diverse responses to ankle exoskeletons are likely due to heterogeneous motor control and musculoskeletal physiology in individuals with motor impairments, though how specific impairments impact gait with exoskeletons remains unclear [4, 24, 67].

In summary, individuals respond to changes in ankle exoskeleton properties, such as stiffness, at the COM, joint, and muscle levels, which can impact gait energetics, stability, and mobility.

Therefore, predicting these complex, high-dimensional responses to exoskeletons is critical to eliciting desired exoskeleton outcomes. For individuals with motor impairments, interindividual differences in motor control and musculoskeletal physiology make exoskeleton personalization particularly challenging [4, 24, 67]. Developing methods to study and predict gait with ankle exoskeletons in individuals with diverse motor impairments may enable data-driven personalization of ankle exoskeletons.

2.3 MODELING AND PREDICTING GAIT WITH ANKLE EXOSKELETONS

Experimental and computational approaches for personalizing exoskeletons exist, though each has limitations for device personalization in individuals with motor impairments [19, 25, 26, 37, 68]. State-of-the-art experimental approaches, such as human-in-the-loop exoskeleton optimization, automatically probe different powered exoskeleton torque profiles in real-time to optimize control policies for an individual's objectives [19]. While this model-free approach does not require knowledge of the user's physiology, it does not provide insight into the exoskeleton-user dynamics and cannot predict responses to novel exoskeleton designs. Conversely, model-based predictions of human gait may provide insight into the underlying biological mechanisms governing responses to ankle exoskeletons and predict responses to un-tested exoskeleton designs. In this section, we discuss the powerful and limiting aspects of existing approaches to predicting responses to ankle exoskeletons. We then discuss alternative perspectives for modeling locomotion from data. Note that we specify three classes of locomotion models, whose nomenclature differs between research fields. We define the three classes as:

- **Physiological models**: Physiologically-detailed models, such as musculoskeletal models, containing biologically-plausible geometry (skeleton), actuators (muscles), and controllers

(objective functions). These models may be tuned from data or use default population-based normative parameter values. Examples include low-degree-of-freedom sagittal-plane models [69]) and high-degree-of-freedom 3D models ([70])

- **Physics-informed models**: Models obeying physical laws and with physically-interpretable structure, such as limbs and joints. While the force-producing elements in these models are not physiological, they have clear physical meaning. Examples include inverted pendula [71-74] and spring-loaded inverted pendula [30, 75-77]. Similar to physiological models, these physics-informed models may use default parameters to synthesize novel gait patterns.
- **Data-driven models**: Non-physiological models whose structure may be motivated by the outcomes, available data, or the hypothesized dynamical structure of the system [78]. Data-driven model parameters are estimated from data. While model structure may be interpretable, it is not constrained by physics. Examples include phase-varying models [79, 80] and the broad set of models under the umbrella of *machine learning* [21, 26].

2.3.1 *Physiological models*

Since the 1950s, conceptual and mathematical models of locomotion have evolved from simple inverted pendula to high-dimensional biological models of walking, termed *musculoskeletal models* [70, 81-84]. In the context of ankle exoskeletons, musculoskeletal model-based forward and inverse simulations may be used to estimate the effects of different exoskeleton designs and torque profiles on muscle activity, energy costs of walking, and kinematics. For ankle exoskeletons, the primary benefits of modeling gait using musculoskeletal models include their

potential to examine responses to novel exoskeleton designs and to provide insight into the biomechanics of responses to exoskeletons.

For example, Uchida and colleagues (2016) used musculoskeletal simulations to compare the potential impacts of powered ankle exoskeletons on metabolic rate in unimpaired adults during running, finding differences in the effectiveness of each exoskeleton design [25]. The authors identified the extent to which individual muscles' energetics were altered by exoskeleton torque, providing insight into the expected impacts of different exoskeleton designs. Similarly, Bregman and colleagues (2011) used a lower-dimensional, physics-based model with torsional springs at the ankles to determine that an intermediate exoskeleton stiffness minimized the energetic demand during walking [85]. These results were later corroborated experimentally in unimpaired adults [9]. While computational models' ability to perform 'what-if' predictions of responses to exoskeleton torque may enable predictions of general trends underlying gait with exoskeletons, predicting the responses of specific individuals remains challenging.

The assumptions encoded in musculoskeletal models limit their ability to predict subject-specific responses to exoskeletons. Musculoskeletal models contain a large number of assumptions about physiology and motor control, typically based on normative datasets from unimpaired adults [70]. Simulation solutions are sensitive to violations of these assumptions, such as inaccurate musculotendon dynamics, as is the case for individuals with cerebral palsy [22, 67]. Musculoskeletal simulation-based predictions of muscle force are even sensitive to uncertainty in exoskeleton mechanical properties [40]. Although time- and resource-intensive, tuning musculotendon parameters or control policies from data may improve predictions of muscle

recruitment and kinematics during walking with exoskeletons and is an active area of research [22, 86]. Modeling frameworks with fewer normative assumptions may enable subject-specific predictions of exoskeleton responses without extensive knowledge about an individual's physiology.

State-of-the-art physiological modeling frameworks, such as predictive simulations, have yet to be applied to walking with ankle exoskeletons for individuals with motor impairments. Predictive musculoskeletal simulations with flexible control laws to synthesize novel gait patterns and study the impacts of gait pathologies on motor function. Such models have been used to simulate the impacts of muscle weakness, prosthesis use, and impaired motor control [69, 83]. Unlike musculoskeletal simulations previously used to study ankle exoskeletons (*e.g.* [25, 40]), predictive simulations do not require experimental data, making them ideal for 'what-if' questions about locomotion. However, similar to tracking-based simulations, predictive musculoskeletal simulations are sensitive to initialization conditions and are sensitive to the accuracy of musculotendon parameters and motor control. Accurate subject-specific predictions may, therefore, require extensive experimental measurements to produce accurate predictions of responses to exoskeletons in individuals with motor impairments [22, 86].

2.3.2 *Physics-informed models*

Physics-based mechanical models have a rich history in modeling locomotion but have rarely been applied to ankle exoskeletons [85]. Inverted pendula constitute the simplest walking models [71, 87]. Prior research has increased the complexity of inverted pendula models, adding joints, springs, dampers, and actuators to understand fundamental aspects of gait [33, 34, 71, 84]. The simplicity

of mechanical models enables lumped-parameter approximations of complex structures, such as approximating the leg as a spring-mass-damper system. Simple models have been applied to evaluate leg stiffness and the mechanisms driving pathological gait patterns in children with cerebral palsy [88, 89]. These low-dimensional models are typically confined to a small and specific set of outcomes.

One framework for selecting physics-based representations of walking was proposed by Full and colleagues in 1999 and is known as the *Templates and Anchors* modeling approach [33]. This framework begins with a generic mechanical "template" model that explains an observed phenomenon across species, experimental conditions, or tasks. The spring-loaded inverted pendulum (SLIP) is a common template that has been used to study, among other questions, control of leg impedance during running and stabilization strategies in cockroaches [27, 75]. Complexity may be added to the template to answer questions about specific mechanisms driving a system's behavior, "anchoring" the model in a system's biological structures. By first omitting physiological detail, templates encode an individual's strategy to a accomplish task, such as walking, whereas anchors describe how joints and muscles are recruited to execute the strategy. Indeed, similar template models have been employed in human walking. Alexander (1995) and Davoodi and colleagues (2019) provided summaries of common walking models of varying complexity, such as inverted pendula, spring-loaded inverted pendula, and walkers with actuators [32, 71]. Similar models have elucidated the roles of transitions between single and double-limb support phases, walk-to-run transition speeds, and ankle push-off work [59, 73, 74]. Such mechanistic insights would be challenging to elucidate from biological models because multiple mechanical or neuromechanical factors may result in similar changes in gait. Therefore, template-

based models may provide insight into changes in walking control with ankle exoskeletons, despite differences in physiology. However, if and how such physics-based walking models reflect changes in gait dynamics with ankle exoskeletons has not been investigated.

2.3.3 *Data-driven models of dynamical systems*

While physiological or physics-based mechanistic models provide insight into mechanisms impacting responses to ankle exoskeletons, non-physiological data-driven models, whose parameters are estimated from data, may generate accurate predictions of walking without population average-based assumptions about physiology. Unlike experimentally tuning the properties of an exoskeleton using optimization, data-driven models contain explicit input-output mappings that enable the prediction of responses to novel torque profiles. Unlike physiological models, data-driven models need not encode a large number of assumptions about the underlying system. Instead, data-driven models require few assumptions about the underlying system. Specifically, studies assume (1) the structure of the system's dynamics (*e.g.* linear or nonlinear) and (2) that the measurements included as model inputs contain information needed to predict the outcomes of interest [27, 80, 90, 91]. Data-driven models may be interpreted to learn about a system's dynamics (*e.g.* using Data-Driven Floquet Analysis [92]), but require large amounts of data to perform these analyses [27]. Note that myriad modeling frameworks for dynamical systems are available to biomechanics researchers and their application is beyond the scope of this dissertation [21, 69, 70, 83, 90, 93]. Rather, the research in this dissertation is distinct from many biomechanics studies using data-driven models in that we model gait with exoskeletons as a

subject-specific dynamical system, rather than a population-specific mapping between measurements and outcomes [21, 78].

The dynamical systems approach to data-driven modeling reflects the rhythmic, high-dimensional, and nonlinear nature of human gait. Specifically, the dynamical systems perspective views gait as a first-order differential equation and uses time-series data to estimate the system's dynamics [94]. Therefore, dynamical systems models encode how a system evolves in time, and are appropriate for representing the dynamics of individual systems (*i.e.* subject-specific models for human gait). Adopting this perspective for human locomotion provides access to a rich suite of analytical tools [78]. In particular, Floquet Theory has been used to model locomotion as a linear phase-varying system, in which the system's dynamics describe the convergence of the system following small perturbations away from a nominal cycle (*e.g.* the average cycle) [27, 28, 80, 91, 94]. Note that many dynamical systems-based models of human gait use gait kinematics and center-of-mass motion [27, 28, 80]. However, any measurements relative to the system's dynamics may be included in such a model. Chapter 4 extends the dynamical systems perspective on data-driven models to predict gait kinematics and muscle activity in response to ankle exoskeleton torque.

Human gait need not be viewed as phase-varying. An alternative dynamical systems-based approach is to view gait as a hybrid system, in which the dynamics are piecewise continuous and the system's evolution is well-described by low-dimensional dynamics. Hybrid regions in human gait are often defined by foot-ground contact configuration, such that walking has four distinct contact configurations: single- and double-limb support which define the times when one or both feet are on the ground, with the right or left leg leading [72, 95]. For example, Drnach and

colleagues (2019) used linear models and automated identification of hybrid dynamics to model responses to functional electrical stimulation [95]. The authors reported strong prediction accuracy of kinematic states and highlighted potential insights gained from examining the model's structure. While hybrid dynamical systems theory has been developed most recently than that of continuous dynamical systems, formal mathematical tools exist to study hybrid systems [96].

Data-driven dynamical systems models have two major limitations for studying human gait. Generating stable dynamical systems models of locomotion can require hundreds to thousands of gait cycles of data [27]. When data collection capacity is limited, reduced-order models may be useful for estimating locomotion dynamics that are robust to both sensor noise and stride-to-stride variations in gait [93, 97-99]. Second, the population-specific dynamical systems models are impractical due to the diversity of human gait, such that long time series must be collected for each individual. While subject-specific dynamical models should provide a higher-resolution picture of an individual's gait dynamics, population-specific models would be more practical to implement in clinical settings. Nonetheless, dynamical systems models of human locomotion represent powerful tools to predict and study exoskeleton responses.

When studying population-specific features of locomotion, descriptive and predictive data-driven models are more common than dynamical systems models in biomechanics research [21, 26, 90]. Such modeling frameworks do not synthesize the time evolution of gait, but rather describe characteristic patterns (*descriptive*) in data or encode time-invariant input-output relationships (*predictive*). Examples of descriptive models include muscle synergies, which describe characteristic muscle coordination patterns ([24, 100, 101]), or the Gait Deviation Index, which

used principal components analysis to identify archetypal kinematic coordination patterns during walking [102]. An example of a predictive modeling framework is that of Ries and colleagues (2015) who used a Random Forest algorithm to predict kinematic responses to different ankle exoskeleton designs in children with CP [26]. The authors used retrospective datasets consisting of ankle exoskeleton type, medical history, physical examination, and barefoot gait kinematics as model inputs. Such models are particularly useful when short time series or a large number of participants are available. However, adjusting for complex interindividual differences in gait remains challenging and may bias scientific findings, particularly in individuals with motor impairments.

This dissertation adopts the perspective that subject-specific physiological, physics-based, and data-driven dynamical models of gait with ankle exoskeletons will provide substantial insight into how gait mechanics and control change with exoskeletons. The following chapters detail applications of each perspective to quantify and predict subject-specific responses to ankle exoskeletons. This dissertation provides a foundation for future investigation into mechanisms driving heterogeneous responses to exoskeletons and other assistive devices. The long-term goal of this work is to enhance mobility by providing researchers and clinicians with knowledge and tools to improve the efficacy of exoskeleton design across individuals with diverse physiology and motor capacity.

Chapter 3. SIMULATED IMPACTS OF ANKLE FOOT ORTHOSES ON MUSCLE DEMAND AND RECRUITMENT IN TYPICALLY-DEVELOPING CHILDREN AND CHILDREN WITH CEREBRAL PALSY AND CROUCH GAIT

PLoS One, 2017 Jul; 12(7): e0180219.

https://doi.org/10.1371/journal.pone.0180219

Michael Rosenberg

Katherine M. Steele

ABSTRACT

Passive ankle foot orthoses (AFOs) are often prescribed for children with cerebral palsy (CP) to assist locomotion, but predicting how specific device designs will impact energetic demand during gait remains challenging. Powered AFOs have been shown to reduce energy costs of walking in unimpaired adults more than passive AFOs, but have not been tested in children with CP. The goal of this study was to investigate the potential impact of powered and passive AFOs on muscle demand and recruitment in children with CP and crouch gait. We simulated gait for nine children with crouch gait and three typically-developing children with powered and passive AFOs. For each AFO design, we computed reductions in muscle demand compared to unassisted gait. Powered AFOs reduced muscle demand 15-44% compared to unassisted walking, 1-14% more than passive AFOs. A slower walking speed was associated with smaller reductions in absolute muscle demand for all AFOs (r^2=0.60-0.70). However, reductions in muscle demand were only moderately correlated with crouch severity (r^2=0.40-0.43). The ankle plantarflexor muscles were most heavily impacted by the AFOs, with gastrocnemius recruitment decreasing 13-73% and correlating with increasing knee flexor moments (r2=0.29-0.91). These findings support the potential use of powered AFOs for children with crouch gait, and highlight how subject-specific kinematics and kinetics may influence muscle demand and recruitment to inform AFO design.

3.1 INTRODUCTION

Crouch gait, characterized by excessive knee flexion during stance, is one of the most common gait patterns among individuals with cerebral palsy (CP) [54]. Children with CP expend significantly more energy to walk than their typically-developing (TD) peers [103], which can hinder participation in activities of daily life. Increased knee flexion during crouch gait increases the muscle force required to support and propel the body [104-106], contributing to increased energy costs [53]. While many treatments aim to improve crouch gait, ankle foot orthoses (AFOs) remain one of the most common interventions. AFOs are often prescribed for children with CP to improve gait kinematics, prevent bone deformities, and potentially reduce energy costs of walking [29, 48]. However, there are many different types of AFOs and their potential to reduce energy costs of walking remains unclear.

Passive AFOs that resist ankle dorsiflexion are the most commonly prescribed orthoses for children with CP [4]. Solid, passive-elastic AFOs generate torque as a function of ankle kinematics and AFO properties. Two properties largely dictate the passive resistance from these AFOs: stiffness and equilibrium angle. Stiffness determines the resistance of the AFO to ankle dorsiflexion and has been shown to vary widely across passive AFO designs, with studies of CP reporting AFO stiffness ranging from 0.2–3.8 N·m/deg [29, 107]. The AFO equilibrium angle (Figure 3.1) is defined as the angle between the AFO shank and footplate at which the AFO starts to generate torque. Displacement of the AFO ankle angle from the equilibrium angle produces a resistive torque proportional to the magnitude of the AFO's angular displacement and the AFO stiffness. Orthotists often adjust these properties during AFO fabrication to customize passive

AFOs for children with CP [108]. Some new AFOs even let orthotists or therapists adjust the stiffness or other properties after fabrication [109].

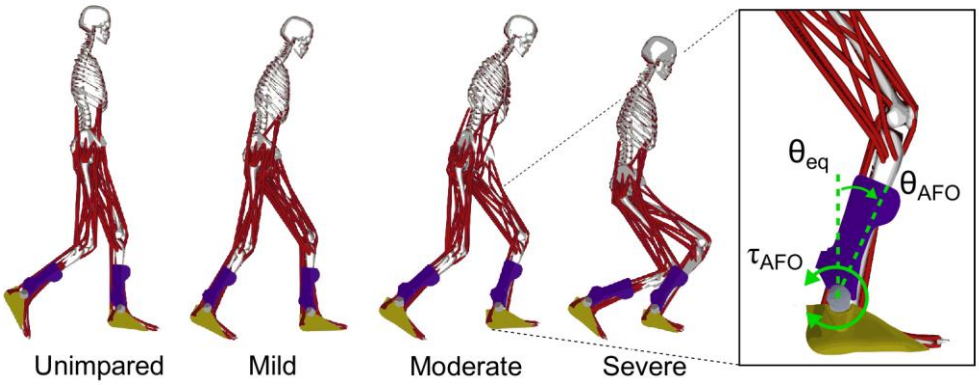

Figure 3.1. Musculoskeletal models with bilateral AFOs. The beginning of second double-limb support is shown for one typically-developing (TD) participant and one participant from each level of crouch severity. Mild (MI), moderate (MO) and severe (SE) crouch gait were defined by the minimum knee flexion angle during stance. AFO torque (τ_{AFO}) was determined by AFO stiffness and AFO angle (θ_{AFO}) for the passive AFOs, and by the OpenSim cost function for the powered AFOs.

If designed properly, a passive AFO's storage and release of mechanical energy can potentially reduce energetic demand during gait. Clinically-prescribed passive AFOs have been shown to reduce energy costs of walking in CP, with energy savings ranging from 6-9% compared to unassisted walking [48, 110]. Greater energetic savings have been observed using experimental AFOs. A recent study of 15 children with spastic CP tested three AFO stiffness levels and found that moderate stiffness AFOs generally provided the greatest reductions in energy costs: 11% reduction compared to unassisted walking [29]. However, predicting an individual's response to different AFOs and identifying optimal AFO properties for each individual remains challenging [4, 29, 48, 111].

Moving beyond passive AFOs, technological advances have motivated the use of powered AFOs, which use actuators, such as electric motors, to generate torques at the ankle for assistance or augmentation [16, 17, 56]. The power generated by these AFOs has the potential to surpass achievable energy storage and return of passive AFOs during gait. Further, powered AFOs provide the opportunity to customize the timing and magnitude of the ankle torque to each individual and different activities of daily life. Unlike passive AFOs, these devices generate controllable torques that are independent of ankle kinematics, giving them the potential to further reduce energy costs of walking. In unimpaired adults, powered AFOs that assist plantarflexion have been shown to reduce energy costs by up to 11% [17, 56], as compared to 7% with passive AFOs [9]. Powered AFOs have not been tested on individuals with CP. A potential disadvantage of powered AFOs is the additional device weight and complexity. Current models often weigh two to four times that of passive AFOs in adults, and may present a larger energetic challenge for children [9, 56]. While battery packs can be mounted at the waist, much of the device mass is located distally, on the foot and shank, which can significantly increase energy costs during walking [112]. Understanding the potential energy savings of powered AFOs during pathologic gait in CP can help inform design specifications for these devices.

Experimental analyses of individuals' responses to different AFO designs can be time-consuming and technically challenging. Measures of metabolic rate, such as oxygen consumption, are noisy and can be slow to stabilize, limiting the number of conditions that can be tested in a single session [113, 114]. Musculoskeletal simulation provides a tool to quickly perform "what-if" experiments, such as testing how different AFO designs impact muscle demand and recruitment. Recently, Uchida et al. [25] used simulation to investigate how powered lower-limb assistive devices may

impact metabolic rate in adults during running. Their findings suggest that massless, powered AFOs may reduce the metabolic power required for running by up to 26%. Hegarty et al. [40] recently combined musculoskeletal simulation and probabilistic methods to evaluate the sensitivity of muscle force estimates on passive AFO mechanical properties for two children with CP. The authors demonstrated that muscle force estimates were sensitive to both AFO stiffness and equilibrium angle, further motivating the need for novel methods to predict optimal passive AFO properties for a given individual.

The goal of this research was to investigate the potential impact of powered and passive AFOs on muscle recruitment and energy costs of walking in TD children and children with crouch gait. We generated musculoskeletal simulations of children with CP and TD children, and evaluated the potential reduction in muscle force with passive and powered AFOs. We hypothesized that powered AFOs would provide greater reductions in muscle force than passive AFOs for both children with CP and TD peers. Understanding how AFOs can impact muscle demand and recruitment may motivate further investigation into the use of powered AFOs and inform AFO design for children with CP.

3.2 METHODS

3.2.1 *Participants*

To evaluate the potential impact of AFOs on muscle recruitment during gait, we used previously-collected experimental kinematics and ground reaction force data from three TD children and nine children with diplegic CP and crouch gait (Table 3.1), which are available from a public data repository [115, 116]. These datasets were generated from motion analysis data originally collected at Gillette Children's Specialty Healthcare (St. Paul, MN), and include one gait cycle of unassisted, barefoot overground walking for each participant at their self-selected speed. The participants with CP were grouped by minimum knee flexion angle (KFA) during stance, representing mild (MI; KFA 15˚-30˚), moderate (MO; KFA 30˚-50˚), and severe (SE; KFA >50˚) crouch gait. These datasets were previously used in simulations to evaluate muscle contributions to mass center accelerations and tibiofemoral forces during crouch gait [106, 117].

Table 3.1. Characteristics of TD children and children with CP used in AFO simulations (average ± 1SD)

	N*	Age (years)	Height (m)	Mass (kg)	KFA** (deg)
Typically-Developing	3	12 ± 2	1.4 ± 0.0	38 ± 5	2 ± 1
Mild	3	9 ± 1	1.2 ± 0.1	24 ± 4	18 ± 3
Moderate	3	11 ± 2	1.4 ± 0.1	43 ± 31	34 ± 2
Severe	3	14 ± 2	1.6 ± 0.1	42 ± 8	64 ± 20

*N, Number of participants in each group
**KFA, Minimum knee flexion angle during stance

3.2.2 *Musculoskeletal modeling*

To generate simulations of walking with and without AFOs, we used scaled musculoskeletal models from the original dataset. These models have 19 degrees of freedom and 92 musculotendon actuators, and were updated for compatibility with version 3.3 of OpenSim, an open-source musculoskeletal modeling program [70, 118]. We used inverse kinematics to generate joint angle trajectories by minimizing the tracking error between virtual and experimental marker trajectories. Average kinematic marker RMS error was 1.2 ± 0.2 cm and the maximum marker error was 2.8 ± 0.8 cm [119]. A residual reduction algorithm was used to improve dynamic consistency and reduce the impact of modeling and experimental errors by making small adjustments to the torso mass center position and joint angles [120]. Peak residual forces were less than 5.0% of participants' total ground reaction forces, and peak residual moments were less than 5.9% of participants' external moments about the center of mass. Residual forces and moments were elevated in these simulations compared to best-practice values [119] due to a number of factors. In particular, arm and torso motion can have important impacts on gait in CP [121]. Arm motion in CP has been shown to contribute to center of mass acceleration more in children with CP compared to TD children [122]. Arm motion was not modeled due to a lack of arm markers during data collection and the torso was modeled as a rigid segment. Other soft tissue artifacts can also contribute to increased residual magnitudes, but we expect arm and torso modeling assumptions to be the primary contributors to residuals in these simulations.

We estimated muscle forces over one gait cycle using OpenSim's static optimization algorithm. Static optimization estimates muscle forces by minimizing the sum of squared muscle activations required to generate experimental kinematics and ground reaction forces at each time point [66].

For each participant, we simulated unassisted walking and walking under four AFO conditions, using the same set of experimental kinematics and ground reaction forces (Figure 3.2). Although prior research has demonstrated that AFOs often produce important changes in kinematics for children with CP [4, 29, 48], changes in kinematics with existing AFOs are often small and variable between individuals [4, 29]. In this study, we aimed to understand the potential impact of AFOs on muscle demand, even if kinematics are unchanged. Thus, we assumed identical kinematics between barefoot and AFO conditions and evaluated the potential impact of AFOs on muscle force during walking.

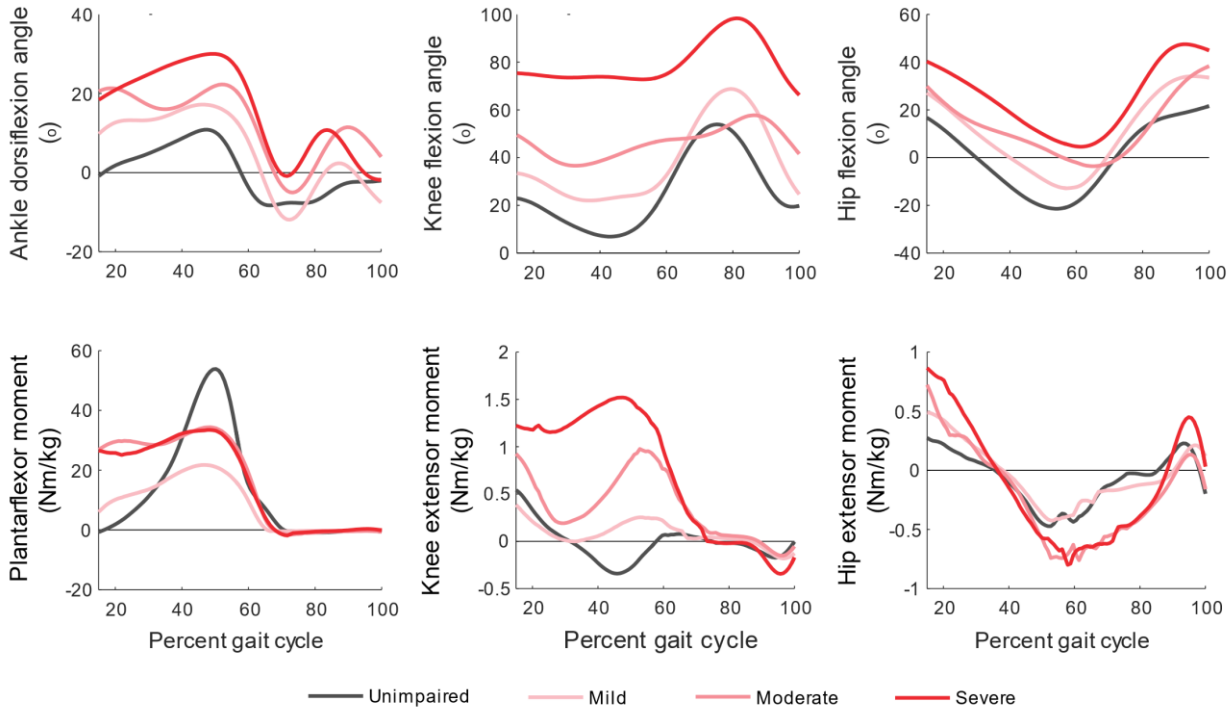

Figure 3.2. Sagittal-plane joint kinematics and internal moments. Top: Ankle, knee and hip kinematics for gait in TD children and children with crouch gait. TD children walked with less ankle dorsiflexion and knee flexion during stance than those with crouch gait. Bottom: Ankle, knee and hip moments for gait in TD children and crouch gait. TD children generated larger peak plantarflexor moments and smaller peak knee extensor moments compared to crouch gait. Knee extensor moments increased with increasing crouch severity.

3.2.3 *Quantification of muscle demand*

Our primary outcome measure was the sum of muscle forces in one leg, integrated over single-limb support and second double-limb support, which we term *leg impulse*. Although this is not a direct measure of metabolic cost, the mechanical work rate of muscle is a major component of metabolic cost and is proportional to muscle force [65]. We analyzed leg impulse during single-limb support and second double-limb support for each participant, which was the range that consistently had clean ground reaction force data across all participants. Simulations showed that 85-92% of the AFOs' impacts on muscle demand occurred during this portion of the gait cycle. This range is consistent with one experiment that reported that changes in active muscle volume during stance accounted for over 85% of the increase in metabolic rate when carrying different loads [123].

Muscle force trajectories from static optimization were processed in MATLAB (MathWorks, Inc., Natick, MA). We interpolated the entire gait cycle to 1000 data points and analyzed only single-limb support and second double-limb support. Muscle forces were normalized by each participant's bodyweight (BW=mass·gravity) and AFO torques were normalized by BW·leg length [124]. For individual muscles, we defined scalar *muscle impulse* as the integral of a muscle's force during single-limb support and second double-limb support. We computed muscle impulse for the soleus (SOL), gastrocnemius (GAS), tibialis anterior (TA), rectus femoris (RF), vasti (VAS), hamstrings (HAMS), gluteus maximus (GMAX), and iliopsoas (ILIO).

3.2.4 *AFO conditions*

An overview of our simulations and analysis pipeline can be found in Figure 3.3. We modeled the passive AFOs as massless, sagittal-plane, constant-stiffness torsional springs at the ankle joint, resisting only dorsiflexion, similar to some AFOs used in studies of children with CP and more advanced devices used to study optimal AFO stiffness in unimpaired adults [9, 29]. The passive AFO torque profile was determined by ankle kinematics, and two AFO properties: torsional stiffness and equilibrium angle (Figure 3.1, right). Equilibrium angle, θ_{eq}, was defined as the sagittal-plane angle between the AFO shank and footplate at which the AFO started generating torque. The passive AFO shank and footplate were fixed to the tibia and calcaneus of the model, respectively. The AFO angle, θ_{AFO}, was therefore equal to the sagittal-plane ankle angle throughout the gait cycle. The plantarflexor torque generated by AFOs, τ_{AFO}, was a linear function of equilibrium angle and ankle dorsiflexion angle (equation 3.1). We defined the optimal combination of AFO stiffness and equilibrium angle for each participant as that which minimized leg impulse.

$$\tau_{AFO}(t) = \begin{cases} k_{AFO} \cdot (\theta_{AFO}(t) - \theta_{eq}(t)) & \theta_{AFO} \geq \theta_{eq} \\ 0 & \theta_{AFO} < \theta_{eq} \end{cases} \quad 3.1$$

To identify optimal passive AFO properties, we simulated gait using different combinations of AFO stiffness and equilibrium angle for each participant. We performed simulations in two iterations. The first iteration simulated a grid of 400 uniformly-distributed combinations of AFO stiffness and equilibrium angle. For the children in this study, we simulated a range of AFO stiffness from 0.0 N·m/deg to 5.0 N·m/deg. These values were determined from studies that tested AFO stiffness values ranging from 0.7-3.8 N·m/deg for children with CP and 0.0-7.0 N·m/deg for unimpaired adults [9, 29]. AFO equilibrium angles ranged from minimum to maximum ankle angle

during gait for each participant. We identified the combination of AFO properties from these simulations that minimized the leg impulse for each participant. We then determined the range of AFO properties around this point that resulted in less than a 5% increase in leg impulse, and simulated an additional 225 uniformly-distributed data points within this range. From these simulations, we defined the optimal AFO properties as the combination of AFO stiffness and equilibrium angle that minimized leg impulse for each participant.

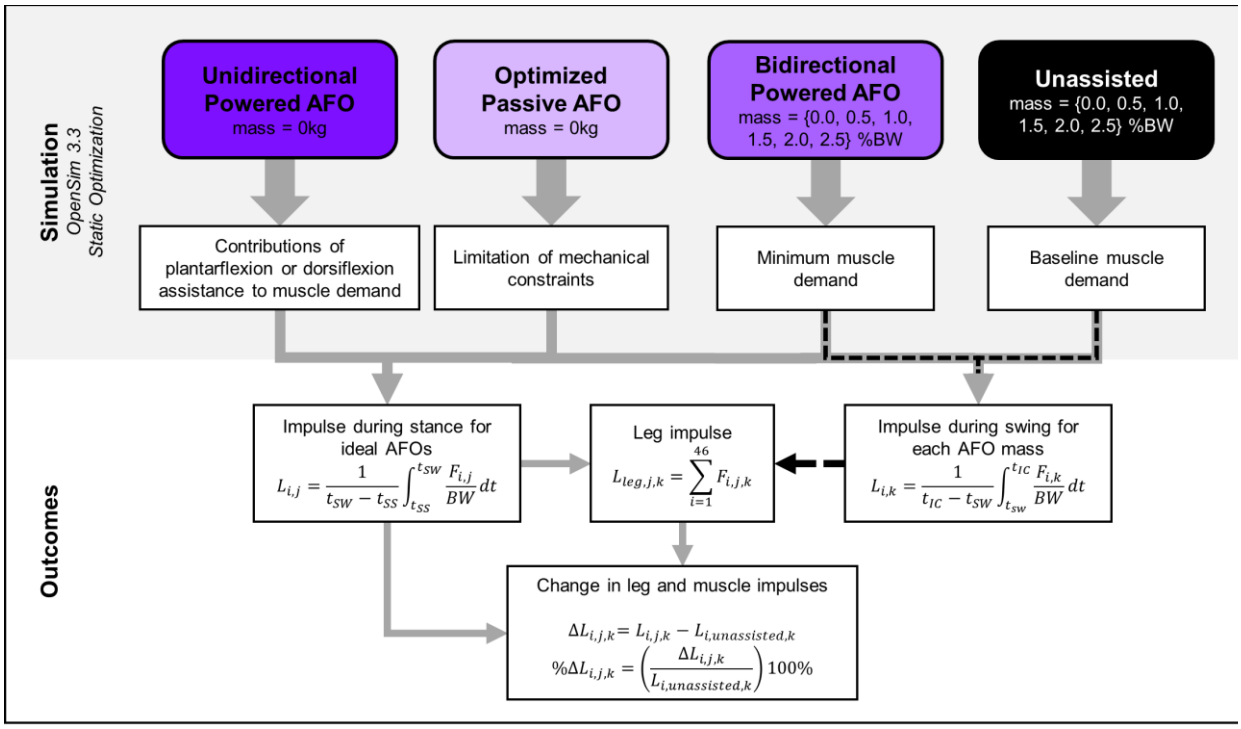

Figure 3.3. Simulation pipeline and outcome measures. Leg ($L_{leg,j,k}$) and muscle ($L_{i,k}$, $L_{i,j}$) impulses were computed for all AFO conditions, including the baseline (Unassisted) condition. Subscripts i, j, k, denote the muscle, AFO condition, and mass, respectively. The muscle impulses used to compare between AFO conditions were computed from the beginning of single-limb support (t_{SS}) to the start of swing (t_{SW}). Muscle impulses for the mass analysis (black dotted line) were computed from t_{SW} to initial contact at the start of the next gait cycle (t_{IC}). Forces were normalized by bodyweight (BW). Leg impulse was computed for each participant's leg that contained the single-limb support and second double-limb support gait phases. Change ($\Delta L_{i,j,k}$) and percent change ($\%\Delta L_{i,j,k}$) in leg and muscle impulses were used to quantify changes in muscle demand between AFO conditions. Abbreviations: $L_{leg,i,j,k}$, Leg impulse for muscle i, AFO j, and mass k; SS, single-limb support phase; SW, swing phase; IC, initial contact; Δ, absolute change; %Δ, percent change.

We modeled the powered AFOs as additional sagittal-plane reserve actuators at the ankle joint. Unlike passive AFOs, the activation level of powered AFOs was included in and determined by the static optimization cost function. Static optimization identified the active AFO torque profile that minimized the sum of squared muscle activations during gait [125], and thus required only a single simulation per subject for each powered AFO design. We set the optimal torque of the powered AFOs to a value of 1 MN·m, such that the AFO torque had a negligible impact on the static optimization cost function. This optimal torque is consistent with prior work examining the impact of exoskeletons on running energetics in unimpaired adults [25], and we found that our simulation results were insensitive to further increases in the AFO's optimal torque. We simulated two powered AFO conditions: a bidirectional AFO, which generated both plantarflexor and dorsiflexor torques, and a unidirectional AFO, which generated only assistive plantarflexor torques. We have made all musculoskeletal models, including actuators and setup files available on (https://simtk.org/projects/crouchgait).

To evaluate the impact of AFO mass, we simulated gait with AFOs with mass both with and without bidirectional actuation. We modeled each AFO as a shank piece and a footplate. The shank piece and footplate contained 66.6% and 33.3% of the AFO mass, respectively, which is consistent with experimental powered AFO designs [56]. AFO mass was increased incrementally from 0.0 to 2.5% of each participant's bodyweight (Figure 3.3). When AFO mass was larger than 2.5% of bodyweight, the peak and RMS residual forces from static optimization exceeded best-practice values [119], and were omitted from analysis. The foot-mounted hardware of recent powered AFOs weigh as little as 1.1 kg per foot [56]. Including the mass of a standard shoe, this would

result in a total mass of approximately 2kg at each foot for children, which corresponds to 2.5–9.0% bodyweight for the children in this study. Commercial passive AFOs for children can weigh as little as 0.3 kg per foot, which, in combination with shoes, would be less than 5.0% of the mass of most children in this study.

Each AFO condition was compared to simulations of unassisted gait and AFOs were applied bilaterally for all simulations. We computed reductions in leg and muscle impulses in each AFO condition as absolute and percent change relative to the unassisted walking condition for each participant. We compared outcomes between AFO conditions by computing absolute and percent changes in leg impulse and the impulse of individual muscles. To compare the impacts of AFOs between groups, we averaged changes in leg and muscle impulses across participants in each group. The sensitivity of leg impulse to AFO mass was determined as the slope of the linear-least squares curve fit between AFO mass and leg impulse. We performed linear regression to investigate whether participant-specific parameters identified from prior research impacted changes in leg impulse. Specifically, we tested peak and average sagittal-plane lower-limb kinematics [53, 126], joint moments [126], and nondimensionalized walking speed [103]. All predictors were computed for the leg analyzed for each participant and over the same portion of the gait cycle used to compute leg impulse. We iterated through each predictor-outcome pair using a robust fitting algorithm to reduce the influence of outliers.

3.3 RESULTS

3.3.1 *Unassisted walking*

Crouch gait required more muscle force than gait in TD children during unassisted walking (Figure 3.4). Leg impulse increased with crouch severity (r^2=0.80, slope=0.06 xBW/deg, $p<0.001$).

Impulses in the SOL (r^2=0.60, slope=0.01 xBW/deg, p<0.005), RF (r^2=0.44, slope=0.004 xBW/deg, p<0.001), GMAX (r^2=0.84, slope=0.003 xBW/deg, p<0.001) and VAS (r^2=0.92, slope=0.04 xBW/deg, p<0.001) increased with crouch severity, while GAS impulse decreased with increasing crouch (r^2=0.47, slope=-0.004 xBW/deg, p<0.02). HAMS impulse was uncorrelated with crouch severity for these participants (r^2<0.06).

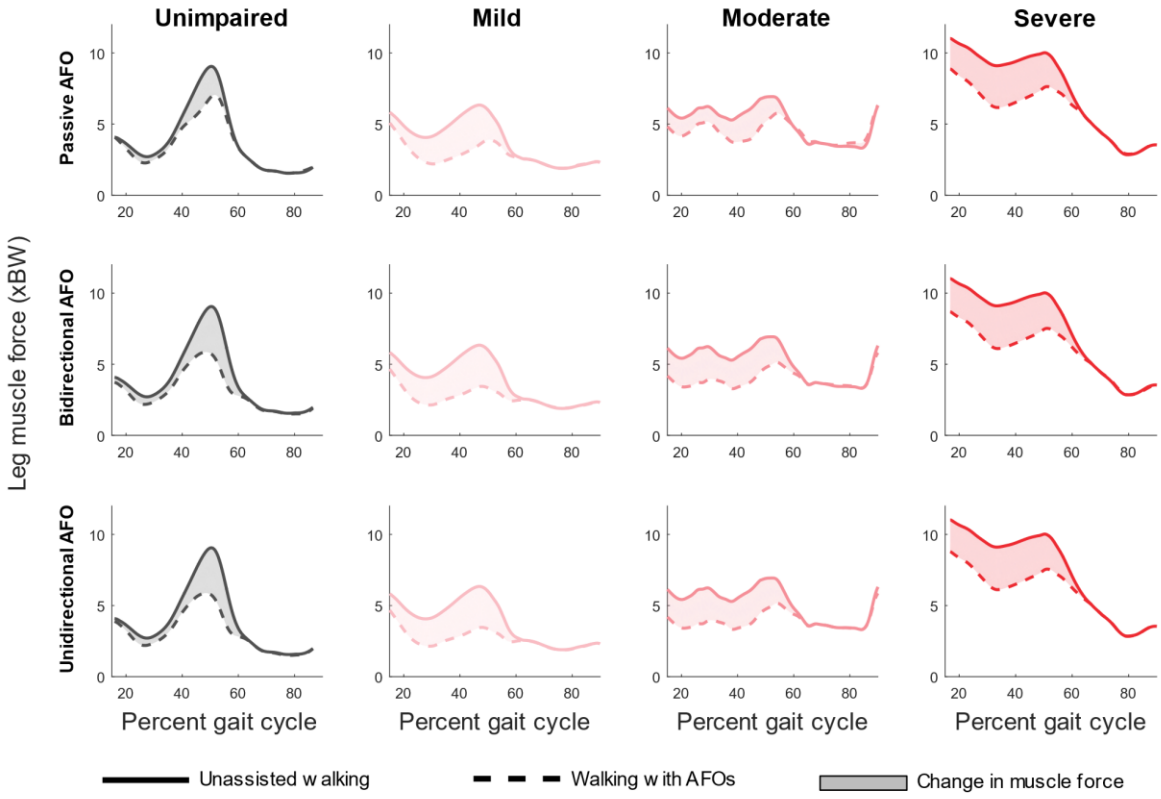

Figure 3.4. Leg muscle force with each AFO condition compared to unassisted walking. Profiles are averaged across participants in each group. Top to bottom: Optimal passive AFO, unidirectional powered AFO, and bidirectional powered AFO. The integral of these curves represents the leg impulse. Reductions in leg muscle force occurred primarily during late stance (40-60% gait cycle) for the TD group, while crouch gait groups saw leg muscle force reduced throughout single-limb support and late stance (20-60% gait cycle). Passive AFOs reduced leg muscle force less than unidirectional powered AFOs during early single-limb support for all groups, and throughout stance for the TD and moderate crouch groups. For some participants, passive and unidirectional powered AFO torque profiles were nearly identical, resulting in only small differences in leg muscle force with different AFOs. Reductions in leg muscle force were nearly identical for the unidirectional and bidirectional powered AFO conditions. Small

differences in leg muscle force between these conditions occurred during swing and corresponded to changes in tibialis anterior force due to dorsiflexion assistance in the bidirectional AFO.

Passive AFOs that resisted dorsiflexion reduced muscle demand during gait for all participants, primarily during terminal stance for TD participants and throughout stance for crouch gait (Figure 3.4). Compared to unassisted walking, leg impulse was reduced 15% in the TD group with passive AFOs, and 31, 17 and 21% in the mild, moderate and severe crouch groups, respectively (Figure 3.5, Table 3.2) Percent reduction in leg impulse was not correlated with crouch severity (r^2<0.01), nor was it strongly correlated with any of the predictors selected from prior studies. However, the absolute reduction in leg impulse increased moderately with increasing crouch severity (r^2=0.40, slope=0.01 xBW/deg, p<0.03), with gait in TD children having the smallest impulse reduction (0.5 xBW). Nondimensional speed (r^2=0.70, slope=-5.20 xBW, p<0.001) and average ankle angle (r^2=0.70, slope=0.03 xBW/deg, p<0.001) were the strongest correlates with absolute reduction in leg impulse. Passive AFO torque profiles did not resemble net ankle moments for TD and moderate crouch gait (Figure 3.5, top).

3.3.2 *Passive AFOs*

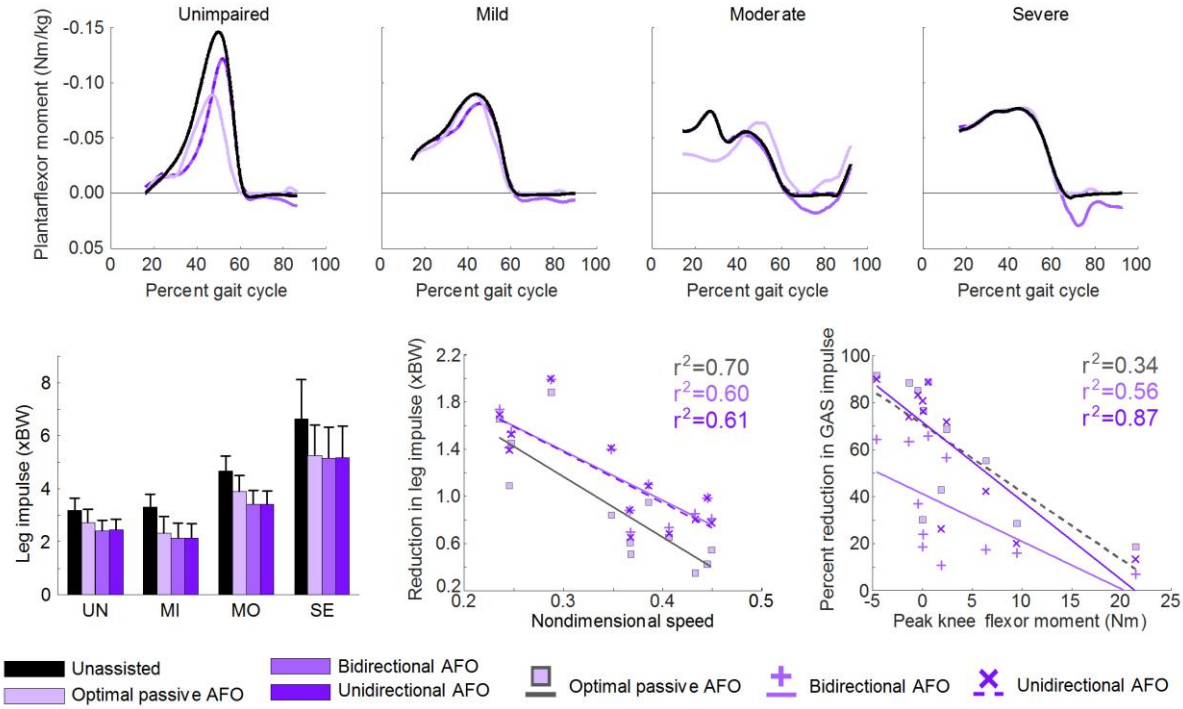

Figure 3.5. AFO torque profiles, leg impulse for each AFO condition and predictors of reductions in leg and muscle impulses. Top: Net ankle moments determined by inverse dynamics and AFO torque profiles for gait in TD children and children with crouch gait. A positive moment corresponds to a plantarflexor torque. Bottom, left: Leg impulse magnitude increased with crouch severity. Bottom, center: Reduction in leg impulse was strongly correlated with nondimensional speed for all AFO conditions. Bottom, right: GAS impulse was most strongly correlated with peak knee flexor moment. GAS activity in one subject with severe crouch was estimated to be near-zero during stance, and was omitted from this figure. Abbreviations: TD, typically-developing; MI, mild crouch; MO moderate crouch; SE; severe crouch; GAS, gastrocnemius muscle group.

Table 3.2. Reduction in leg impulse versus unassisted gait, showing average absolute (xBW, ± SD) and percent change (± SD) in leg impulse.

	Typically-Developing	**Mild**	**Moderate**	**Severe**
Passive AFO	0.5 ± 0.1 15 ± 5 %	1.0 ± 0.4 31 ± 13 %	0.8 ± 0.3 17 ± 7.8 %	1.4 ± 0.7 21 ± 9 %
Powered AFO, Unidirectional	0.7 ± 0.1 12 ± 2 %	1.2 ± 0.3 36 ± 11 %	1.3 ± 0.2 27 ± 5 %	1.5 ± 0.7 22 ± 9 %
Powered AFO, Bidirectional	0.8 ± 0.1 25 ± 2 %	1.2 ± 0.3 36 ± 11 %	1.3 ± 0.2 27 ± 5 %	1.5 ± 0.7 22 ± 9 %

For individual muscles, only the ankle plantarflexors had a reduction in muscle impulse of more than 20% with passive AFOs compared to unassisted gait (Figure 3.6). Passive AFOs reduced GAS impulse by 34-69% and SOL impulse by 71-97%. Percent reduction in GAS impulse with passive AFOs decreased with increasing peak knee flexor moment (r^2=0.50, slope=-98.0 xBW/(N·m/kg), $p<0.02$). TA impulse increased with passive AFOs for the TD, mild and moderate crouch groups (82-369%), but this change corresponded to only a 0.03-0.14 xBW absolute increase in impulse. Reductions in VAS (2-11%) and RF (1-18%) impulses largest for muscles not spanning the ankle, and were variable between groups with passive AFOs.

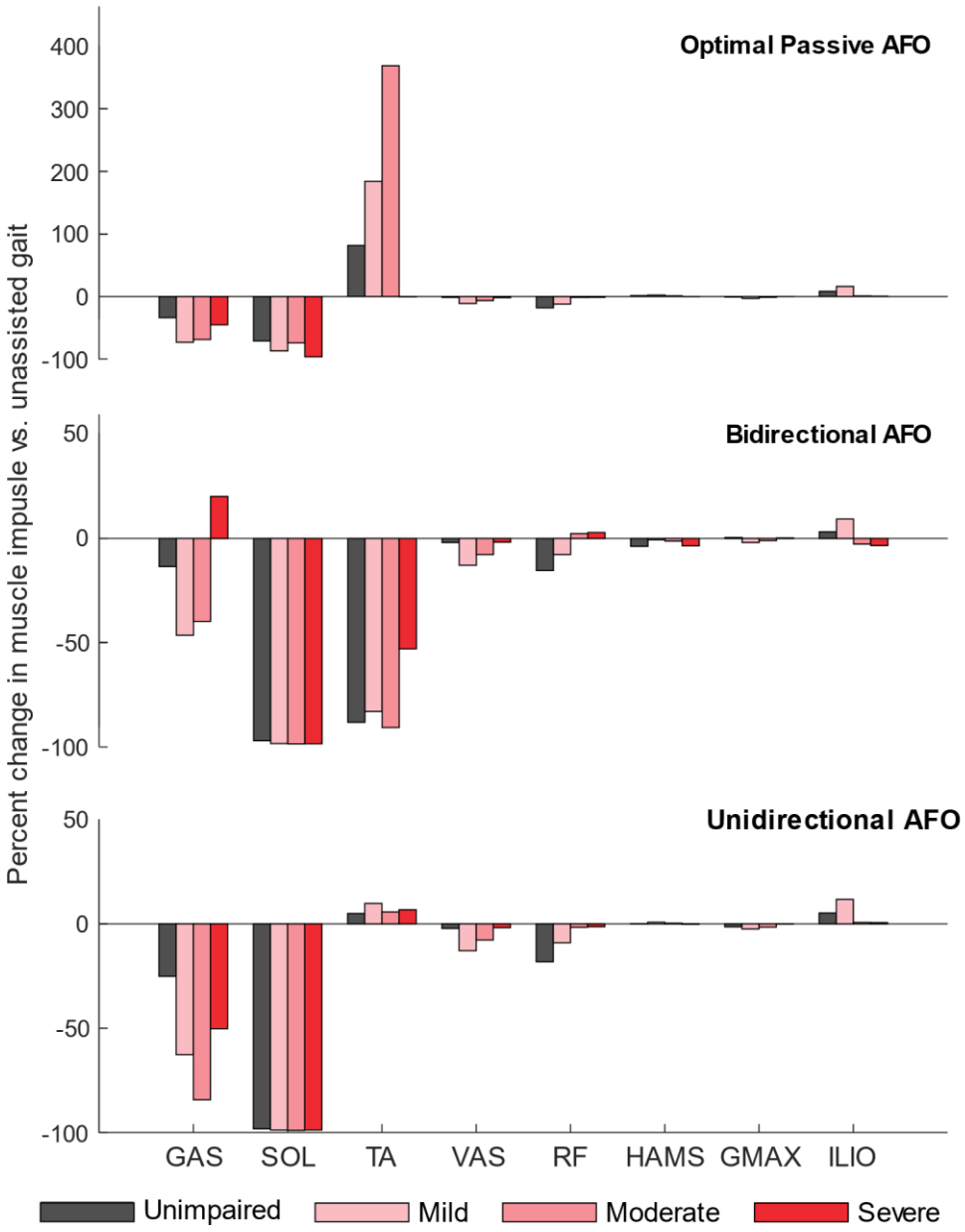

Figure 3.6. Percent change in impulse of individual muscles across AFO conditions. The GAS and SOL were most impacted by all AFO conditions, with relatively small changes occurring in other muscles. Top: The TA impulse increased with passive AFOs to overcome the AFO's stiffness and maintain ankle kinematics. The large percent increase in TA impulse for the optimized passive AFO corresponds to only a small absolute increase in TA impulse compared to unassisted gait. Middle: The unidirectional powered AFO had similar reductions in muscle impulses as the bidirectional AFO, except for the GAS. Bottom: Only the bidirectional powered AFO reduced TA impulse, but this corresponded to a smaller percent reduction in GAS impulse. Impulses in muscles spanning the knee and hip changed by less than 20%, with the VAS having the largest reductions in muscle demand within these groups. Abbreviations: GAS, gastrocnemius; SOL, soleus; TA, tibialis anterior; VAS, vasti; RF, rectus femoris; HAMS, biarticular hamstrings; GMAX, gluteus maximus; ILIO, iliopsoas.

The average AFO stiffness that produced the greatest reduction in leg impulse was 4.6 ± 1.4 N·m/deg for gait in TD children and 2.3 ± 1.4 N·m/deg for crouch gait. Normalizing AFO stiffness by participant mass resulted in different optimal stiffness values in each CP group: 0.12 ± 0.04 N·m/(kg·deg) for gait in TD children and 0.09 ± 0.06, 0.05 ± 0.02, and 0.05 ± 0.02 N·m/(kg·deg) for the mild, moderate, and severe crouch gait, respectively. The normalized passive AFO stiffness correlated most strongly with peak ankle plantarflexor moment (r^2=0.75, slope=-0.11 deg^{-1}, $p<0.001$). The AFO equilibrium angle that resulted in the largest reduction in leg impulse was largest for severe crouch (12.8 ± 7.3 deg) and smallest for gait in TD children (3.5 ± 5.6 deg). This angle increased (*i.e.*, a more dorsiflexed equilibrium angle) as peak plantarflexion angle decreased (r^2=0.88, slope=-0.4, $p<0.001$).

3.3.3 *Powered AFOs*

Unidirectional powered AFOs reduced leg impulse for all subjects, with an average reduction of 23 ± 2% and 28 ± 10% compared to unassisted gait for the TD and crouch groups, respectively. This corresponds to a 10 ± 4% and 7 ± 5% greater reduction than passive AFOs for the TD and crouch groups, respectively. The largest reductions in leg impulse with the unidirectional powered AFO occurred during single-limb support for all groups, and throughout stance for the TD and moderate crouch groups (Figure 3.4). Large reductions in leg impulse with the unidirectional powered AFO represent the benefit of powered AFOs over passive AFOs of comparable design. However, the difference in leg impulse reductions between AFO designs was variable, with participants experiencing a 1% to 13% difference between powered and passive AFOs. Leg impulse reductions were smallest for participants whose passive AFO torque profiles most closely

matched their unidirectional powered AFO torque profiles. Minimum KFA during stance was moderately correlated with the absolute reduction in leg impulse (r^2=0.41, slope=0.01 xBW/deg, p<0.03), but was not correlated to percent reduction in leg impulse (r^2<0.07). Similar to passive AFOs, nondimensional speed (r^2=0.60, slope=-4.21 xBW, p<0.004) was most strongly correlated with the absolute reduction in leg impulse.

Walking with bidirectional powered AFOs reduced leg impulse similar to the unidirectional powered AFOs (Figure 3.5, Table 3.2). During gait in TD children, the average reduction in leg impulse was 25%, while leg impulse was reduced 36, 27 and 22% for mild, moderate and severe crouch groups, respectively, compared to unassisted walking (Table 3.2, Figure 3.5). Bidirectional powered AFOs assisted both ankle plantarflexion and dorsiflexion as much as needed, and thus returned the maximum achievable reductions in leg impulse from our simulations. However, dorsiflexion assistance corresponded to only a 1% greater reduction in leg impulse compared to the unidirectional AFOs. Regression results were nearly identical to the unidirectional AFO condition: Percent reductions in muscle demand were not correlated with crouch severity (r^2<0.05), or any other pre-selected predictor. Participants with greater crouch severity had larger reductions in leg impulse: 0.8, 1.2, 1.3 and 1.5 xBW for gait in TD children and mild, moderate and severe crouch gait, respectively. Minimum KFA during stance was moderately correlated to these reductions (r^2=0.43, slope=0.01 xBW/deg, p<0.03). Similar to the passive AFO, average ankle angle (r^2=0.70, slope=0.03 xBW/deg, p<0.001) and nondimensional speed (r^2=0.61, slope=-4.20 xBW, p<0.003) were most strongly correlated to absolute reduction in leg impulse. Both bidirectional and unidirectional AFO torque profiles closely resembled net ankle moments for

crouch gait and more closely resembled net ankle moments compared to passive AFOs for gait in TD children (Figure 3.5, top).

Similar to passive AFOs, the powered AFOs primarily reduced muscle demand in the ankle plantarflexors, with reductions in muscle impulse of more than 20% in only the GAS and SOL for both powered AFOs, as well as in the TA for the bidirectional AFO (Figure 3.6). Unlike the passive AFO condition, SOL impulse reduction was similar for all crouch groups (97-98%) for both powered AFO conditions. The percent reduction in GAS impulse decreased with increasing peak knee flexor moment for the unidirectional AFOs (r^2=0.91, slope=-225.0 %/(N·m/kg), $p<0.001$) and bidirectional AFOs (r^2=0.29, slope=-65.3 %/(N·m/kg), $p<0.1$). Percent reductions in GAS impulse ranged from 25-84% for the unidirectional AFO condition, and 13-46% for the bidirectional AFO condition. The smaller reduction in GAS impulse with the bidirectional AFO compared to unidirectional AFOs was due to the bidirectional AFOs' dorsiflexion assistance. By generating a dorsiflexor torque during swing, the bidirectional AFOs enabled the GAS to contribute to knee flexion moments more than during unassisted walking, reducing demand on the HAMS (Figure 3.6). Consequently, bidirectional assistance resulted in small reductions in both the TA and HAMS impulses in these simulations. Minimum KFA was correlated with the reduction in GAS impulse only for the unidirectional AFOs (r^2=0.57, slope=-1.07 xBW/deg, $p<0.01$). TA impulse was reduced 53-91%, only when walking with bidirectional powered AFOs. Powered AFOs' impacts on muscles spanning the knee and hip were similar to those of passive AFOs, with the VAS (2-13%) and RF (1-18%) muscles showing the largest reductions in impulse compared to unassisted gait. Although the change was small (<5.0%), the bidirectional AFO was the only device to reduce HAMS recruitment compared to unassisted gait.

Leg impulse increased with increasing AFO mass in all participants, but sensitivity to AFO mass decreased with increasing crouch severity. Leg impulse increased at a rate of 0.14, 0.18, 0.15, 0.10 xBW/kg_{AFO} for the gait in TD children, and mild, moderate and severe crouch groups, respectively (Table 3.3). Powered AFO actuation increased sensitivity to AFO mass by less than 0.03 xBW/kg_{AFO} compared to the unactuated AFO. Increases in muscle impulse due to AFO mass occurred primarily in the knee flexors and hip flexors during swing, but were not correlated with minimum KFA during stance. Hip flexor force increased in early swing, while knee flexor force increased most during mid and late swing.

Table 3.3. Sensitivity of leg impulse to AFO mass (xBW/kgAFO).

	Mass sensitivity (xBW/kg_{AFO})*	
	Unactuated	Bidirectional
Typically-Developing	0.14 ± 0.06	0.15 ± 0.06
Mild	0.18 ± 0.05	0.21 ± 0.05
Moderate	0.15 ± 0.10	0.17 ± 0.11
Severe	0.10 ± 0.08	0.10 ± 0.09

*Sensitivity is defined as the slope of the leg impulse vs. AFO mass curve.

3.4 DISCUSSION

We simulated the effects of passive and powered AFOs on muscle demand and recruitment during walking in TD children and children with CP and crouch gait. We hypothesized that powered AFOs would reduce leg impulse more than passive AFOs. The simulation results supported this hypothesis, with leg impulse being reduced 1-15% more with powered AFOs than passive AFOs, supporting the potential use of powered AFOs as assistive devices for CP. Unlike passive AFOs, powered AFO torque profiles are independent of ankle kinematics which increases the ability to customize torque profiles to an individual's gait pattern. We also found, as anticipated, that all AFO designs primarily impacted the ankle plantarflexor muscles; however, reductions in muscle impulse were only moderately correlated with crouch severity, emphasizing the diverse factors that influence an AFO's impact on muscle demand, even among children with similar gait patterns.

As idealized models of passive and powered AFOs, the results of this study provide an estimate of the potential of AFOs to reduce muscle demand during gait for children with CP independent of changes in kinematics. Prior studies with passive AFOs reported reductions in metabolic cost ranging from 6-10% [29, 48], though no prior studies have investigated the impact of powered AFOs on muscle demand in CP. In this study, we observed 10-41% reductions in leg impulse with AFOs, which is one of the primary contributors to metabolic cost of walking. However, there are other factors such as cardiovascular health or selective motor control which may influence reductions in metabolic cost beyond reductions in muscle demand. Our results suggest that appropriate tuning of AFO mechanical properties to an individual may optimize reductions in muscle demand for children with CP. Further, the results from this study highlight the importance of optimizing AFOs across multiple parameters to minimize muscle demand during walking.

Passive AFO optimization protocols have been proposed, but typically select between only a few different AFO stiffness values or designs [26, 127], possibly limiting the "optimality" of selected AFO properties.

Identifying the optimal AFO properties for a given individual remains an open challenge, though musculoskeletal simulation may be used to inform subject-specific device design. Testing over many potential AFO tuning parameters is time and resource intensive, making simulation-based predictions of AFOs attractive. We found that absolute reductions in leg impulse with all AFO designs correlated most strongly with nondimensional speed, and that percent reductions in GAS impulse correlated most strongly with peak knee flexor moments. This highlights the importance of activity-level (walking speed) and mechanical-level (kinematics, kinetics) measurements in predicting the impacts of AFOs on gait in CP [128]. The complex interaction between mechanical and activity-level aspects of gait suggests that a multivariate approach to predicting AFO impacts on muscle demand and recruitment is necessary. A post-hoc multiple linear regression analysis found that a linear combination of lower-limb kinematics and joint moments was strongly correlated with both absolute and percent reductions in muscle demand. This is consistent with one study that found that a similar linear combination of mechanical-level measures explained 89% of the variance in net metabolic cost during uphill walking in unimpaired adults [126]. While our regression analysis suggested that nondimensional speed may be a useful way to quantify the potential impact of AFOs on muscle demand if kinematic or kinetic data are unavailable, new methods are needed to evaluate the potential benefit of AFO designs. The simulation paradigm presented in this research may be used to help identify a near-optimal set of mechanical AFO

properties for an individual and potentially inform biofeedback or other training regimes to optimize muscle recruitment while walking with a new AFO.

There were similarities in the optimal AFO properties predicted in our study and prior experimental results. The optimal passive AFO stiffness values predicted for the TD children were larger than a prior study that identified the passive AFO stiffness that most reduced metabolic costs in unimpaired adults (4.6 N·m/deg vs 3.1 N·m/deg [9]). Similarly, for crouch gait, our optimal stiffness of 2.3 N·m/deg was slightly larger than a reported optimal of 1.6 N·m/deg for passive AFOs that minimized energy costs of walking in CP [29], though this study evaluated three AFO stiffness conditions with a maximum stiffness of 3.8 N·m/deg. These differences may be due in part to the instantaneous "adaptation" to AFOs that occurs during simulation, compared to slow and complex motor adaptation in human gait. Further, simulated AFO stiffness has been shown to alter the strain of elastic elements in the ankle plantarflexors, which leads to changes in metabolic power in these muscles during gait [37]. Consistent with our findings, this suggests that the comparatively simple musculotendon model used in static optimization may over-predict optimal AFO stiffness values. Passive AFO equilibrium angle is less studied than AFO stiffness [39], but correlated well with peak ankle plantarflexion angle. Thus, basing passive AFO equilibrium angle on ankle kinematics may generate a good initial guess prior to tuning AFOs to minimize muscular demand during gait. The range of optimal AFO properties found in this study emphasizes the importance of appropriate AFO actuator design and mechanical properties based on an individual's gait pattern.

Powered AFOs outperformed passive AFOs in this study and may be more effectively tuned to a specific individual. However, their use may not be justifiable if powered AFOs are too heavy.

Consider that our reported sensitivity of leg impulse to AFO mass (~0.1 xBW/kg_{AFO}) was similar to the contribution of powered AFO dorsiflexion assistance to reductions in leg impulse (0.1-0.2 xBW). This implies that the additional hardware required for powered dorsiflexion assistance would have to weigh less than 1kg to reduce leg impulses. Moreover, some participants received only a small (<3%) benefit of powered AFO assistance over passive assistance. Since powered AFOs can weigh four times as much as passive AFOs, the additional weight of powered actuation may not be justifiable if energetic savings is a primary objective [9, 56]. The small linear increase in muscle demand due to AFO mass applied to the foot and shank was qualitatively consistent with experimental studies of unimpaired walking that found that metabolic rate increased linearly with mass added to the foot and shank [112]. This suggests that results from small AFO masses may be extrapolated to masses larger than 2.5% of participants' bodyweights. For example, our results suggest that the weight of powered AFOs [56] may increase leg impulse by 10% for a child with mild CP, which could eliminate the potential advantage of powered AFOs over passive AFOs in reducing muscle demand during walking. However, the sensitivity to AFO mass decreased as crouch severity increased, which may be explained by a reduced mass moment of inertia of the AFO mass about the hip and knee in the sagittal plane [129]. Thus, individuals with more severe crouch gait, whose limbs may have less rotational inertia with about the hip, may be less sensitive to mass added to the foot and shank. These results collectively suggest that AFO actuator design, mass, and mass distribution should all be considered and informed by an individual's gait analysis.

There are also other important factors that may limit achievable reductions in metabolic costs with AFOs for children with CP. In particular, children with CP have been shown to have less complex motor control strategies than their TD peers, which may limit their ability to adapt muscle

recruitment to AFOs [24, 130]. If muscle coordination is restricted to synergistic motor patterns, a child may not be able to modulate muscle activity and take advantage of the potential energy savings. Prior studies with varying AFO properties for children with CP have provided short training periods, which may also limit resulting changes in muscle activity and reductions in metabolic cost. The results of this study support the potential of passive and powered AFOs to reduce energy costs in CP, but highlight the need to evaluate changes in neuromuscular control and train appropriate changes in muscle recruitment with assistive devices.

AFOs primarily impacted ankle plantarflexor activity and the results of this study demonstrate the complex and important role these muscles play during gait. Prior experimental studies of unimpaired adults have demonstrated a reduction in ankle plantarflexor activity with both passive and powered AFOs [9, 16, 18]. However, prior experimental studies have not investigated changes in plantarflexor muscle activity with AFOs in children with CP [29, 40, 48]. We found that reductions in GAS recruitment were not only important for ankle dynamics, but also correlated with peak knee flexor moments, which decreased with crouch severity [131]. This highlights the potential of AFOs to indirectly influence knee flexor moments. Reduced GAS recruitment with simulated AFOs also reduced the GAS's contribution to knee flexor moments during stance, which in turn reduced the demand of the knee extensor muscles. This effect was reflected in reductions in VAS and RF impulses with all AFOs. Since the knee extensors are active during most of stance in crouch gait [106], a smaller knee flexor moment contribution of the GAS may also enable the knee extensor muscles to further extend the knee, possibly enabling a less crouched posture. We must acknowledge, however, that crouch gait can arise from myriad factors. Simply reducing knee extensor demand may not reduce crouch [132, 133]. For example, if short hamstrings contribute

to crouch, reduced demand on the knee extensors with AFOs may not improve crouch [134]. Conversely, if coactivation or spasticity influences crouch, altered muscle demand with AFOs may enable the quadriceps to more effectively extend the knee. These results may also inform future studies of myoelectric control of powered AFOs for children with CP. Myoelectric feedback control of powered AFOs typically uses SOL activation signals for control during unimpaired gait [16, 135]. Using GAS activation signals for feedback control of powered AFOs may enable children with crouch gait to better influence both knee and ankle dynamics.

The results of this study should be taken in the context of the study's limitations. Our inverse simulations were constrained by one set of experimental kinematics and kinetics for each individual to evaluate potential reductions in muscle demand independent of changes in gait pattern. In contrast, clinically-prescribed passive AFOs are often designed to alter gait kinematics, and powered AFOs have been shown to alter lower-limb joint moments compared to unassisted walking [16, 18]. For example, allowing powered AFOs to reduce extensor moments at the knee may enable greater simulated reductions in knee extensor impulse compared to unassisted gait. Predicting changes in gait after an intervention remains a grand challenge of biomechanics which may further enhance our ability to identify optimal, customized orthoses. Maintaining constant kinematics and kinetics across AFO conditions provides a reasonable method to evaluate potential energy savings of a wide range AFO designs, prior to experimentation [4, 25]. Also, we used OpenSim's static optimization algorithm to estimate muscle activity, which does not model excitation-activation or tendon dynamics, both of which may influence muscle force during dynamic tasks [37, 136]. Conversely, OpenSim's computed muscle control algorithm (CMC) [120] includes tendon dynamics, but over-predicts muscle forces [25, 40]. We compared these

algorithms and found that CMC predicted greater overall muscle activity, and our outcome measures and conclusions were insensitive to algorithm choice. Finally, bone deformities, contracture, and spasticity are common in CP and were not captured in our models. This dataset was originally selected to include participants with minimal bone deformities [137], but minimal information regarding muscle physiology and spasticity were available for these participants. Incorporating individual changes in muscle properties, such as contracture or weakness, may further improve the ability of these methods to predict optimal AFO design for a given individual. Future simulation-based orthosis optimizations may also want to consider maximum allowable reductions in muscle activity to help prevent atrophy or exacerbate muscle weakness. Even with more accurate subject-specific modeling and simulation methods, researchers should acknowledge the importance of patient feedback in the AFO prescription process. Device users provide important feedback that is not captured by musculoskeletal models, such as comfort or interactions of soft-tissue with the AFO. The simulation pipeline presented in this work can be used to complement clinician expertise and help customize AFO design for rehabilitation and performance goals.

3.5 Conclusions

Optimizing the design of powered or passive AFOs has the potential to reduce muscle demand and improve metabolic efficiency for children with CP, even without changes in an individual's gait pattern. These changes are clinically important because children with CP have inefficient gait patterns compared to TD peers and optimizing AFOs to reduce energy costs may reduce fatigue and increase participation in daily life. Musculoskeletal simulation provides a platform to evaluate and test AFO designs and inform training by predicting optimal patterns of muscle recruitment.

Although crouch gait represents one of the most common gait pathologies in CP [54], many other common gait pathologies exist that could benefit from similar analyses. Further understanding of the role of concomitant impairments such as muscle weakness, spasticity, or contracture represent important areas for future investigation. To encourage expansion of musculoskeletal simulation to assistive device applications, we have made our simulations available for others to use and build upon (https://simtk.org/projects/crouchgait). Adaptation to and optimization of AFOs remain challenging topics [4, 135], and future work comparing predictions with experimental tests will further enhance these methods. This study informs future clinical design and prescription of AFOs for children with CP and motivates further investigation into powered AFOs as assistive devices for children with CP.

Chapter 4. PREDICTING WALKING RESPONSE TO ANKLE EXOSKELETONS USING DATA-DRIVEN MODELS

Journal of the Royal Society Interface, 2020 Oct; 17(171): 20200487.

https://doi.org/10.1098/rsif.2020.0487

Michael C. Rosenberg

Bora S. Banjanin

Samuel A. Burden

Katherine M. Steele

ABSTRACT

Despite recent innovations in exoskeleton design and control, predicting subject-specific impacts of exoskeletons on gait remains challenging. We evaluated the ability of three classes of subject-specific phase-varying models to predict kinematic and myoelectric responses to ankle exoskeletons during walking, without requiring prior knowledge of specific user characteristics. Each model – phase-varying (PV), linear phase-varying (LPV), and nonlinear phase-varying (NPV) – leveraged Floquet Theory to predict deviations from a nominal gait cycle due to exoskeleton torque, though the models differed in complexity and expected prediction accuracy. For twelve unimpaired adults walking with bilateral passive ankle exoskeletons, we predicted kinematics and muscle activity in response to three exoskeleton torque conditions. The LPV model's predictions were more accurate than the PV model when predicting less than 12.5% of a stride in the future and explained 49–70% of the variance in hip, knee, and ankle kinematic responses to torque. The LPV model also predicted kinematic responses with similar accuracy to the more-complex NPV model. Myoelectric responses were challenging to predict with all models, explaining at most 10% of the variance in responses. This work highlights the potential of data-driven phase-varying models to predict complex subject-specific responses to ankle exoskeletons and inform device design and control.

4.1 INTRODUCTION

Ankle exoskeletons are used to improve kinematics and reduce the energetic demands of locomotion in unimpaired adults and individuals with neurologic injuries [9, 18, 29, 39, 55]. Customizing exoskeleton properties to improve an individual's gait is challenging and accelerating the iterative experimental process of device optimization is an active area of research [19, 138]. Studies examining the effects of exoskeleton properties – sagittal-plane ankle stiffness or equilibrium ankle angle for passive exoskeletons and torque control laws for powered exoskeletons – on kinematics, motor control, and energetics have developed design and control principles to reduce the energetic demand of walking and improve the quality of gait [9, 19, 26, 38]. Predicting how an individual's gait pattern responds to ankle exoskeletons across stance may inform exoskeleton design by enabling rapid evaluation of exoskeleton properties not tested experimentally. Additionally, for powered exoskeletons, which prescribe torque profiles using feedforward or feedback (*e.g.* kinematic or myoelectric) control laws, predicting responses over even 10–20% of a stride may improve tracking performance or transitions between control modes [16, 45, 55, 139]. However, predicting subject-specific responses to exoskeletons remains challenging for unimpaired individuals and those with motor impairments [4, 29, 45].

Common physics-based models, including simple mechanical models and more physiologically-detailed musculoskeletal models, use principles from physics and biology to analyze and predict exoskeleton impacts on gait. For example, one lower-limb mechanical walking model predicted that an intermediate stiffness in a passive exoskeleton would minimize the energy required to walk, a finding that was later observed experimentally in unimpaired adults [9, 85]. More physiologically-detailed musculoskeletal models have been used to predict the impacts of

exoskeleton design on muscle activity during walking in children with cerebral palsy and running in unimpaired adults [25, 140]. While these studies identified hypothetical relationships between kinematics and the myoelectric impacts of exoskeleton design parameters, their predictions were not evaluated against experimental data.

Challenges to accurately predicting responses to ankle exoskeletons with physics-based models largely stem from uncertainty in adaptation, musculoskeletal physiology, and motor control, which vary between individuals and influence response to exoskeletons. While individuals explore different gait patterns to identify an energetically-optimal gait, exploration does not always occur spontaneously, resulting in sub-optimal gait patterns for some users [141]. Popular physiologically-detailed models of human gait typically assume instantaneous and optimal adaptation, which do not reflect how experience and exploration may influence responses to exoskeletons, possibly reducing the accuracy of predicted responses [22, 70]. Additionally, when specific measurement sets are unavailable for model parameter tuning, population-average based assumptions about musculoskeletal properties and motor control are required [24, 37, 67, 141]. However, musculoskeletal properties and motor control are highly uncertain for individuals with motor impairments, today's most ubiquitous ankle exoskeleton users [22, 24, 67, 142]. Musculotendon dynamics and motor complexity are known to explain unintuitive exoskeleton impacts on gait energetics, suggesting that uncertain musculotendon parameters and motor control may limit the accuracy of predicted changes in gait with ankle exoskeletons [22, 37, 143]. Predictions of exoskeleton impacts on gait using physiological models, therefore, require accurate estimates of adaptation, musculotendon parameters, and motor control.

Conversely, data-driven approaches address uncertainty in user-exoskeleton dynamics by representing the system entirely from experimental data. For instance, human-in-the-loop optimization provides a model-free alternative to physics-based prediction of exoskeleton responses by automatically exploring different exoskeleton torque control strategies for an individual [19, 138]. This experimental approach requires no prior knowledge about the individual: optimization frameworks identify torque control laws that decrease metabolic rate relative to baseline for an individual using only respiratory data and exoskeleton torque measurements. However, experimental approaches to exoskeleton optimization require the optimal design to be tested, potentially making the search for optimal device parameters time-intensive. Alternatively, machine learning algorithms, such as the Random Forest Algorithm, have used retrospective gait analysis and clinical exam data to predict changes in joint kinematics in response to different ankle-foot orthosis designs in children with cerebral palsy [26]. This study reported good classification accuracy, though predictions may not generalize to new orthosis designs. Unlike physiologically-detailed or physics-based models, human-in-the-loop optimization and many machine learning models are challenging to interpret, limiting insight into how a specific individual's physiology influences response to exoskeleton torque. A balance between physiologically-detailed and model-free or black-box data-driven approaches may facilitate the prediction and analysis of responses to ankle exoskeletons without requiring extensive knowledge of an individual's physiology.

In this work, we investigated a subject-specific data-driven modeling framework – phase-varying models – that may fill the gap between physiologically-detailed model-based and model-free experimental approaches for predicting gait with exoskeletons. Phase-varying models typically have linear structure whose parameters are estimated from data, enabling both prediction and

analysis of gait with exoskeletons [27, 79]. Unlike physiologically-detailed models, phase-varying models do not require knowledge of the physics or control of the underlying system. Unlike experimental approaches, the model-based framework enables prediction of responses to untested exoskeleton designs or control laws.

Phase-varying models leverage dynamical properties of stable gaits derived from Floquet Theory, which ensures that the convergence of a perturbed trajectory to a stable limit cycle may be locally approximated using time-varying linear maps [94]. Similar principles have been shown to generalize to limit cycles in non-smooth or hybrid systems, such as human walking [96]. Moreover, phase-varying modeling principles have been applied to biological systems, identifying linear phase-varying dynamics to investigate gait stability and predict changes in kinematics in response to perturbations [27, 79, 80, 97, 144]. Responses to ankle exoskeleton torques may be similarly defined as perturbations off an unperturbed (*i.e.* zero torque) gait cycle, suggesting that the principles of phase-varying models will generalize to walking with exoskeletons. To the best of our knowledge, phase-varying models have never been used to study walking with exoskeletons and the extent to which the principles underlying phase-varying models of locomotion generalize to walking with exoskeletons is unknown.

To determine if phase-varying models represent useful predictive tools for locomotion with exoskeletons, the purpose of this research was to evaluate the ability of subject-specific phase-varying models to predict kinematic and myoelectric responses to ankle exoskeleton torque during walking. We predicted responses to exoskeletons in unimpaired adults walking with passive ankle exoskeletons under multiple dorsiflexion stiffness conditions. We focused on three related classes

of phase-varying models with different structures, complexity, and expected prediction accuracies: a phase-varying (PV), a linear phase-varying (LPV), and a nonlinear phase-varying (NPV) model. Since passive exoskeletons typically elicit small changes in joint kinematics and muscle activity, we expected the validity of Floquet Theory for human gait to extend to gait with exoskeletons, indicating that the LPV model should accurately predict responses to passive exoskeleton torque [9, 27, 79, 80, 94]. We, therefore, hypothesized that the LPV models would predict kinematic and myoelectric responses to torque more accurately than the PV model and as accurately as the NPV model. To exemplify the potential utility of subject-specific phase-varying models in gait analysis with ankle exoskeletons, we show how varying the length of model prediction time horizon may inform measurement selection for exoskeleton design and control. To assess the viability of data-driven phase-varying models in gait analysis settings, we evaluated the effect of limiting the size of the training dataset on prediction accuracy.

4.2 METHODS

4.2.1 *Experimental protocol*

We collected kinematic and electromyographic (EMG) data from 12 unimpaired adults (6 female / 6 male; age = 23.9 ± 1.8 years; height = 1.69 ± 0.10 m; mass = 66.5 ± 11.7 kg) during treadmill walking with bilateral passive ankle exoskeletons at a self-selected speed (Table 4.1). Each participant performed two sessions – practice and data collection – on separate days within a one-week span.

TABLE 4.1. ADULT ANKLE EXOSKELETON PARTICIPANT CHARACTERISTICS

Subjects	Gender (M/F)	Age (years)	Mass (kg)	Height (m)	Walking speed (m/s)
P01	M	25	73.5	1.78	1.36
P02	F	24	61.2	1.65	1.40
P03	F	20	49.9	1.60	1.30
P04	F	22	65.8	1.73	1.50
P05	F	25	55.0	1.55	1.30
P06	F	23	49.4	1.52	1.30
P07	M	27	59.9	1.68	1.35
P08	M	23	77.1	1.73	1.55
P09	M	24	80.7	1.84	1.40
P10	M	25	73.9	1.73	1.20
P11	M	25	83.9	1.83	1.40
P12	F	24	68.0	1.70	1.22

M = male, F = female; kg = kilograms; m = meters; s = seconds

In the first session, we modified the exoskeletons for fit and comfort and performed a 20-minute practice session. We ensured that the appropriately sized footwear was selected, that the exoskeleton cuff was at a comfortable height, and any points of discomfort were adequately padded. Participants were instructed to stop if they experienced pain or modified their gait pattern to avoid discomfort. Each participant performed 20 minutes of walking practice under three exoskeleton stiffness conditions (K0, K1, K3), spanning the range of conditions used during data collection. Participants walked at three nondimensional speeds (0.35, 0.45, 0.55) and three cadences (100, 120, and 140 steps/minute), set by a metronome, for one minute each. The ordering of the speed and cadence conditions was (1) middle, (2) high, and (3) low. Nondimensional speed, $\hat{v}$, was defined as $\hat{v} = \frac{v}{\sqrt{gL}}$, where v is the walking speed in meters/second, g is the gravitational constant, and L is the leg length measured from the lateral malleolus of the ankle to the anterior superior iliac spine point on the pelvis (Figure 4.1) [124]. Walking speeds during practice ranged from 0.88 m/s to 1.67 m/s. Following the practice session, each participant selected a preferred

walking speed corresponding to a "pace that they could comfortably sustain for 60 minutes while walking with the exoskeletons." Beginning at the intermediate nondimensional speed, the treadmill speed was changed according to the participant's requests (faster/slower), until the participant identified a preferred speed. If a participant did not explore speeds above/below their selected speed, a second iteration was performed, beginning at a speed below/above the selected speed to encourage exploration of walking speeds during the selection process, which is known to influence gait pattern selection [145]. All participants selected walking speeds within the range of nondimensional speeds used during practice ($0.40 \leq \hat{v}_{selected} \leq 0.53$). *Additional detail regarding experimental setup, input variable calculations, modeling algorithms, and statistical analyses can be found in Appendix A1*.

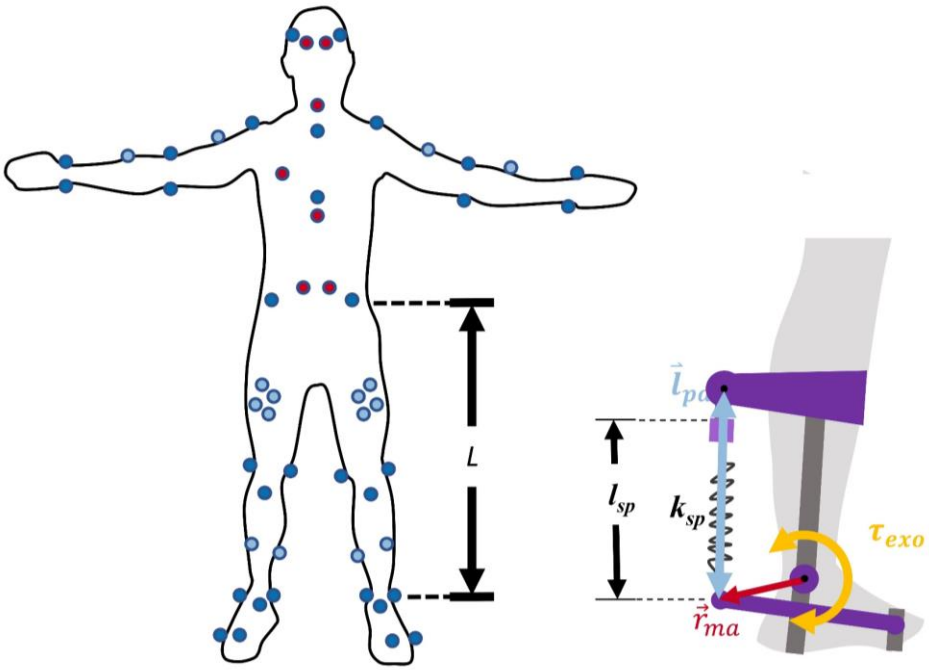

Figure 4.1. Left: A modified Helen Hayes marker set used in this study [146]. The depicted participant is facing forward. Dark blue markers were visible from an anterior view of the participant and were placed on bony landmarks on the body. Light blue markers were tracking markers and were also visible from an anterior view but were not placed on bony landmarks. Red markers were visible from a posterior view of the participant and were placed on bony landmarks. The distance *L* represents leg length. Right: A depiction of the exoskeleton components as listed in Eqn. 4.1. The exoskeleton torque, τ_{exo}, is determined by l_{pd}, the distance between the proximal and distal moment arms, l_{eq}, the equilibrium length of the spring cable, the spring stiffness, k_{sp}, and the moment arm vector between the spring insertion and the ankle joint, r_{ma}.

Data were collected during the second session. We monitored changes in kinematics using a modified Helen-Hayes marker set [146] and a 10-camera motion capture system (Qualisys AB, Gothenburg, SE; Figure 4.1), and measured muscle activity using 14 wireless EMG sensors (Delsys Inc., Natick, USA). The EMG sensors were placed bilaterally on the soleus, medial gastrocnemius, tibialis anterior, vastus medialis, rectus femoris, lateral hamstrings, and gluteus medius following SENIAM guidelines [147]. Participants performed four randomized trials on a split-belt instrumented treadmill (Bertec Corp., Columbus, USA) at their self-selected speed under different exoskeleton conditions (Figure 4.2). Each trial included two-minutes of walking to adapt to the new exoskeleton condition and participants could rest as needed between trials.

Unlike many clinical exoskeletons (ankle-foot orthoses), whose torque profiles are smooth functions of ankle angle, the passive exoskeletons used in this study generated ankle plantarflexion torques as a piecewise-linear function of the user's ankle angle, and the exoskeleton's neutral angle and rotational stiffness. The exoskeletons did not resist plantarflexion, similar to other experimental devices [9, 39]. The four exoskeleton conditions were set to sagittal-plane stiffness values: K_0 (0 Nm/deg), K_1 (1.17 Nm/deg), K_2 (3.26 Nm/deg), and K_3 (5.08 Nm/deg), a range

known to alter kinematics and myoelectric signals during gait (Figure 4.2) [9]. Participants walked for six minutes per trial, the last four of which were recorded, and could rest between trials.

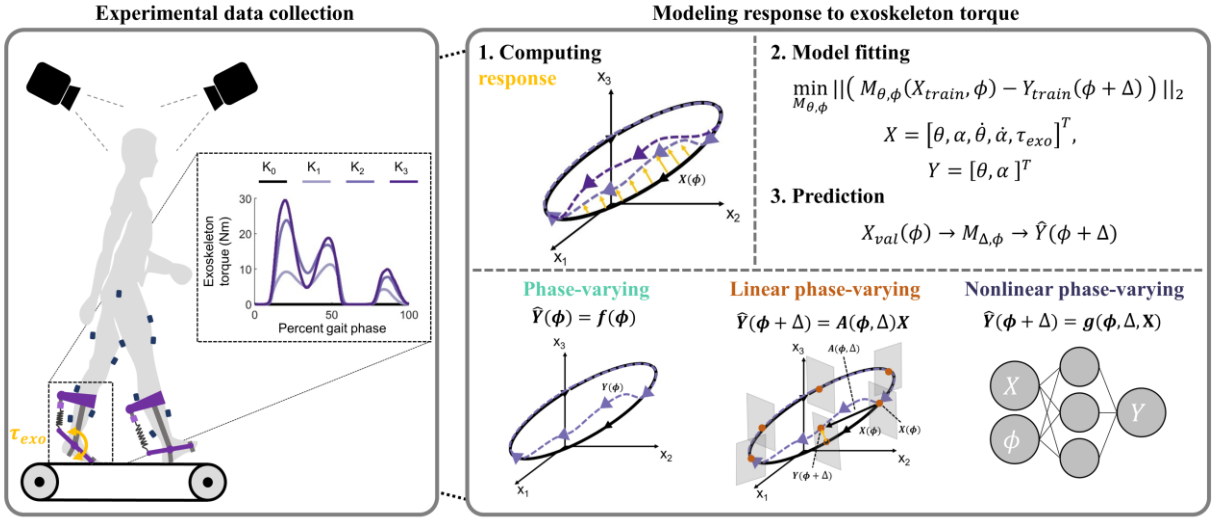

Figure 4.2. Left box: Data were collected during treadmill walking with bilateral ankle exoskeletons that used linear springs to resist dorsiflexion. Increasing exoskeleton stiffness (K_0–K_3) increased exoskeleton torque (τ_{exo}, yellow). Right box: (1) Purple dashed arrows represent responses to exoskeleton torque, which were defined as deviations from the average zero-torque gait cycle (K_0). (2) Response data from the training set were used to fit each model. Input variables included joint kinematics, muscle activity, their time derivatives, and exoskeleton torque. (3) Models were validated by predicting responses from the held-out torque condition using the models fit in (2). Right box (bottom): The three phase-varying models were fit and evaluated on the same training and validation sets.

$M_{\Delta,\phi}$ = generic model function of prediction horizon and phase; X = experimental inputs; Y = experimental outputs; $\hat{Y}$ = predicted outputs; ϕ = phase; Δ = prediction horizon; A = linear function; f, g = nonlinear functions; θ = joint kinematics; α = muscle activation; τ_{exo} = exoskeleton torque.

To compute linear EMG envelopes, we high-pass filtered the EMG data at 40 Hz, rectified the data, and low-pass filtered at 10 Hz [38]. Kinematic and EMG data were pre-processed using custom scripts in MATLAB (MathWorks, Natick, USA). The marker trajectories were low-pass filtered at 6 Hz using a zero-lag fourth-order Butterworth filter [18]. We computed joint kinematics by scaling a generic 29 degree-of-freedom skeletal model to each participant's skeletal geometry

and body mass using the inverse kinematics algorithm in OpenSim 3.3 to convert marker trajectories into joint kinematics [70, 148]. First, we scaled a generic 29 degree-of-freedom skeletal model to each participant's skeletal geometry [148]. The subtalar, metatarsophalangeal, wrist flexion, and wrist deviation degrees of freedom were locked. We ensured that root-mean-squared marker errors were less than 1 cm and maximum marker errors were less than 2 cm. Joint kinematics were then computed using OpenSim's inverse kinematics algorithm. The inverse kinematics algorithm identifies joint angle trajectories to minimize error between model markers, which are fixed on rigid body segments of the model, and the experimental marker trajectories. The knee joint range of motion was increased to permit up to five degrees of hyperextension for participants who appeared to hyperextend their knee during walking. We evaluated model quality using experimental marker errors, in line with best-practices [119]. Root-mean-squared marker errors were less than 2 cm and maximum marker errors were less than 4 cm for each trial.

4.2.2 *Estimating exoskeleton torque profiles*

For a passive exoskeleton, the torque, τ_{exo}, depended approximately linearly on the user's ankle kinematics, θ_{ankle}, exoskeleton equilibrium angle, θ_{eq}, and exoskeleton's rotational stiffness, k_{exo} (equation 4.1) as:

$$\tau_{\mathrm{exo}}(\mathrm{t}) = \begin{cases} -\mathrm{k}_{\mathrm{exo}}\left(\theta_{ankle}(t) - \theta_{eq}\right), & \theta_{ankle} \geq \theta_{eq} \\ 0 & \theta_{ankle} < \theta_{eq} \end{cases} \quad 4.1$$

Unlike many clinical exoskeletons, whose torque profiles are smooth functions of ankle angle, torque in the exoskeletons used in this work were piecewise-smooth functions of ankle angle, providing plantarflexion assistance similar to other experimental devices (Figure 4.2) [9, 39].

The linear approximation in Eqn 4.1 was deemed sufficient based on calibration trials with pilot datasets, during which tension load cells (Omega Engineering, Norwalk, CT) were attached in series to each exoskeleton spring (equation 4.2). The measured torque from the load cell, τ_{exo}, was,

$$\tau_{\mathrm{exo}}(\mathrm{t}) = \vec{r}_{\mathrm{ma}}(\mathrm{t}) \times \left[-k_{sp}\left(\vec{l}_{pd}(t) - l_{eq}\right)\right], \qquad 4.2$$

where l_{pd} is the distance the proximal and distal spring attachment points, and l_{eq} is the equilibrium length of the spring cable, which we estimated by having the subject dorsiflex until they felt the spring engage with the exoskeleton raised off the ground. The spring stiffness is denoted by k_{sp}. The cross product of the spring force vector and the vector between the moment arm at the distal end of the spring cable and the exoskeleton ankle joint, r_{ma}, defined the exoskeleton torque. Preliminary analyses showed small differences between torque profiles estimated from the nonlinear torque-ankle angle relationship (equation 4.2) and the linear relationship (equation 4.1) that we employed in our analysis.

4.2.3 *Gait phase and phase-varying models*

Unlike the typical gait cycle definition – the percentage of time between successive foot contact events – we used a gait phase based on kinematic posture, which we expected to improve predictions of a system's response to perturbations from the exoskeletons [149]. Using a posture-based gait phase groups kinematically-similar measurements at a specific phase, reducing variance in the data at any point in the cycle, and ensuring that similar postures across exoskeleton conditions were used during model fitting and prediction. Moreover, Floquet Theory ensures that phase is well-defined using any periodically-varying measurements [94]. We used the *Phaser* algorithm, which estimates a system's phase using arbitrary input signals considered to be phase-

locked, to generate gait phase estimates as a function of left and right leg hip flexion angles, similar to a phase variable proposed to control robotic prostheses [144, 149]. Following gait phase estimation, we modeled gait using three subject-specific models of response to exoskeletons:

4.2.4 *Phase-varying model*

The phase-varying (PV) model, F_{pv}^{w}, was our simplest model and predicts outputs purely as a function of gait phase. Rather than taking exoskeleton torque as an input, PV model predictions are similar to guessing the average of the training data at a certain gait phase (**Table 4.2**) [144, 150]. The PV model takes a phase estimate as an input and returns a prediction of the system's outputs, $\hat{Y}_{\phi} \in \mathbb{R}^{M}$, where *M* is the number of outputs. The PV model was parameterized using a seventh-order Fourier Series as a function of phase and served as a lower bound on prediction accuracy (equation. 4.3).

$$F_{pv}^{w} = \frac{1}{2}w_0 + \sum_{h=1}^{7} w_{2h-1}\cos(h\phi) + w_{2h}\sin(h\phi) \tag{4.3}$$

4.2.5 *Linear phase-varying model*

The linear phase-varying (LPV) model is a discrete-time model that predicts system outputs at a future phase based on measurements at an initial phase (Table 4.2). For any phase, ϕ, from 0-100% of a stride and a prediction horizon, Δ, the LPV model estimates a map $A_{\phi,\Delta} \in \mathbb{R}^{M\times N+1}$, from the initial phase to the final phase, where $N+1$ denotes the number of input variables (N) plus a constant term. At 64 initial phases spaced equally over the gait cycle, we fit discrete maps between initial and final phases using weighted least-squares regression [27, 79, 80]. We weighted

each observation based on the proximity of its phase estimate to the prescribed initial phase using a Gaussian weighting scheme. For each prediction horizon, the LPV model was represented as a continuously phase-varying function, $F_{LPV,\Delta}(\phi) \approx A_{\phi,\Delta}$, parametrized by a Fourier Series. We expected the LPV model's prediction accuracy to exceed that of the PV model [94].

4.2.6 *Nonlinear phase-varying model*

While the LPV model should approximate nonlinearities in the dynamics of response to torque, we selected a nonlinear phase-varying (NPV) model that serves as an upper bound on prediction accuracy. Specifically, we used a three-layer feedforward neural network – a universal function approximator (Table 4.2) [151]. Neural networks are considered state-of-the-art predictors and are used in numerous domains, including image recognition and robotics [152]. The NPV model's parameters were tuned for each prediction horizon and included phase as an input. We expected the NPV model's prediction accuracy to meet or exceed that of the LPV model.

TABLE 4.2. SUMMARY OF PHASE VARYING MODEL STRUCTURE AND EXPECTED PERFORMANCE

Model	Functional form	Linear terms	Nonlinear terms	Expected prediction accuracy
Phase-varying (PV)	$\hat{Y}_{\phi} = F_{PV}(\phi)$	None	Phase	Low
Linear phase-varying (LPV)	$\hat{Y}_{\phi+\Delta} = F_{LPV,\Delta}(\phi)X_{\phi}$	Inputs	Phase	Moderate
Nonlinear phase-varying (NPV)	$\hat{Y}_{\phi+\Delta} = G_{NPV,\Delta}(\phi, X_{\phi})$	None	Phase Inputs	Moderate-High

F = model functions parameterized by a Fourier Series; G = feedforward neural network model; ϕ = phase; Δ = prediction horizon; X = inputs; $\hat{Y}$ = predicted outputs

4.3 INPUTS AND OUTPUT VARIABLES

To reflect clinically-relevant measurements and the dynamics of the neuromusculoskeletal system, we selected input variables expected to encode musculoskeletal dynamics and motor control: 3D pelvis orientation and lower-limb and lumbar joint angles, processed EMG signals, and their time derivatives at an initial phase, ϕ [9, 29, 62]. We appended ten time-history exoskeleton torque samples per leg – uniformly distributed between the initial and final phases – to the inputs, resulting in $N = 80$ inputs [19, 45]. Our decision to use exoskeleton torque samples was motivated by Floquet Theory, according to which an individual's posture at a future time is a linear function of their initial posture and the exoskeleton torque signal between initial and final times [94]. Model outputs ($M = 20$) included right and left leg sagittal-plane hip, knee and ankle kinematics, and EMG signals from each muscle at a future phase, $\phi + \Delta$, offset from the initial phase by prediction horizon Δ. While phase-varying models may also predict joint moments, we omitted prediction of kinetic outcomes due to the presence of sporadic poor force plate strikes for some gait cycles in our dataset. We modeled response to exoskeleton torque as the deviation from the unperturbed gait cycle (*i.e.* the zero-torque, K_0 condition) by subtracting the phase-averaged zero-torque gait cycle from each exoskeleton condition [79, 80]. All data were de-meaned and scaled to unit variance of the training set. *Additional detail regarding the selection of torque as model inputs and experimental ground reaction forces can be found in Appendix A2.*

We first computed each model's ability to predict responses to torque within the range of exoskeleton stiffness levels used to train the models (interpolation) by training each model using the K_0, K_1 and K_3 datasets and validating by predicting outputs from the held-out K_2 dataset using inputs from the same dataset at an initial gait phase. While "what-if" predictions – predicting

responses to "untested" (held-out) torques using nominal kinematics and EMG from a "tested" condition (*e.g.* K_0) – are needed to for predictions to inform passive exoskeleton design, we chose to predict using the held-out inputs to provide unambiguous interpretation of each model's prediction accuracy. In "what-if" predictions, errors stem from both poor model fit and poor matches between the "tested" and "untested" input data at the initial phase. By instead predicting using "untested" inputs, our predictions errors reflect only the models' fits to each participant's dynamics and provide upper bounds on the potential accuracy of "what-if" predictions. We selected the K_2 condition for validation in our experimental design because responses in this intermediate torque condition should be encoded by the K_0, K_1, and K_3 conditions. During validation, experimental outputs from the K_2 condition were compared to the corresponding model predictions.

We quantified each model's prediction accuracy using the relative remaining variance (RRV) of model predictions compared to the held-out experimental data [27]. The RRV is calculated as the ratio of the variances of the prediction error and the experimental data. An RRV value of zero implies a perfect prediction, while unity RRV values can be achieved by predicting the mean of the validation data. Since we de-meaned the data and predicted deviations from the zero-torque condition, RRV values below unity indicate that predictions are more accurate than guessing constant (*e.g.* zero) response to exoskeleton torque. We computed RRV values for each output using a bootstrapping procedure with 200 iterations [27]. We computed RRV values for each model over the entire validation time series of approximately 240 strides. During analysis, the right and left leg RRV values for each output variable were averaged, as we expected nearly symmetric responses from our unimpaired participants.

We evaluated the LPV and NPV models' prediction accuracies for the K_2 condition over a range of prediction horizons, in increments of 6.25% ($1/16^{th}$ of a stride), between 6.25 and 100% of a gait cycle. When optimizing exoskeleton torque profiles, predicting responses using measurements at an initial phase (*e.g.* initial contact of the foot with the ground) to achieve a desired outcome at some final phase may be of interest, such as improving midstance knee kinematics in children with cerebral palsy [29, 39]. However, as the prediction horizon increases, coherence between measurements at initial and final phases decreases due to nonlinearities in musculoskeletal dynamics, resulting in prediction accuracies reducing to those of the average prediction (*i.e.* the PV model), rather than a stride-specific prediction [62, 153, 154]. Identifying the maximum prediction horizon at which initial measurements improve predictions at a final phase may inform exoskeleton control laws or design criteria. Therefore, we identified the largest prediction horizon lengths at which RRV values were significantly less than those of the PV model, which were constant across prediction horizons.

The amount of data required to accurately predict response to exoskeletons will restrict the settings in which phase-varying models are practical, such as in clinical gait analysis where datasets typically contain only a few gait cycles [26, 29]. We quantified the impact of training set size on prediction accuracy by determining the amount of training data needed for prediction accuracies of the K_2 condition to approach to their values when models were fit using the entire training set (RRV_{full}). We iteratively reduced the training set size by 10% of the full size (approximately 24 strides per exoskeleton condition), removing data from the end of each torque condition in the

training set, providing a range of 24-240 strides of training data per condition. For all training set sizes, we evaluated models using the full-length validation set.

To test each model's generalizability across a range of exoskeleton torque conditions, we separately predicted responses to torque in the K_1, K_2, and K_3 datasets, termed *held-out conditions*, at a 12.5% stride prediction horizon ($1/8^{th}$ of a stride). Predictions over these conditions evaluated both the models' ability to interpolate (K_1 and K_2) and extrapolate (K_3) responses to exoskeleton torques included in the training set. For each held-out condition (K_1, K_2, or K_3), we trained the models using kinematic, EMG, and exoskeleton torque inputs from the zero-torque (K_0) condition and the two non-zero-torque exoskeleton conditions not held out for validation. We evaluated each model by predicting output variables from the held-out exoskeleton condition using input data at an initial gait phase in the same condition. We compared prediction accuracies across held-out conditions.

To compare differences in performance across the three models, we identified differences in the models' prediction accuracies using repeated-measures analysis of variance tests at a significance level of $\alpha = 0.05$. When significant differences between models emerged, we identified pair-wise differences between models using post-hoc paired t-tests ($\alpha = 0.05$) and a Holm-Sidak step-down correction for multiple comparisons [38, 155]. We report percent reductions in RRV values compared to the PV model and percent differences between the LPV and NPV models.

4.4 RESULTS

The ankle exoskeletons had the largest impact on ankle kinematics, smaller impacts on knee and hip kinematics, and variable impacts on muscle activity (Figure 4.3). Compared to the K_0

condition, the peak ankle dorsiflexion angle during single-limb support decreased significantly in the K_2 (36.7%) and K_3 (40.0%) conditions ($p < 0.020$). Average integrated EMG increased slightly, but not significantly in the hamstrings and tibialis anterior ($p > 0.066$) in the K_2 and K_3 conditions compared to the K_0 condition.

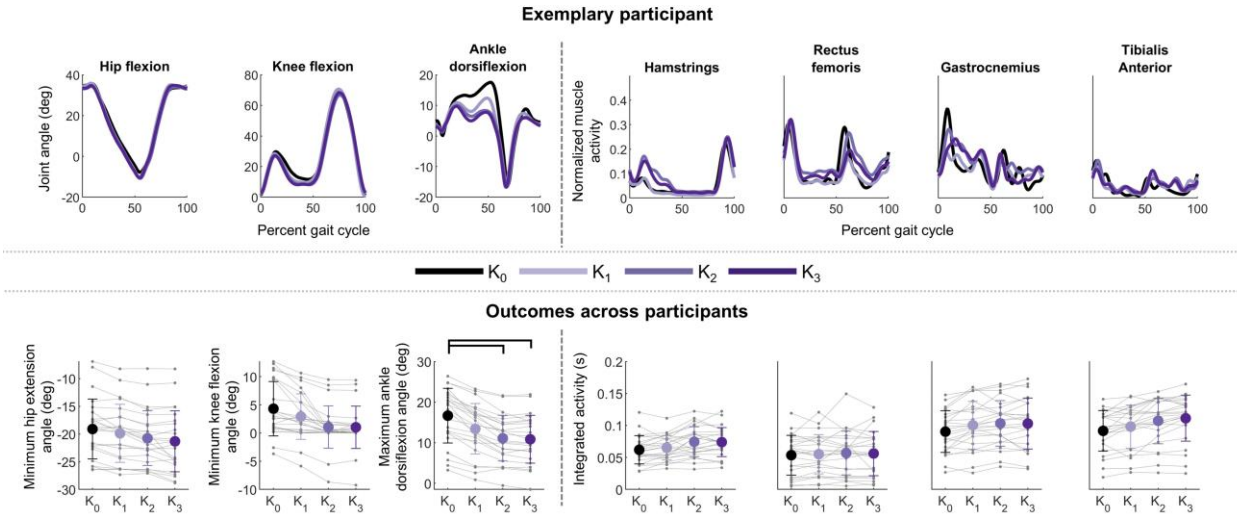

Figure 4.3. Top: Average kinematic (left) and EMG (right) data for one participant who exhibited large, repeatable responses to exoskeleton torque and high model prediction accuracies (P03). Black lines show the zero-torque condition (K_0) that was subtracted from all conditions to reflect responses to exoskeleton torque. Bottom: Average (±1SD) kinematic and myoelectric responses for all participants in each torque condition. Brackets denote significant differences between exoskeleton conditions according to post-hoc paired t-tests ($\alpha = 0.05$) and a Holm-Sidak step-down correction. Thin gray lines represent individual legs.

When validating on the held-out K_2 condition, all three models predicted kinematic but not myoelectric responses to exoskeleton torque (Figure 4.4, dashed lines). At a prediction horizon of $\Delta = 12.5\%$ of a stride, the LPV model's prediction accuracy at the ankle – where the largest responses to torque were observed – was 41.6 ± 16.0% more accurate than the PV model ($p < 0.001$) but not the NPV model ($p = 0.130$; Figure 4.5; Table 4.3). Similarly, the LPV model's prediction accuracy at the hip was 41.7 ± 12.7% better than the PV model ($p < 0.001$). However, as prediction horizon increased, the average LPV and NPV model prediction accuracies of all

outputs except the ankle approached those of the PV model. Changes in knee and hip kinematics were predicted more accurately than the baseline PV model for prediction horizons shorter than Δ = 18.75% of a stride ($p < 0.001$) in the LPV model and Δ = 12.5% of a stride ($p < 0.001$) in the NPV model (Figure 4.6). At the ankle, the LPV model predicted kinematics 29.1–60.0% more accurately than the PV model for all prediction horizons ($p < 0.001$). The NPV model's predictions were significantly more accurate than those of the PV model for all prediction horizons except 25.0% and 75.5–81.3% of a stride ($p < 0.001$).

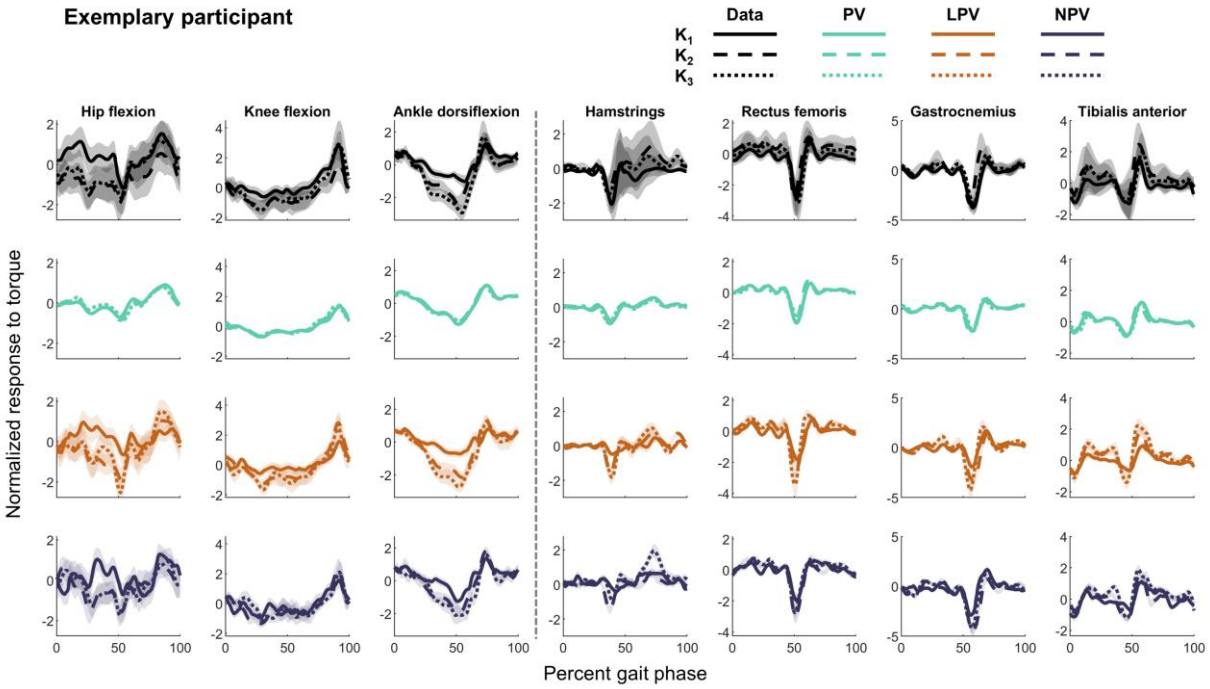

Figure 4.4. Kinematic and myoelectric experimental (black) and predicted (colors) responses to torque for one participant who exhibited large responses to the exoskeletons (P03). Predictions are shown for a prediction horizon of 12.5% of a stride for the PV (green), LPV (orange), and NPV (purple) models. The three held-out conditions are denoted with solid (K_1), dashed (K_2), and dotted (K_3) lines. Lines represent the average (±1SD; shaded region) data and predictions over all gait cycles in the corresponding validation dataset. The experimental data show that the K_2 and K_3 responses to torque were more similar to each other than to the K_1 response. The PV model predictions were similar across held-out conditions, while the LPV and NPV models scaled with exoskeleton torque. Full joint trajectories may be reproduced by rescaling and adding the average unperturbed gait cycle to the predictions. All comparisons used paired t-tests ($\alpha = 0.05$) with a Holm-Sidak step-down correction for multiple comparisons.

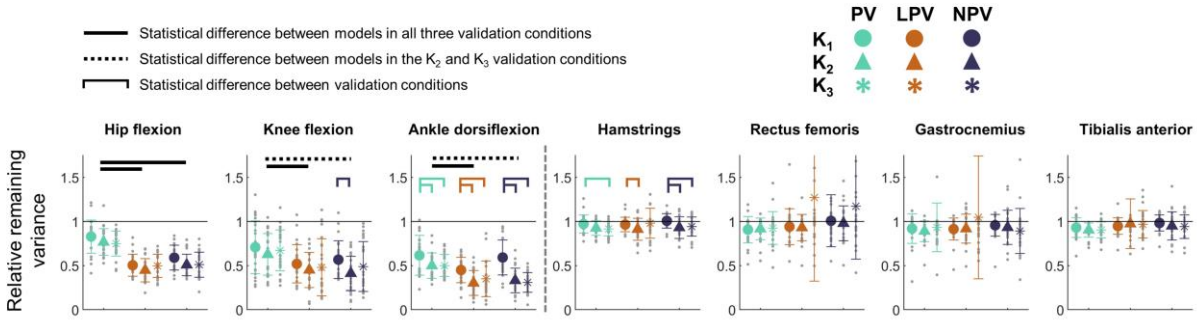

Figure 4.5. Average (±1SD) prediction accuracies for all participants and held-out conditions at a prediction horizon of 12.5% of a stride. Gray dots represent individual legs. Colored brackets denote statistically significant differences between held-out conditions for each model. Black horizontal bars denote significant differences between models across all three (solid) or two (dashed) held-out conditions. The large variance in the LPV model's predictions of rectus femoris and gastrocnemius responses in the held-out K_3 condition were due to bad predictions (RRV > 2) in a small number of legs. All comparisons used paired t-tests ($\alpha = 0.05$) with a Holm-Sidak step-down correction for multiple comparisons.

Predictions of myoelectric responses were poor (RRV ≈ 1.00) across all muscles and models, except at the shortest prediction horizon ($\Delta = 6.25\%$). At the shortest prediction horizon, both the LPV and NPV models' predictions for the hamstrings, rectus femoris, and gastrocnemius were 10.7–15.0% more accurate than those of the PV model ($p < 0.001$; Figure 4.6).

TABLE 4.3. AVERAGE (± 1SD) RRV VALUES FOR KINEMATIC AND MYOELECTRIC PREDICTIONS AT A 12.5% PREDICTION HORIZON.

Output	PV	LPV	NPV
Ankle angle†‡	0.50 ± 0.14	0.30 ± 0.14	0.33 ± 0.14
Knee angle†‡	0.62 ± 0.24	0.45 ± 0.20	0.41 ± 0.19
Hip angle†‡	0.77 ± 0.15	0.44 ± 0.13	0.51 ± 0.12
Tibialis anterior	0.90 ± 0.08	0.97 ± 0.28	0.95 ± 0.15
Soleus	0.86 ± 0.21	1.02 ± 0.66	1.04 ± 0.64
Gastrocnemius	0.89 ± 0.12	0.91 ± 0.16	0.93 ± 0.19
Vastus medialis	0.92 ± 0.12	0.93 ± 0.15	0.98 ± 0.20
Rectus femoris	0.87 ± 0.21	0.91 ± 0.38	0.94 ± 0.42
Lateral hamstrings	0.93 ± 0.08	0.91 ± 0.13	0.93 ± 0.12
Gluteus medius	0.95 ± 0.08	0.96 ± 0.10	0.98 ± 0.10

LPV = Linear phase-varying model; NPV = Nonlinear phase-varying model; PV = Phase-varying model

† Significant difference in prediction accuracy between the PV and LPV models

‡ Significant difference in prediction accuracy between the PV and NPV models

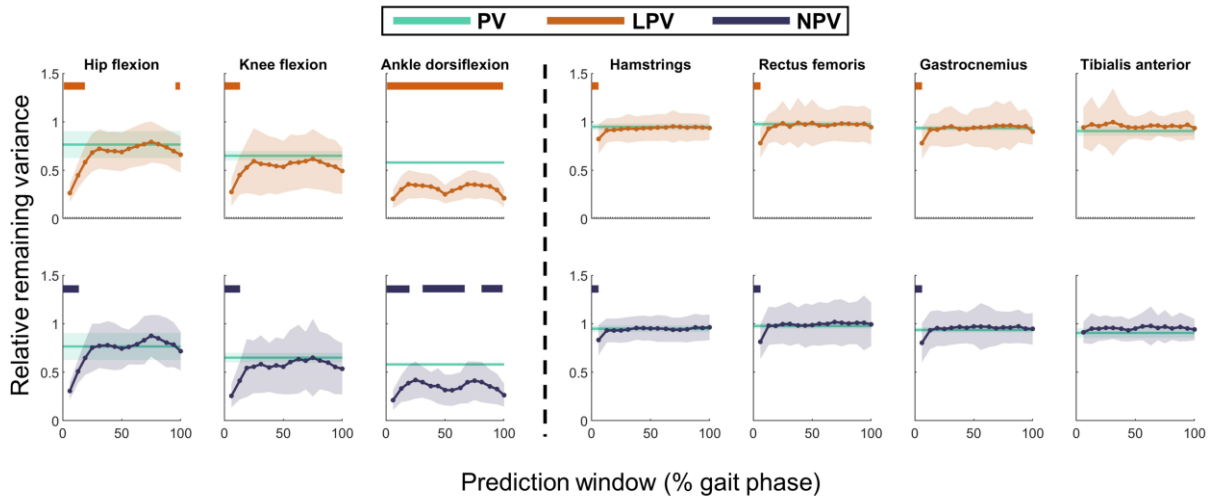

Figure 4.6. Prediction accuracy decreased with increasing prediction horizon. The PV model's predictions (green) were constant across prediction horizons. Horizontal bars denote predictions that were significantly more accurate than the PV model. The LPV (top; orange) and NPV (bottom; purple) models' prediction accuracies approached nearly constant values for prediction horizons beyond 25.0% of a stride for kinematic responses and 6.25% of a stride for myoelectric responses. The LPV and NPV models' predictions of ankle kinematics remained more accurate

than PV model predictions across almost all prediction horizons, while knee and hip kinematic predictions were similar to those of the PV model beyond 25.0% of a stride.

The LPV and NPV models' prediction accuracies improved with increasing training set size. As expected, the PV model's prediction accuracy was nearly constant across training set sizes ($p > 0.005$; Figure 4.7). For a prediction horizon of $\Delta = 12.5\%$ of a stride, the LPV model's hip (RRV = 0.81) and knee (RRV = 0.78) prediction accuracies were significantly worse than RRV_{full} when using less than 50 strides of training data per exoskeleton condition ($p < 0.001$). Similarly, the NPV model's hip and knee prediction accuracies approached RRV_{full} with approximately 50 strides of training data per condition ($p < 0.001$). The LPV model required more data – up to 150 strides per condition – for prediction accuracies to approach RRV_{full} at the ankle, gastrocnemius, and tibialis anterior ($p < 0.001$), though predictions were only 0.02–0.05 RRV points greater than RRV_{full} with 75 strides of training data per condition. The NPV model's myoelectric prediction accuracies approached RRV_{full}, in 25–75 strides of training data per condition ($p < 0.001$; Figure 4.7).

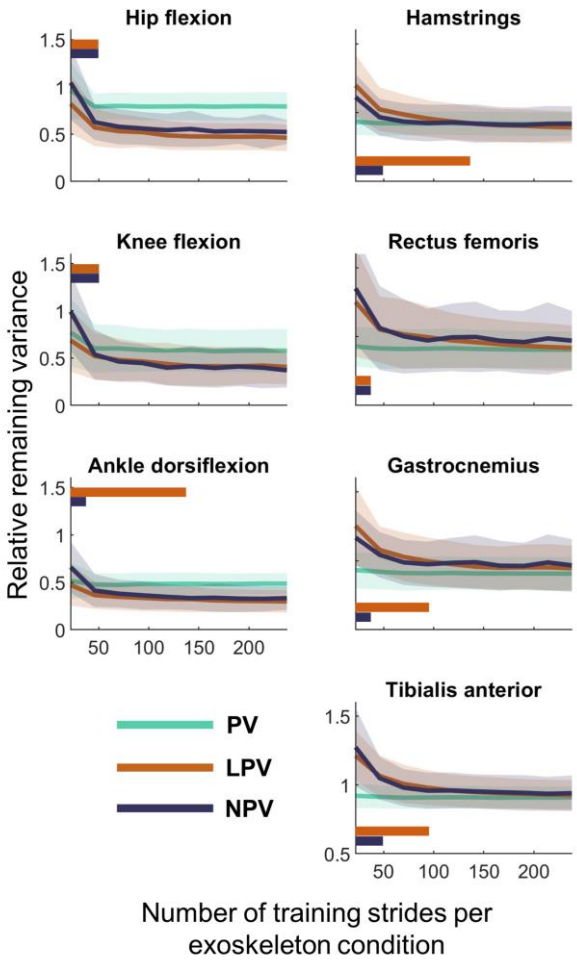

Figure 4.7. Average (±1SD; shaded region) prediction accuracy of kinematic (left) and myoelectric (right) outputs for the PV (green), LPV (orange), and NPV (purple) models over training set sizes ranging from 24 to 240 cycles (RRV_{full}). Prediction accuracies were reported at a 12.5% stride prediction horizon. Orange (LPV) and purple (NPV) horizontal bars denote the training set sizes that yielded significantly worse predictions than those of the full training set. The PV model's prediction accuracies were not significantly different from RRV_{full} at any training set size.

When validating on the held-out K_1, K_2, and K_3 conditions, the LPV and NPV model predictions reflected experimental changes in response between conditions (Figure 4.4). For all models at a 12.5% stride prediction horizon, predictions of responses in the held-out K_1 condition (interpolation) were 0.10–0.28 RRV points at the ankle and 0.04–0.09 points in the hamstrings less accurate than predictions of the K_2 or K_3 datasets ($p < 0.001$). Conversely, no statistical differences in prediction accuracies of the held-out K_2 (interpolation) and K_3 (extrapolation) conditions were

identified (Figure 4.5). Improvements in kinematic prediction accuracy of the LPV model compared to the PV model were identified across the held-out K_1, K_2, and K_3 conditions ($p < 0.001$). Differences between the NPV and PV models' kinematic prediction accuracies in the held-out K_1 condition did not reach significance at the knee or ankle.

4.5 DISCUSSION

We evaluated the ability of subject-specific phase-varying models to predict kinematic and myoelectric responses to ankle exoskeleton torques during treadmill walking. When predicting across three exoskeleton torque conditions, both linear and nonlinear models predicted kinematic responses to exoskeletons without knowledge of the specific user's physiological characteristics, supporting their potential utility as predictive tools for exoskeleton design and control. To our knowledge, this is the first study to predict kinematic and myoelectric responses to ankle exoskeletons using phase-varying models. Consistent with Floquet Theory and prior models of human locomotion, LPV models appear appropriate for predicting responses to exoskeleton torque over short prediction horizons, evidenced by its similar prediction accuracy to the more complex NPV model and improved prediction accuracy over the less complex PV model [27, 79, 80, 94].

The small and variable responses to exoskeleton torque exhibited by the unimpaired adults in this work highlight the challenge of altering kinematics with passive ankle exoskeletons. We found that even stiff exoskeletons (K_3 = 5.08 Nm/deg) only altered ankle kinematics on average by six degrees and integrated muscle activity by 14%. These small changes may correspond to larger changes in joint powers or metabolic demands and indicate that the present study is a rigorous test case [9, 18, 29, 143]. Despite small changes in gait, the LPV model's predictions explained more

of the variance in kinematic responses to exoskeletons than the PV model, regardless of whether predictions interpolated (K_1 and K_2) or extrapolated (K_3) relative to the training set. The LPV model's ability to predict kinematics within and slightly beyond the available training data supports its potential utility for predicting responses to untested exoskeleton designs or control laws. However, predictions of the held-out K_1 condition highlight the importance of selecting experimental conditions that encode complex responses to torque.

Our hypothesis that the LPV model would predict kinematic and myoelectric responses more accurately than the PV model and as accurately as the NPV model was partially supported. The LPV model's kinematic and myoelectric predictions were more accurate than those of the PV model only for prediction horizons less than 18.75% and 6.25% of a stride, respectively, but the LPV and NPV models exhibited similar prediction accuracies across prediction horizons. The LPV and NPV models' similar predictions support research demonstrating that nonlinear spring-loaded inverted pendula (SLIPs) have similar predictive accuracy to linear models of human movement [27]. Compared to a nonlinear SLIP, the NPV model's feedforward neural network imposed fewer restrictions on model structure and enabling greater differences in prediction accuracy compared to a linear model. Therefore, the similarity of LPV and NPV model predictions supports the extension of Floquet Theory to gait with exoskeletons and indicates that, for rhythmic locomotion at a constant speed over level ground, linear phase-varying models have sufficiently complex structure to predict kinematic responses to exoskeletons [27, 79, 80, 94].

We observed comparable kinematic prediction accuracy to studies using physics-based and data-driven models of locomotion. Maus et al. evaluated multiple models' abilities to predict center-of-

mass height during running and reported accuracies ranging from RRV ≈ 0.15 at a 15% prediction horizon to RRV ≈ 0.85 beyond an 80% stride prediction horizon, for an exemplary participant [27]. Within a similar range of prediction horizons, the LPV model predicted kinematics across participants with average accuracies ranging from ($0.30 < RRV < 0.45$) at a 12.5% prediction horizon and ($0.34 < RRV < 0.77$) at an 81.3% prediction horizon. Similarly, Drnach et al. [95] used a hybrid linear model to predict response to functional electrical stimulation, reporting median RRV values (transformed from a fitness score) ranging from approximately 0.11-1.04. However, the average unperturbed gait cycle was not subtracted from the data before computing the fitness score in [95]. The average unperturbed cycle accounts for a substantial portion of the variance in the perturbed signals, providing a less conservative prediction accuracy statistic than the RRV presented here. For example, if the unperturbed cycle had not been subtracted from the data in the present study, the LPV model's ankle predictions for one participant who exhibited large responses to torque would be RRV = 0.08 rather than the more conservative 0.21 reported. Comparable prediction accuracies to prior work indicate that phase-varying models are potentially useful predictive tools for locomotion with ankle exoskeletons and may have similar predictive power to physics-based models of locomotion.

The convergence of LPV and NPV models' prediction accuracies to an approximately constant value at large prediction horizons (*e.g.* $RRV_{LPV} \approx 0.70$ for knee kinematics at $\Delta > 25.0\%$ of a stride) may be useful when selecting measurements for device design or control. The LPV and NPV models' kinematic prediction accuracies decreased rapidly from 6.25% to 18.75% stride prediction horizons, before reaching an approximately constant value. Ankle predictions remained better than those of the PV model across prediction horizons. Higher prediction accuracy at the

ankle was unsurprising due to large responses to exoskeletons and the ankle's direct piecewise-linear relationship to passive exoskeleton torque. Since we trained on multiple exoskeleton conditions, the dynamics predicting future ankle kinematics are higher-dimensional than the simple exoskeleton torque-ankle angle relationship, suggesting that accurate predictions of ankle kinematics over large prediction horizons are likely for powered exoskeletons as well. Unlike the ankle, hip and knee kinematics were indirectly impacted by exoskeleton torque and their RRV values approached those of the PV model for prediction horizons above 18.75% of a stride. This result indicates that stride-specific initial posture and exoskeleton torque were predictive of indirect exoskeleton impacts on kinematics only for short prediction horizons. At large prediction horizons, measurements at an initial phase did not, on average, improve predictions of future posture. However, some participants' hip and knee kinematics were predicted up to 0.30 RRV points more accurately by the LPV and NPV models than the PV model across prediction horizons, suggesting that the prediction horizon at which stride-specific measurements no longer improve predicted responses to exoskeletons depends on the magnitude of the individual's response. The LPV and NPV models' accurate predictions over short prediction horizons make them primarily useful for exoskeleton control [16, 139]. For individuals that exhibit large responses to exoskeletons, however, LPV model-based predictions over stance may inform passive exoskeleton parameter selection. Guided adaptation and extended practice sessions [9, 141] or powered ankle exoskeletons [18, 19] may elicit larger responses than those observed in this study and increase the maximum prediction horizons at which measurements at an initial posture improve predicted responses to torque, potentially expanding the settings in which model predictions are useful.

A major limitation of all three models was their inability to predict myoelectric responses. The LPV and NPV models predicted myoelectric signals more accurately than the PV model only for the shortest prediction horizon ($\Delta = 6.25\%$). While exoskeleton torque and stiffness are known to impact average plantarflexor activity, we found that the average unperturbed gait cycle accounted for only 30-60% of the variance in the K_2 data, compared to 60-95% in kinematic signals [9, 38, 45]. Consequently, poor prediction accuracy may be partially attributed to small changes in muscle activity between the exoskeleton conditions. Alternatively, kinematic and myoelectric input variables may fail to encode nonlinear musculotendon dynamics, which are impacted by ankle exoskeletons, between the initial and final phases [37, 153]. Studies predicting muscle activity using physiologically-detailed models accounted for 60-99% of the variance in myoelectric signals, though they evaluated predictions on unperturbed walking conditions only [76, 156]. Still, the difference in prediction accuracy between the phase-varying models and physiologically-detailed models indicates that encoding musculotendon dynamics in the input variables is likely needed to improve myoelectric predictions for data-driven phase-varying models and represents an interesting area of future research.

Another limitation of subject-specific data-driven models, compared to physiologically-detailed models, is the amount of training data required to predict changes in gait with exoskeletons, which impacts models' utility in settings where minimizing data collection duration is critical to mitigating physical and logistical burdens on participants and families, such as in clinical gait laboratories. Improvements in prediction accuracy of the LPV and NPV models were small beyond 75–100 strides of training data per exoskeleton condition. The LPV model required more training data at the ankle, but a similar amount at the hip and knee to that used by Drnach et al., who trained

a hybrid linear model using 45 seconds of data across two experimental conditions [95]. For unimpaired, steady-state locomotion, data-driven linear models appear to require 75–125 strides of training data per condition, which supports their feasibility only in gait analysis settings with treadmills or long walkways [19, 138]. Additional dimensionality reduction, such as via sparse regression, may reduce the LPV model's complexity and demand for training data [27, 97, 157]. However, when only one training condition or a few strides are collected, as is standard in clinical gait analysis, phase-varying model predictions will be poor and physiologically-detailed or population-specific models may generate more accurate predictions [22, 26, 76, 156].

Subject-specific data-driven phase-varying models of gait with exoskeletons have benefits and limitations compared to predictive musculoskeletal models. While we investigated only a specific subset of phase-varying models, we showed that this class of model can predict kinematic responses to exoskeletons without detailed knowledge of the physiological and neuromuscular factors influencing responses to exoskeletons. Conversely, uncertainty in the mechanisms driving complex responses to exoskeletons may limit physiologically-detailed models' accuracy [4, 143]. While predictive musculoskeletal models may generate "what-if" predictions without experimental data, data may be needed to specify initial postures and tune subject-specific parameters. Phase-varying models can similarly perform subject-specific "what-if" predictions when application-specific training data are available. Unlike physiologically-detail models, this and prior work exemplify phase-varying models' ability to take arbitrary measurements as inputs, enabling their application using a range of experimental resources [27, 79, 97]. Extending data-driven predictions to "what-if" scenarios and improving predicted myoelectric responses to exoskeletons, combined with analytical tools for phase-varying systems(*e.g.* [97]), may facilitate

prediction and analysis of individualized exoskeleton impacts on gait mechanics and motor control.

4.6 CONCLUSIONS

To our knowledge, this is the first study to predict subject-specific responses to ankle exoskeletons using phase-varying models. Without making assumptions about individual physiology or motor control, an LPV model predicted short-time kinematic responses to bilateral passive ankle exoskeletons, though predicting myoelectric responses remains challenging. Results support the utility of LPV models for studying and predicting response to exoskeleton torque. Improving data-driven models and experimental protocols to study and predict myoelectric responses to exoskeletons represents an important direction for future research. Modeling responses to exoskeletons or other assistive devices using a phase-varying perspective has the potential to inform exoskeleton design for a range of user groups.

Chapter 5. QUANTIFYING TEMPLATE SIGNATURES OF CENTER-OF-MASS MOTION DURING WALKING WITH ANKLE EXOSKELETONS

In preparation

Michael C. Rosenberg

Joshua L. Proctor

Katherine M. Steele

ABSTRACT

Ankle exoskeletons are used to assist walking and improve gait mechanics. However, interindividual differences in physiology and motor control make predicting subject-specific changes in gait with ankle exoskeletons challenging, limiting device efficacy across individuals with diverse physiology. Understanding and predicting variable responses to ankle exoskeletons may first require understanding how task-level variables, such as whole-limb control of center-of-mass (COM) motion changes with exoskeletons. We evaluated the subject-specific impacts of ankle exoskeletons on whole-limb (COM) control in unimpaired adults and one stroke survivor with hemiparesis while walking in shoes-only and with passive ankle exoskeletons. We used a novel data-driven modeling algorithm, Hybrid-SINDy, to select from a library of candidate mechanisms those that best encoded each individual's COM accelerations. Consistent with literature on the dynamics of walking, Hybrid-SINDy selected spring-loaded inverted pendulum mechanisms (leg stiffness and leg length) throughout stance in all participants, while sagittal- and frontal-plane rotary stiffness mechanisms were selected in 40-50% of participants. In unimpaired adults, template signatures did not change with the addition of the exoskeleton ($p > 0.13$). Conversely, in our stroke participant, paretic leg stiffness increased by 11% with the addition of the exoskeleton frame, while both paretic and non-paretic limb rotary stiffness increased by 11% with the addition of exoskeleton stiffness. These results suggest that unimpaired individuals maintain whole-limb COM dynamics when walking with passive ankle exoskeletons, while individuals with motor impairments may alter COM dynamics to maintain stable or efficient gait. Further, we showed that common reduced-order representations of walking dynamics may be constructed from data using a library of candidate mechanisms, which may accelerate the rate of discovery of mechanisms driving diverse responses to ankle exoskeletons.

5.1 INTRODUCTION

Ankle exoskeletons are prescribed and designed to improve walking function and gait mechanics, with individuals with cerebral palsy and stroke being the most common ankle exoskeleton users [4, 20, 29]. While commonly prescribed ankle exoskeletons are passive devices, customized powered ankle exoskeletons have recently shown promise to further improve walking function and muscle coordination in both unimpaired adults and individuals with motor impairments [9, 12, 17, 19, 20, 55]. However, changes in gait in response to ankle exoskeletons are highly variable, especially for individuals with motor impairments, making customization critical to improving device efficacy. For example, ankle exoskeletons have highly variable impacts on gait mechanics, walking speed, step length, and the energetic cost of walking in adults post-stroke and children with cerebral palsy [4, 20, 29, 55]. Understanding the mechanisms that drive variable responses to ankle exoskeletons may enable clinicians and designers to personalize exoskeletons without requiring extensive experimental tuning.

Variable responses to ankle exoskeletons may stem form inter-individual differences in musculoskeletal physiology and motor control [4, 20, 22, 24, 64]. Human gait is the product of high-dimensional, nonlinear interactions between the neural and biomechanical systems. Small differences in physiology or control may have large impacts on baseline gait and exoskeleton responses [158]. These complex interactions make identifying the mechanisms driving an individual's response to exoskeletons particularly challenging. For example, Ries and colleagues (2014) used a Random Forest algorithm to predict changes in gait kinematics with passive ankle exoskeletons using kinematic and clinical exam measurements from over 300 children with cerebral palsy [26]. Despite the large dataset, the algorithm explained only 19-28% of the variance in kinematic responses to exoskeletons. Not only does significant variance remain unexplained by these models, but the specific gait features that may predict or dictate an individual's response remains unclear.

Recent advances in computing power and neuromusculoskeletal simulation has enabled investigations into mechanisms driving exoskeleton responses [25, 37, 140, 143] and altered gait patterns following neurological injury [22, 83]. For example, musculotendon fascicle length and Achilles tendon compliance have been shown to impact energetic responses to powered [143] and passive [37] ankle exoskeletons. While this approach shows promise in identifying mechanisms driving exoskeleton responses, neuromusculoskeletal models must be extensively tuned to encode the unique physiology of individuals with motor impairments [22, 86, 159]. Due to these models' complexity, similar solutions may be achieved using different model properties, especially for a single walking condition [158]. Consequently, identifying mechanisms driving exoskeleton responses may benefit from first understanding how the parameters of less complex models impact exoskeleton responses.

A potential solution to this challenge may be found in early models of locomotion. These models focused on how task-level goals, such as moving the center-of-mass (COM) stably and efficiently, are achieved during locomotion [72, 75, 160-162]. By ignoring physiological detail, this approach enables the investigation of fundamental characteristics of human gait despite uncertainty in the biological mechanisms describing COM accelerations. For example, modeling the leg as an inverted pendulum during stance has been widely used to describe and study COM motion and energetics during walking [71, 87, 161]. Contemporary musculoskeletal models used to study the function of biological mechanisms emerged from these simple mechanical representations of gait.

To study locomotion at the task level, Full & Kodistchek (1999) proposed the notion of using *template* models of locomotion to quantify strategies employed to achieve task-level goals, such as controlling the COM during walking [33]. The authors suggested that template models could provide a foundation upon which physiological detail may be added to study specific biological mechanisms impacting gait. Templates models satisfy task objectives by applying forces on the COM using lumped-parameter mechanisms, which often span the entire leg [32, 33, 74, 160, 162-165]. Each mechanism within a template, therefore, encodes a hypothesis about how neural and biomechanical subsystems interact to achieve task-level objectives, such as using leg spring mechanisms to encode whole-limb strategies for achieving the double-hump ground reaction forces (GRFs) during walking [76]. Consequently, the dynamics describing whole-limb control of COM motion may be characterized by two main features of a template model's dynamics:

1. *Template structure* defines mechanisms that are critical to capturing the magnitude and timing of COM accelerations.
2. *Template parameters* describe how mechanisms are regulated to accelerate the COM.

Template models' structure and parameters during walking have provided numerous influential insights into strategies to control the COM. For example, simple inverted pendulum templates with rigid legs have been used to study COM energetics and the transition from walking to running [74, 160], as well as strategies for energetically-efficient COM accelerations [59, 87, 166] and lateral stabilization [162, 167]. Alternative template structures, such as the bipedal spring-loaded inverted pendulum (SLIP) and its variants have been used to improve predictions of GRFs in the sagittal plane and study COM stabilization strategies across different speeds [32, 164, 165, 168]. Extensions of the bipedal inverted pendulum and SLIP templates include additional leg damping

elements, rotary springs, or curved feet and have been used to study quantify differences in COM dynamics in individuals with motor impairments [88, 163, 169, 170]. Additionally, template models have shown that whole-limb contributions to COM motion may be altered following neurological injury, which may be described by changes in both template structure and parameters [88, 169]. Therefore, template structure and parameters may be individualized. To emphasize the subject-specific nature of template dynamics, we denote an individual's unique template structure and parameters as their *template signature*.

Understanding how whole-limb COM dynamics – described by template signatures – change with exoskeletons may provide targets for future investigations into biological mechanisms driving exoskeleton responses. To our knowledge, template signatures have never been used to study changes in whole-limb dynamics in response to ankle exoskeletons or other assistive devices. Consequently, our ability to select mechanisms to include in the signatures based on prior literature is limited. Further, heterogeneous responses to exoskeletons in individuals with motor impairments suggests that template signature structures and their changes with exoskeletons may not be fixed across individuals.

Recent advances in data-driven modeling and machine learning have introduced new algorithms to flexibly identify and select dynamics from data in rhythmic systems [23, 93, 157]. **Hybrid-SINDy** (*SINDy: Sparse identification of nonlinear dynamics*; [157]) is a germane approach for identifying template signatures in that the algorithm identifies sparse, nonlinear dynamics in hybrid systems from time-series data [23]. Importantly, Hybrid-SINDy identifies a large number of candidate dynamical models (e.g. template signatures) from an arbitrary library of possible mechanisms. The algorithm then uses information criteria to provide levels of support for each

candidate model and selects models that are both sparse and highly representative of the system [171].

The purpose of this study was to identify changes in whole-limb COM dynamics in response to ankle exoskeletons and evaluate the how neurological injuries may alter whole-limb dynamics in response to exoskeletons. We used the Hybrid-SINDy algorithm to identify template signatures explaining COM accelerations during walking in unimpaired adults and how those signatures changed with hinged and stiff ankle exoskeletons. We hypothesized that ankle exoskeletons would primarily increase limb stiffness. Additionally, to examine the potential of template signatures to encode changes in COM dynamics in response to ankle exoskeletons in individuals with neurological injuries, we present a case study comparing the template signatures in an individual with post-stroke hemiparesis. To our knowledge, this work is the first to employ physics-informed data-driven modeling techniques to select low-dimensional, interpretable, representations of whole-limb COM dynamics with ankle exoskeletons.

5.2 METHODS

5.2.1 *Data collection*

We collected data from twelve unimpaired adults (6M/6F; age = 23.9 ± 1.8 years; height = 1.69 ± 0.10 m; mass = 66.5 ± 11.7 kg) and one stroke survivor with lower-limb hemiparesis (sex not disclosed; age = 24; height = 1.70 m; mass = 68.0 kg). Participants walked on an instrumented split-belt treadmill (Bertec Corp., Columbus, USA) in shoes-only and with bilateral passive ankle exoskeletons that resisted ankle dorsiflexion (Figure 5.1). A detailed description of the experimental protocol and data preprocessing can be found in [172]. Briefly, participants

completed a practice session consisting of 30 minutes of walking with the exoskeletons and selected their preferred walking speed. Data were collected in a follow-up visit, during which participants walked at their self-selected speed for six minutes per condition, the last four of which were recorded. To mitigate fatigue, the stroke participant walked under the same protocol, but for only four minutes per condition, the last three of which were recorded.

We collected kinematic marker trajectories using retroreflective markers and a ten-camera motion capture system (Qualisys AB, Gothenburg, SE) and recorded ground reaction forces (GRFs). We preprocessed kinematic and kinetic data, and estimated body segment kinematics using OpenSim 3.3 [70, 148]. We used OpenSim's *Body Kinematics* algorithm to estimate the COM and foot positions in the for three conditions: walking in shoes-only, zero stiffness (K_0) exoskeletons, and high stiffness (K_H = 5.1 Nm/deg) exoskeletons. This study was approved by the University of Washington Institutional Review Board (#47744) and all participants provided informed consent prior to the training session.

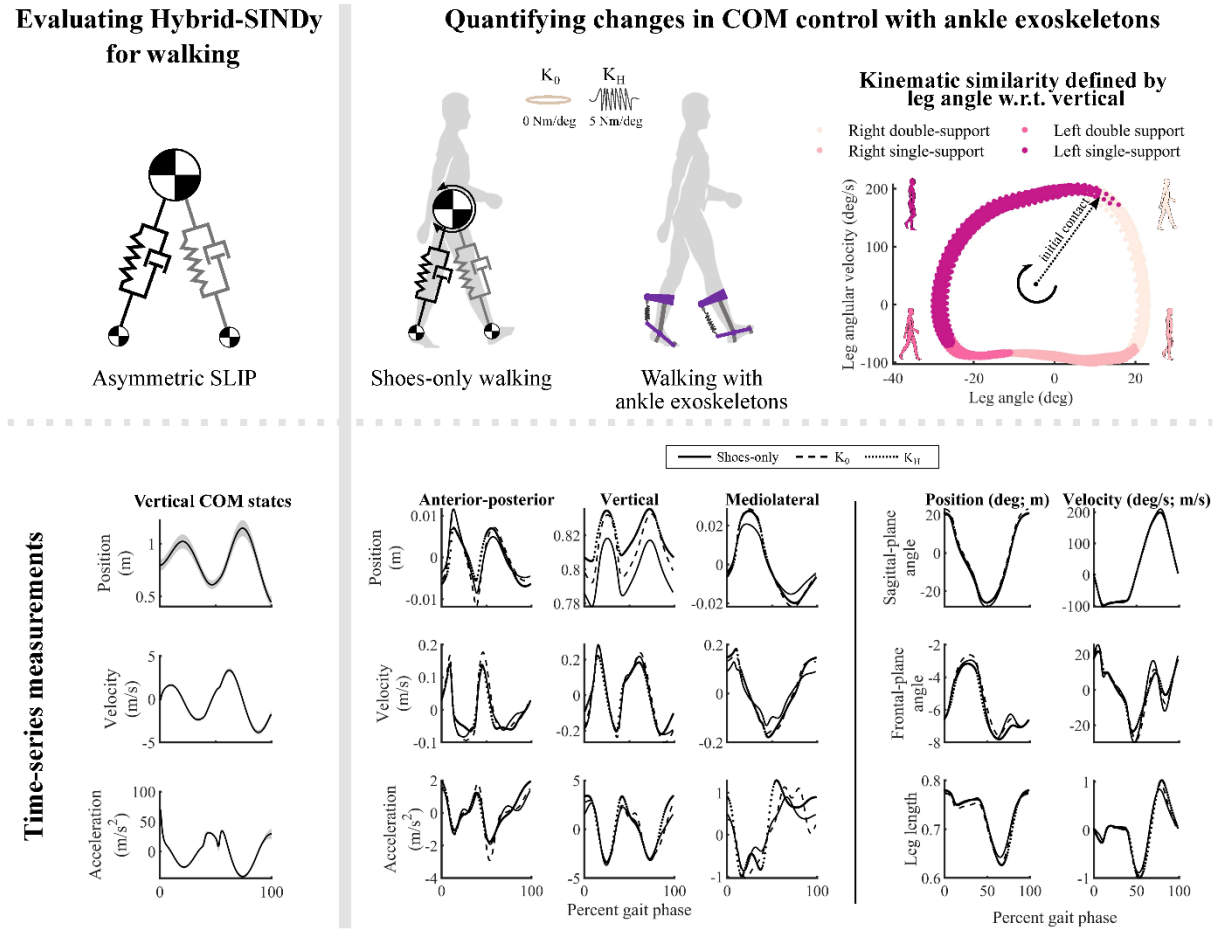

Figure 5.1. Top: Two-dimensional depictions of the simulated SLIP (left) and human walking conditions (right). The simulated SLIP had leg springs and dampers, as well as foot masses. Participants walked on a treadmill in shoes-only and in ankle exoskeletons under zero-stiffness (K_0) and high-stiffness (K_H) conditions. The pink phase portrait shows the leg angle and angular velocity relative to vertical, which was used as a phase variable to cluster kinematically-similar measurements. Colors denote gait phases corresponding to the four foot-contact configurations: first and second double-limb support, single-limb support, and swing. Bottom: Time-series measurements of COM position, velocity, and acceleration for the simulated SLIP (left) and an exemplary unimpaired adult participant (right). For the simulated SLIP, the shaded regions show ±1SD over the stride. For human walking, 3D COM states (middle) and leg states (right) are shown for the three exoskeleton conditions: shoes-only walking (solid lines), zero-stiffness exoskeleton walking (K_0; dashed lines), and high-stiffness exoskeleton walking (K_H; dotted lines). The leg length and velocity, and sagittal- and frontal-plane leg angles determined leg forcing, while COM position and leg length determined the direction of forcing.

5.2.2 *Estimating template signatures with Hybrid-SINDy*

To identify mechanisms describing COM acceleration, we used the Hybrid-SINDy algorithm to identify template signatures with and without ankle exoskeletons. In this section, we briefly describe the SINDy and Hybrid-SINDy algorithms in the context template signatures. We refer the readers to [157] and [23] for detailed descriptions of these algorithms. Consider the continuous-time system with *n*=3 outputs:

$$\frac{d^2}{dt^2}\boldsymbol{q}(t) = \ddot{\boldsymbol{q}}(t) = f\big(\boldsymbol{q}(t), \dot{\boldsymbol{q}}(t)\big), \tag{5.1}$$

$$\boldsymbol{q}(t) = [\boldsymbol{x}(t) \quad \boldsymbol{y}(t) \quad \boldsymbol{z}(t)],$$

where time is denoted by $t \in \mathbb{R}^{m\times 1}$, and $q(t)$ and $\dot{q}(t)$ represent COM positions and velocities relative to the feet in $\mathbb{R}^{m\times n}$, respectively, in the anterior-posterior (x), vertical (y), and mediolateral (z) directions. The system dynamics are described by $f(q(t), \dot{q}(t))$ and predict COM accelerations, $\ddot{q}(t)$. We assume that only a small number of terms in $f(q(t), \dot{q}(t))$ describe most of the system's behavior. We omit the time notation in the remaining sections.

5.2.2.1 Sparse Identification of Nonlinear Dynamics (SINDy)

The SINDy algorithm ([157]) is a powerful system identification tool that recovers sparse nonlinear dynamics from a library of candidate dynamics terms. The dynamics library may consist arbitrary nonlinear functions the system measurements. Adopting the notation from [23], we can rewrite the dynamics in equation 5.1 as:

$$\ddot{\boldsymbol{q}} = \boldsymbol{\Theta}(\boldsymbol{q}, \dot{\boldsymbol{q}})\boldsymbol{\Xi}, \tag{5.2}$$

where $\boldsymbol{\Xi} \in \mathbb{R}^{p \times n}$, is a linear map from nonlinear transformations of system measurements, $\Theta(q, \dot{q})$, to COM accelerations, $\ddot{q}$. The function $\Theta \in \mathbb{R}^{m \times p}$ defines a library of dynamics terms encoding mechanisms that may describe COM accelerations. Therefore, the coefficients in $\boldsymbol{\Xi}$ represent template signatures parameters, while Θ encodes template signature structure. We included $p = 14$ terms in the function library, described in a later section. The SINDy algorithm promotes sparsity using sequential least-squares regression with hard thresholding, with the threshold defined by the sparsity parameter, λ (equation 5.3). This thresholding approach penalizes the zero-norm of Ξ and solves [23]:

$$\min_{\boldsymbol{\Xi}} || \boldsymbol{\Theta}(\boldsymbol{q}, \dot{\boldsymbol{q}})\boldsymbol{\Xi} - \ddot{\boldsymbol{q}}||_2 + \lambda \|\boldsymbol{\Xi}\|_0, \qquad 5.3$$

5.2.2.2 Hybrid-SINDy

Hybrid-SINDy extends SINDy in two important ways. First Hybrid-SINDy uses clustering of the training data to generalize SINDy to hybrid systems. Applying SINDy to clusters of walking data enables unique dynamics to be identified in each hybrid regime defined by contact configuration (*i.e.* single- and double-limb support) [34, 72, 74]. Second, Hybrid-SINDy identifies multiple sets of system dynamics of different sparsity by sweeping a range of sparsity thresholds (λ) and uses information theory to automatically select the dynamics that best describe the system. This technique enables competing hypotheses about which mechanisms in a template signature best describe COM acceleration to be rapidly and systematically compared. For example, Mangan and colleagues (2019) showed that Hybrid-SINDy correctly selected both compression and flight dynamics of a spring-mass hopper using a function library defined by a polynomial expansion of the mass position and velocity [23].

5.2.3 *Applying Hybrid-SINDy to walking*

We applied the Hybrid-SINDy algorithm to human gait using the following steps for each participant and walking condition (Figure 5.2). Note that we modified the Hybrid-SINDy algorithm to evaluate the ability to reconstruct COM accelerations, rather than positions or velocities, use fixed contact configuration-based hybrid regimes during model selection, and use multi-model inference to select a single template signature when multiple signatures represent the data similarly well (Step 5). Our algorithm used the following steps:

1. *Clustering*: For each sample in the training set, we created data clusters consisting of the 800 nearest neighbors to the samples and identified the centroid of each cluster. This cluster size spanned approximately 7.4% of a stride, shorter than double-limb support. We used the right leg angle and angular velocity with respect to vertical as our clustering parameters. These variables were selected as thigh kinematics have been previously used as a phase variable to identify similar lower-limb kinematic postures [149].
2. *Model estimation*: For each cluster, we used SINDy to estimate template signatures, mapping the function library, $\boldsymbol{\Theta}(\boldsymbol{q}, \dot{\boldsymbol{q}})$ to COM accelerations, $\ddot{q}$. We identified multiple signatures per cluster by sweeping 40 sparsity threshold values (λ), ranging from the largest to smallest coefficients in the full-dimensional template signature. Each signature within a cluster had unique dimensionality (*i.e.*, number of non-zero terms). Typically, only 5-15 unique signatures were identified per cluster.
3. *Model evaluation*: Using held-out data, we evaluated the ability of each template signature to reconstruct COM accelerations in the anterior-posterior, vertical, and mediolateral directions. We computed the average reconstruction error compared to the observations for 120 gait phases, ϕ, spanning 0-100% of a stride (equation 5.4).

$$\text{error}_{\phi} = |\boldsymbol{\Theta}(\boldsymbol{q}, \dot{\boldsymbol{q}})\boldsymbol{\Xi} - \ddot{\mathbf{q}}|_{\phi} \quad 5.4$$

4. *Model selection*: We selected template signatures based on two criteria: First, we discarded signatures that were identified in less than 1% of training clusters (36 clusters). Frequently identified template signatures are more likely to be robust to measurement noise or stride-to-stride variability, making them better representations of an individual's gait.

   Second, for each hybrid regime, we selected the frequently-occurring template signatures that had the highest likelihood of being the correct signature describing COM accelerations according to the Akaike Information Criterion (AIC) [171, 173]. The AIC is widely used to compare candidate hypotheses about a system – template signatures, in our case – according to their number of free parameters and log-likelihood [171]. The AIC favors parsimonious, but highly-representative dynamics, which is ideal for identifying simple mechanistic dynamics of gait, such as template signatures. Like Mangan and colleagues (2019), we used the AIC corrected for finite sample sizes (AICc) and compared signatures according to their relative AICc score ($\Delta_j = AICc_j - AICc_{min}$ for signature *j*) [23, 171]. The relative AICc score ensures that the best model, according to the AICc, has a score of $\Delta_j = 0$, and all other models have higher scores. Burnham and Anderson (2004) remarked that models with $\Delta_j \leq 2$ have substantial support, while $\Delta_j > 7$ have low support [171]. We adopted a more generous threshold of [23] and selected template signatures with $\Delta_j \leq 3$. We consider all signatures satisfying this criterion to be *plausible* template signatures for the participant and walking condition.

5. *Multi-model inference*: Unlike the spring-mass hopping model used in [23], we did not expect a single template signature to be selected as plausible in each hybrid regime for human walking. To construct a single template signature in each hybrid regime, we computed a weighted-average model using Akaike weights, ω_j, where j is the j^{th} plausible model in a hybrid regime [171]. Akaike weights are computed as

$$\omega_j = \frac{\exp\left(-\frac{\Delta_j}{2}\right)}{\sum_{r=1}^{R}\exp\left(-\frac{\Delta_r}{2}\right)}, \qquad 5.5$$

where $\exp\left(-\frac{\Delta_j}{2}\right)$ defines the likelihood of the j^{th} template signature given the observations [171]. Therefore, this approach weights each signature based on its likelihood relative to the other plausible signatures. This procedure produced four weighted average template signatures corresponding to right and left leg single- and double-limb support phases.

6. *Uncertainty estimation*: To evaluate the robustness of the final template signatures to noise and stride-to-stride variations in the data, we performed 200 bootstrapped estimates of template signatures parameters using the data in the corresponding hybrid regimes. The template signatures were characterized by the mean and standard deviation of the bootstrapped parameters. The template signatures from this step were used during analysis.

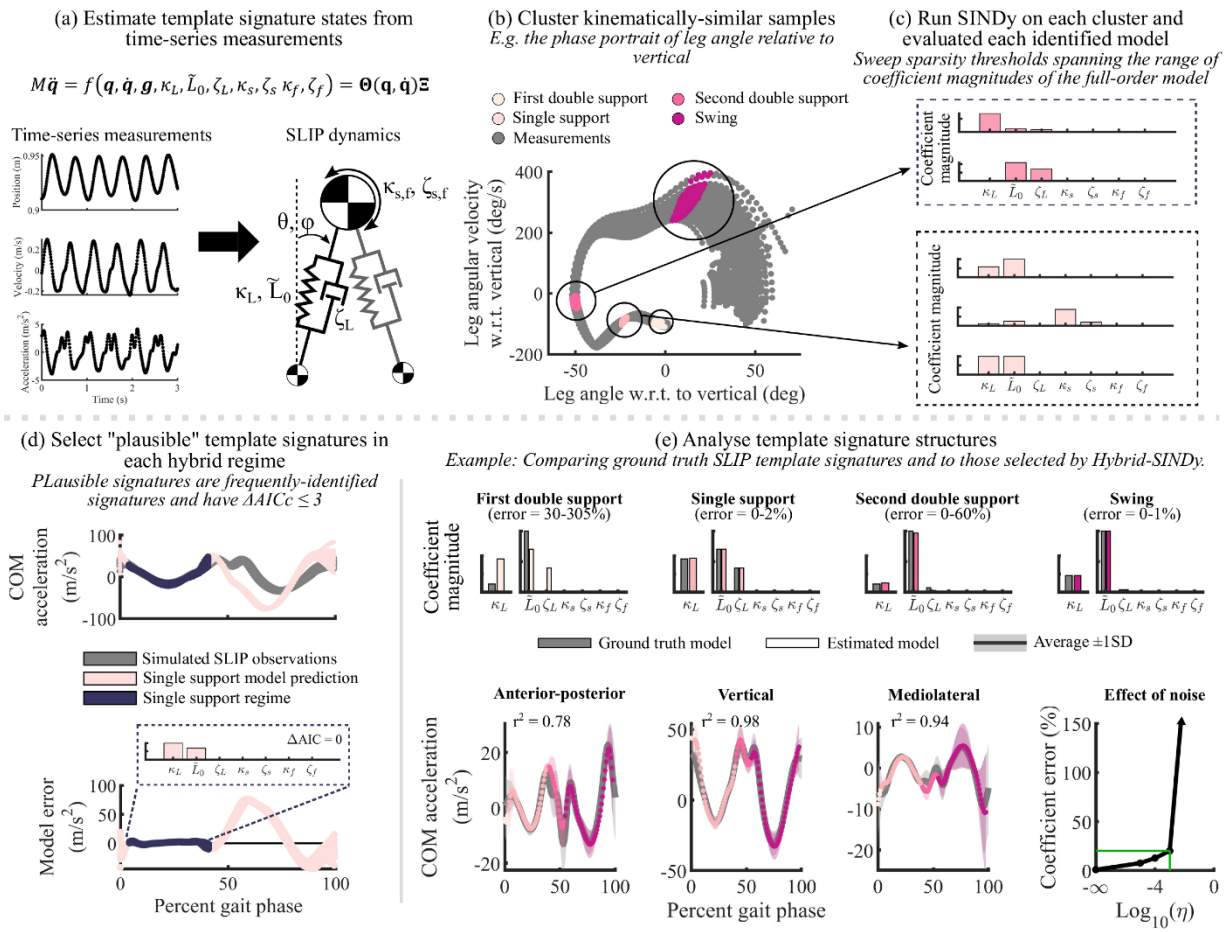

Figure 5.2. The Hybrid-SINDy algorithm, applied to a simulated 3D-SLIP walking model. (a) COM and foot measurements from the simulated SLIP were used to approximate nonlinear SLIP states, $\boldsymbol{\Theta(q, \dot{q})}$, as shown in the equation and the SLIP diagram. Variables can be found in Table 5.1. (b) We used leg kinematics to cluster the data (gray). The colors denote clusters that were each in a different gait regime (*e.g.*, single- or double-limb support). (c) Example models from two clusters are shown. For each cluster, multiple models of different complexity were identified. (d) Each model was evaluated in the hybrid regime containing the cluster centroid. The top plot shows measured (gray) and predicted COM accelerations (pink) using one model in single-limb support (purple). The lower plot shows the prediction error, which was large outside of single-limb support. Error in this regime was used to compute AICc scores for each model. In each hybrid regime, frequently-identified models with low relative AICc ($\Delta AICc$) were considered *plausible*. (e) Top: Ground-truth (gray) and identified (colors) template signatures in each hybrid regime. The reported errors are percent errors compared to the ground-truth signatures. Bottom: Average (±1SD) observed (gray) and predicted (colors) COM accelerations for the simulated SLIP. Colors denote each hybrid regime. The rightmost plot shows the average percent error in the estimated coefficients during single-limb support and swing as measurement noise (η) increased. Green lines denote the approximate noise level of marker-based motion capture.

5.2.4 *Template signatures mechanisms and dynamics*

To model COM anterior-posterior ($\ddot{x}$), vertical ($\ddot{y}$), and mediolateral ($\ddot{z}$) accelerations during walking, we selected the following candidate mechanisms bilaterally based on prior literature (Table 5.1):

- *Rigid legs*, which reflected pendular gait in stance [34, 71, 74, 162, 166, 174]. Pendular gait is energetically passive and reflects kinetic and potential energy transfer during walking [175]. However, pendular walking lacks a double-limb support phase and cannot explain GRFs [163].
- *Leg springs* ([32, 76, 163-165]) and *dampers* ([170]) that produced force along the leg. Leg springs are commonly used to model walking and running and represent energetically-conservative gait while enabling a double-limb support phase. Leg dampers are less common, but have been used to reflect the non-conservative nature of human gait [170].
- *Rotary springs* ([32, 163]) and *dampers* in the sagittal and frontal planes, which enable forcing transverse to the leg axis. For example, Antoniak and colleagues (2018) showed that the addition of a rotary springs helped explain anterior-posterior GRFs in a sagittal-plane bipedal SLIP [163]. We did not identify rotary damping elements in prior literature, but include them as a potential mechanism.

The dynamics of a three-dimensional bipedal SLIP augmented with damping and rotary mechanisms may be written as

$$M(\ddot{\boldsymbol{q}} - \boldsymbol{g}) = \sum_{j=R,L} \left(-\left[k_L(L - L_0) + c\dot{L}\right]\frac{\boldsymbol{q}}{L} - \left[k_s\theta + c_s\dot{\theta}\right]\frac{\boldsymbol{q}}{L_s^2} - \left[k_f\phi + c_f\dot{\phi}\right]\frac{\boldsymbol{q}}{L_f^2}\right)_j, \quad 5.6$$

where *M* is the system mess, $\boldsymbol{g}$ is the gravity vector, ϕ describes the traverse-plane leg angle, and θ describes the leg angle from vertical in the direction defined by ϕ. The summation represents total force generated by the right and left legs on the COM. The left-most brackets contain mechanisms that impart forces radially along the leg: k_L is the leg stiffness, L is the instantaneous leg length, L_0 is the leg resting length, c_L is the leg damping, $\dot{L}$ is the instantaneous leg velocity. Note that we describe L_0 as *leg length* for clarity. The middle bracket contains mechanisms that impart rotary forces transverse to the leg axis in the sagittal plane: k_s is the sagittal-plane rotary stiffness and c_s is the sagittal-plane damping, and L_s denotes the leg projection in the sagittal plane. Analogously in the right-most brackets, k_f and c_f represent the frontal-plane rotary stiffness and damping, respectively, and L_f denotes the leg projection in the frontal plane.

5.2.5 *Nondimensional template mechanisms*

To account for interindividual differences in walking speed and body size, we nondimensionalized the template signatures prior to analysis as follows (Table 5.1): Leg stiffness was multiplied by leg length measured during quiet standing (L_{bio}) and divided by mass-times-gravity ([23, 75, 163]). Leg resting length was normalized by the measured leg length [163, 170]. Damping was converted to a damping ratio (Kim 2011). Rotary stiffness divided by the measured leg length, mass, and gravity and rotary damping was converted to a damping ratio [163]. The nondimensional leg, sagittal-plane, and frontal-plane stiffness mechanisms are denoted by $\kappa_L, \kappa_s,$ and κ_f, respectively. The nondimensional leg, sagittal-plane, and frontal-plane damping mechanisms are denoted by $\zeta_L, \zeta_s,$ and ζ, respectively. Nondimensional leg length is denoted $\tilde{L}_0$. We can rewrite equation 5.6

as a linear combination of our nondimensional coefficients and nonlinear transformations of our states:

$$M(\ddot{\boldsymbol{q}} - \boldsymbol{g}) = [\kappa_L \quad \kappa_L \tilde{L}_0 \quad \zeta_L \quad \kappa_s \quad \zeta_s \quad \kappa_f \quad \zeta_f]_j \, \boldsymbol{\Theta}(\boldsymbol{q}, \dot{\boldsymbol{q}}), \quad j = \{R, L\} \tag{5.7}$$

The nonlinear function $\boldsymbol{\Theta}(\boldsymbol{q}, \dot{\boldsymbol{q}})$ represents our function library, which contained transformations of our system states corresponding to each mechanism described in equation 5.6 for the left and right limbs, totaling p=14 terms. The COM position and velocity relative to the feet were used to compute leg lengths and lengthening velocities, sagittal-plane leg angles and angular velocities relative to vertical, and frontal-plane leg angles and angular velocities relative to vertical.

Table 5.1. List of template signature terms.

Term	Symbol	Nondimensional form
Leg stiffness	κ_L	$\frac{k_L L_{bio}}{Mg}$
Leg resting length	$\tilde{L}_0$	L_0/L_{bio}
Leg damping	ζ_L	$\frac{c_L}{2\sqrt{k_L M}}$
Sagittal-plane rotary stiffness	κ_s	$\frac{k_s}{MgL_{bio}}$
Sagittal-plane rotary damping	ζ_s	$\frac{c_s}{\sqrt{\kappa_s M L_{bio}^2}}$
Frontal-plane rotary stiffness	κ_f	$\frac{k_f}{MgL_{bio}}$
Frontal-plane rotary damping	ζ_f	$\frac{c_f}{\sqrt{\kappa_f M L_{bio}^2}}$

c_L=leg damping; c_s=sagittal-plane rotary damping; c_f=sagittal-plane rotary damping; g = gravitational acceleration; k_L=leg stiffness; k_s=sagittal-plane rotary stiffness; k_f=sagittal-plane rotary stiffness; L_{bio} biological leg length; M = body mass

5.2.6 *Evaluating subject-specific template signatures*

To evaluate the ability of the Hybrid-SINDy algorithm to identify walking dynamics we first tested the algorithm using surrogate data of a simulated bipedal SLIP walker with known dynamics (Figure 5.1 & Figure 5.2) [76]. The bipedal SLIP had asymmetric leg stiffness and damping, and masses representing the pelvis (M = 56 kg) and feet (M_f = 7 kg) to simulate a full gait cycle (Table 5.2). For simplicity, we omitted rotary mechanisms from the SLIP dynamics, but used the same function library described above. To emulate the human-subjects datasets, we simulated 120 gait cycles from randomly perturbed initial conditions with an average initial velocity of 1.20 m/s. We identified template signatures using Hybrid-SINDy as described above and evaluated algorithm performance according to the number of correctly-selected mechanisms and the accuracy of estimated coefficients. To evaluate the impact of sensor noise on algorithm performance, we added Gaussian noise ($\eta = 0, 1e-1, 1e-2, \ldots, 1e-5$ mm) to the position measurements.

Table 5.2. Bipedal SLIP normalized simulation parameters.

	[Right leg, Left leg]			
Term	**DS_1**	**SS**	**DS_2**	**SW**
κ_L	[10.8, 9.1]	[25.1, 18.82]	[9.03, 10.68]	[36.6,25.3]
$\tilde{L}_0$	[1.0, 1.0]	[1.0, 0.7]	[1.0, 1.0]	[0.7, 0.7]
ζ	[0.04, -0.07]	[-0.03, -0.04]	[0, 0]	[-0.40, -0.57]
κ_s	0	0	0	0
ζ_s	0	0	0	0
κ_f	0	0	0	0
ζ_f	0	0	0	0

We estimated unique template signatures that predicted COM accelerations using the Hybrid-SINDy algorithm for each participant and ankle exoskeleton condition. For training, 90 seconds of data (10800 samples) were used for clustering. We identified clusters near samples in the first

30 seconds (3600 samples) of the training data. An additional 30 seconds of held-out data were used for model evaluation and selection.

5.2.7 *Evaluating template signatures*

5.2.7.1 Are COM dynamics consistent across unimpaired adults?

To evaluated the extent to which a common set of mechanisms described COM accelerations in unimpaired adults, we analyzed the proportion of participants for whom each template signature coefficient was identified. Signature terms that are frequently identified represent mechanisms that are important for describing COM dynamics across individuals, while infrequently identified signature terms mechanisms describe individual-specific COM acceleration strategies.

5.2.7.2 Do unimpaired COM dynamics change with ankle exoskeletons?

To evaluate whether the structure of unimpaired COM dynamics during shoes-only walking generalized to walking with ankle exoskeletons, we evaluated the plausibility of the shoe-walking template signature structures to reconstruct COM accelerations in the K_0, and K_H conditions. We tested this condition by estimating template signature parameters for the K_0 and K_H conditions while enforcing the shoes-only template signature structure. We then computed the relative AICc ($\Delta AICc$) scores between these signatures and those selected specifically for the K_0 and K_H conditions. We used one-sample paired t-tests ($\alpha = 0.05$) to determine if shoes-only template signatures were less plausible (*i.e.,* $\Delta AICc \geq 3$) than signature structures selected for the K_0 and K_H conditions.

Similarly, to evaluate how the parameters of COM dynamics changed with ankle exoskeleton, we compared template signature coefficients between the K_0 and Shoe conditions, and between the

K_H and K_0 conditions. We compared exoskeleton coefficients using paired two-sample t-tests with Holm-Sidak step-down corrections for multiple comparisons ($\alpha = 0.05$) [155]. Because template signature coefficients may change when signature structure changes, we enforced the template signatures structure from the shoes-only condition, described above. Significant differences in signature coefficients would indicate how template signatures were impacted by ankle exoskeleton mass (K_0-Shoe) and stiffness (K_H-Shoe).

5.2.7.3 How are COM dynamics affected post-stroke?

To evaluate if COM dynamics may be altered post-stroke, we first computed the percent difference in the non-paretic and paretic limb template signature parameters during shoes-only walking in one individual with post-stroke hemiparesis. To evaluate if changes in COM dynamics in response to ankle exoskeletons may be altered post-stroke, we computed percent changes in template signatures coefficients for the K_0 condition compared to shoes-only walking and the K_H condition, compared to the K_0 condition.

5.3 RESULTS

5.3.1 *Hybrid-SINDy identified hybrid walking dynamics of a simulated SLIP*

The Hybrid-SINDy algorithm correctly identified template signatures in a simulated SLIP during single-limb support (Figure 5.2). Specifically, for our SLIP model, we would expect Hybrid-SINDy to identify non-zero leg stiffness (κ_L), resting length ($\tilde{L}$), and damping (ζ_L) terms only – consistent with the dynamics of the system. In the noise-free condition, 86% of terms were correctly selected and only one term, leg damping in first double-limb support, was incorrectly selected. The incorrect term was selected in first double-limb support. Both double-limb support

regimes were very short in the simulated SLIP: 1.3% and 4.6% of samples in first and second double-limb support – smaller than the 7.4% of the training data comprised by each cluster. Consequently, all clusters with centroids in the double-limb support regimes consistent of samples originating from both double- and single-limb support dynamics. Hybrid-SINDy incorrectly omitted only damping terms, which had small coefficients (Table 5.2). Without measurement noise, in single-limb support and swing, coefficients selected by Hybrid-SINDy were within 2% of the ground truth values, while there were errors up to 306% in double-limb support. When we introduced measurement noise with a standard deviation of 1 mm – similar to that of our motion capture system – Hybrid-SINDy correctly selected only 63% of mechanisms, entirely due to decreased accuracy in double-limb support. Template signatures coefficients were estimated with an average error of less than 29% in single-limb support and swing. For sufficiently large hybrid regimes, such as single-limb support, Hybrid-SINDy was still able to estimate large coefficients (*i.e.*, leg stiffness and resting length) with less than 1% error.

5.3.2 *Shoes-only template signatures highlighted common and subject-specific COM mechanisms*

Data from human walking with shoes-only demonstrated SLIP-like COM dynamics across unimpaired participants. In both double-limb and single-limb support, SLIP mechanisms – leg stiffness and leg length – were selected in 96-100% of limbs (Figure 5.3). Template signatures were similar between legs ($p > 0.01$; $\alpha_{Sidak} = 0.002$). Template signatures varied more during double-limb support: Rotary stiffness terms were selected in 58-67% of limbs in the first double-limb support and 83-95% of limbs during second double-limb support. Except for sagittal-plane damping, damping terms were selected in less than 20% of limbs. As expected during swing, when

the limb is not expected to contribute to COM motion, no terms were selected. We omit the swing regime from remaining analyses.

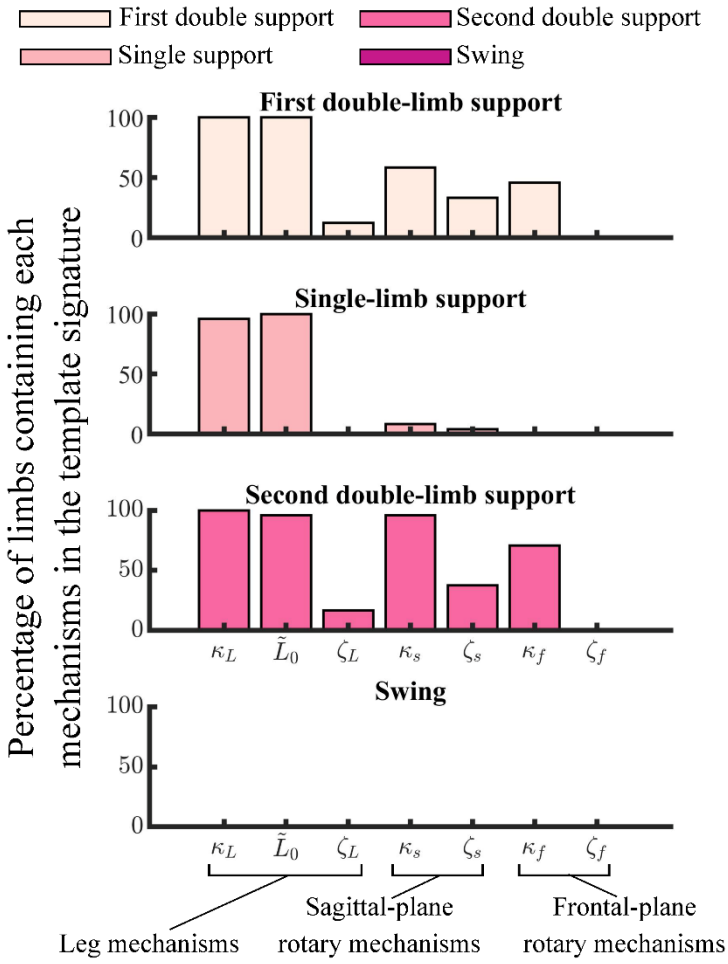

Figure 5.3. The percentage of unimpaired limbs (24 limbs) whose template signatures contained each mechanism in each hybrid regime. Colors denote the different hybrid regimes. Mechanisms selected in a larger percentage of legs suggest common representations of COM dynamics, while less frequently-selected mechanisms reflect individual specific features of COM dynamics.

For each participant, template signatures were robust to stride-to-stride variations in single-limb support. During single-limb support, stiffness and leg length exhibited coefficients of variation (CVs) less than 0.021 ± 0.015. In both double-limb support phases, CVs of stiffness and sagittal-

plane rotary damping, which were selected in 30-50% of signatures, ranged from 0.11 – 0.26. Less frequently selected mechanisms in double-limb support – leg damping and frontal-plane damping – were highly variable, with CVs ranging from 0.082 – 0.442. Across participants, template signature parameters varied (Figure 5.4; top). Single-limb support leg length was most consistent across unimpaired participants (CV = 0.03), while leg stiffness was more variable (CV = 0.28). Interindividual variability in double-limb support leg and rotary stiffness were larger (CV = 0.43 – 1.94). Despite this variability, template signatures reconstructed participants' COM accelerations well, 32-85% of the variance in 3D COM accelerations (Figure 5.4; bottom).

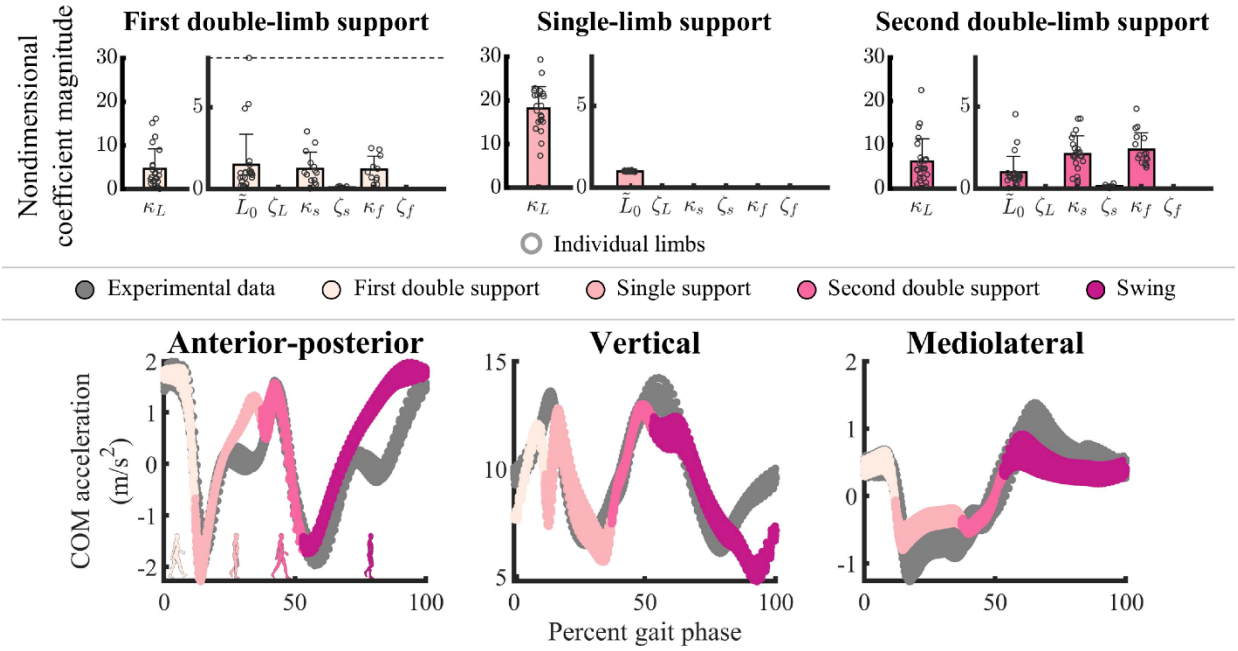

Figure 5.4. Nondimensional template signatures (top) and reconstructed COM accelerations (bottom) for shoes-only walking in each hybrid regime. Top: Bars denote the average template signature (+1SD) in single- and double-limb support. The small circles represent individual limbs. The number of circles in each bar differs based on the number of limbs for which each mechanism was selected. Note that we omitted mechanisms that were selected in less than 25% of participants. The dashed lines truncate large terms for clarity. Bottom: Experimental and predicted COM accelerations from the test dataset of an exemplary unimpaired participant in the anterior-posterior (left), vertical (center), and mediolateral (right) directions. The gray dots

denote the experimental accelerations, while the colors correspond to the predicted accelerations in each hybrid regime. Hybrid regimes are defined based on right leg contact configuration.

5.3.3 *Template signatures did not change with ankle exoskeletons in unimpaired adults*

Template signatures did not change significantly when walking with ankle exoskeletons among unimpaired adults. First, the shoes-only template signatures were plausible representations of COM dynamics with ankle exoskeletons, according to the AICc. Compared to the template signatures selected from K_0 and K_H data, the shoes-only template signature structures were not significantly less plausible in the K_0 ($\Delta AICc = 0.2 \pm 0.7$; p = 0.93) and K_H ($\Delta AICc = 0.7 \pm 2.9$; p = 0.24) conditions (Figure 5.5). Shoe template signatures were less consistently plausible for the K_0 or K_H conditions during double-limb support, with relative AICc scores ranging from $-118 \leq \Delta AICc < 220$, though the median relative AICc scores were less than three. Therefore, to compare signature coefficients between exoskeleton conditions, we constrained each participant's template signatures to that selected in the shoes-only condition. Using this approach, we did not identify any differences in template signature coefficients between walking in shoes-only and the K_0 or K_H conditions. ($p > 0.05$). Specifically, we found that neither ankle exoskeleton mass and frame (K_0) nor stiffness (K_H) had a significant impact on limb stiffness in any gait phase ($p > 0.13$; Figure 5.5).

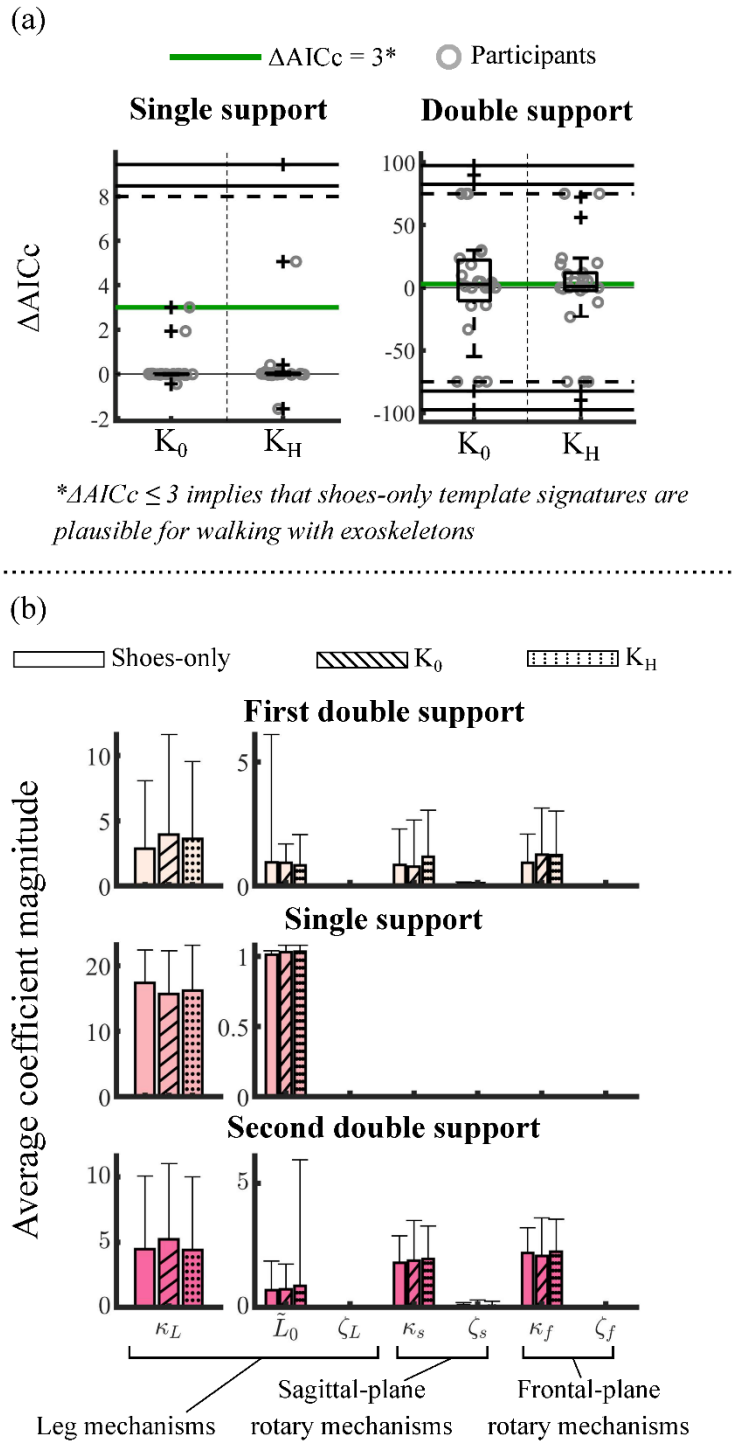

Figure 5.5. (a) Relative AICc ($\Delta AICc$) between template signatures identified specifically for the K_0 and K_H conditions and signatures constrained to the shoes-only signature structures. Positive $\Delta AICc$ values indicate that shoes-only signature structures were less plausible than those identified specifically for each condition. $\Delta AICc$ scores are shown for single-limb support (left) and double-limb support (right). $\Delta AICc \leq 3$ (green lines) denote plausible shoe template

signature structures. For double-limb support, large $\Delta AICc$ scores are truncated at $\Delta AICc = \pm 75$ for clarity. (b) Template signatures of walking in shoes only (solid bars), zero-stiffness (K_0; slashed bars) exoskeletons, and high-stiffness exoskeletons (K_H; dotted bars) during single and double-limb support. Each row corresponds to one hybrid regime, with colors matching those in all other figures. Bars represent the average (+1SD) template signature. Leg stiffness (κ_L) is included on a separate subplot for clarity. The shoes-only condition matches that ofFigure 5.4. The large variability in leg length during double-limb support is due one limb with a high resting length.

5.3.4 *Template signatures reflected a stroke survivor's impairment*

During shoes-only walking in the participant with post-stroke hemiparesis, template signatures were symmetric between the paretic and non-paretic limbs during single-limb support, consisting of only leg stiffness and resting length. During first double-limb support, leg damping and rotary stiffness were selected in only the paretic limb, while in second double-limb support both paretic and non-paretic rotary stiffness mechanisms were selected by the Hybrid-SINDy algorithm (Figure 5.6). In first double-limb support, the stroke survivor's non-paretic limb was 62% stiffer and had a 27% shorter leg length than the paretic limb. During single-limb support, the stroke survivor's paretic limb was 31% stiffer and had a 3% shorter leg length than the non-paretic limb. Conversely, during second double-limb support, the non-paretic leg stiffness was only 20% of the paretic leg stiffness.

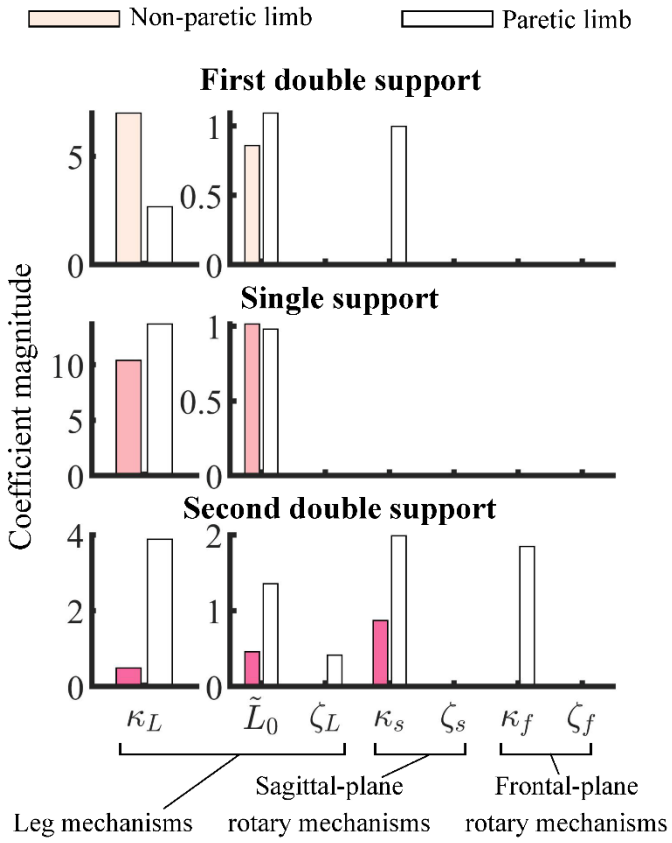

Figure 5.6. Non-paretic (colored bars) and paretic (whited bars) template signatures for one individual with post-stroke hemiparesis. This participant's template signatures differed in the paretic and non-paretic limbs in double-limb support, as shown by the zero-values for non-paretic sagittal-plane rotary stiffness in first double-limb support (top row) and the leg damping and frontal-plane stiffness in double-limb support (third row).

5.3.5 *Template signatures changed with ankle exoskeletons for a stroke survivor*

The exoskeleton mass and frame primarily impacted paretic leg stiffness and non-paretic leg rotary stiffness. Compared to walking in shoes only, the paretic leg stiffness was 11% greater in the zero-stiffness (K_0) exoskeleton condition in single-limb support and over twice as stiff in double-limb support (Figure 5.7; slashed bars). Responses to the K_0 exoskeleton condition were asymmetric, with the non-paretic leg being 3% less stiff in the K_0 condition than the shoes-only condition in single-limb support, while sagittal-plane stiffness was 41% larger in second double-limb support.

Conversely, exoskeleton stiffness had small impacts on paretic template signatures. In the high-stiffness (K_H) exoskeleton condition, single-limb support paretic leg stiffness was only 1% larger than in the K_0 condition (Figure 5.7; dotted bars). Both paretic and non-paretic leg rotary stiffness were 11% greater in second double limb support than in the K_0 condition. Non-paretic leg stiffness reduced by 49% compared to zero-stiffness exoskeletons in single-limb support.

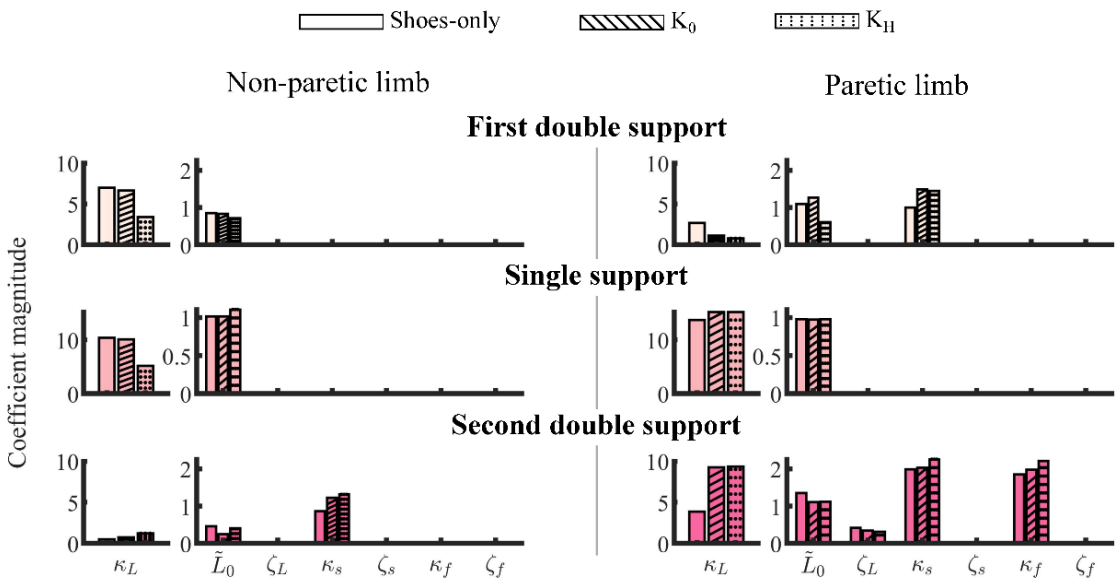

Figure 5.7. Template signatures of a stroke survivor walking in the shoes-only (clear bars), zero-stiffness (K_0; slashed bars), and high-stiffness (K_H; dotted bars) ankle exoskeleton conditions for the non-paretic (left) and paretic (right) limbs. Bars represent the average template signatures over 200 bootstrapped model fitting iterations. Colors correspond to each hybrid regime.

5.4 DISCUSSION

5.4.1 *Template signatures provide insight into changes in whole-limb COM dynamics in response to ankle exoskeletons*

We evaluated the impacts of passive ankle exoskeletons on subject-specific whole-limb COM dynamics – described by template signatures – using a recently-developed data-driven modeling framework, Hybrid-SINDy. To our knowledge, this is the first study to parameterize the impacts of ankle exoskeletons on whole-limb COM dynamics. Contrary to our hypothesis, leg stiffness did not change in response to ankle exoskeleton mass (K_0 condition) or stiffness (K_H condition) in unimpaired adults. Further, template signatures identified for shoe walking were plausible representations of COM dynamics when walking with ankle exoskeletons. These results suggest that unimpaired strategies to accelerate the COM during walking are unaffected by passive ankle exoskeletons, despite changes in gait kinematics and muscle activity [172]. Since template signatures are impacted by the biological limb and the exoskeleton, this finding suggests that biological dynamics may be modulated to maintain similar COM dynamics in response to exoskeletons. Conversely, if biological dynamics were insensitive to ankle exoskeletons, we would expect template signatures to change with ankle exoskeletons. This explanation is consistent with work by Collins and colleagues (2015), who observed small changes in total COM power with passive exoskeletons compared to walking in shoes-only, but larger changes in biological contributions to COM power [9]. Our results suggest that these small changes in COM power are accompanied by only small changes in COM dynamics for unimpaired adults. As COM motion is task-relevant during walking, this result implies that task-level strategies to accelerate the COM

may largely be maintained when walking with ankle exoskeletons, while joint or muscle-level control may change in response to exoskeletons [9, 37, 38, 172].

Conversely, in one individual post-stroke, ankle exoskeletons impacted whole-limb COM dynamics. The addition of exoskeleton mass and frame (K_0) increased paretic limb sagittal-plane rotary stiffness in first double-limb support and leg stiffness in single-limb and second double-limb support. Increased paretic-limb stiffness is likely due to the exoskeleton frame restricting ankle inversion, which the participant noted during data collection. As the participant's paretic ankle was severely affected, restricting frontal-plane ankle motion may result in increased leg stiffness by enabling the less affected knee and hip to produce greater moments during stance. The latter possibility is supported by observations that exoskeleton stiffness alters leg power during hopping in unimpaired adults [176]. This result emphasizes the importance of quantifying the impacts of other ankle exoskeleton properties, such as restriction to frontal-plane ankle motion, in explaining exoskeleton impacts on gait following neurological injury. For example, Ries and colleagues (2015) observed that rigid ankle exoskeletons increased walking speed more than passive-elastic exoskeletons prescribed to children with diplegic cerebral palsy [4]. Passive-elastic exoskeletons are typically less stiff than rigid exoskeletons and do not restrict ankle inversion, which may influence walking speed for individuals with severely impaired ankles.

The insensitivity of the paretic limb template signatures to exoskeleton stiffness during single-limb support suggests that, for this individual, exoskeleton stiffness did not alter body weight support strategies in this gait regime [63]. One explanation for this may be that the participant appeared to walk with a more pendular gait in the paretic limb, such that exoskeleton stiffness did not further

increase leg stiffness. Conversely, during double-limb support, paretic-limb sagittal- and frontal-plane rotary stiffness were larger than those of the zero-stiffness condition. Restricted ankle dorsiflexion due to exoskeleton stiffness in terminal stance may enable increased propulsive force in the paretic limb, which could alter rotary mechanism contributions to gait. Additionally, the ankle plantarflexors accelerate the COM laterally, such that increased force-generating capacity in the paretic limb may contribute to frontal-plane motion as well [177, 178]. For this participant, changes in only rotary dynamics suggest that the individual's strategy to support the COM was maintained, while strategies to propel and stabilize the COM changed in response to exoskeleton stiffness. While these impacts likely vary between individuals post-stroke [20], our results highlight potential differences in the impacts of exoskeleton frame and stiffness on whole-limb COM dynamics that can be described using template signatures.

5.4.2 *Template signatures quantify interindividual and inter-limb differences in whole-limb contributions to COM acceleration*

Both unimpaired and post-stroke template signatures highlighted inter-individual and inter-limb differences in COM dynamics. While SLIP mechanisms described COM accelerations in all unimpaired limbs, rotary mechanisms were plausible in only 50% of limbs during double-limb support. The uniform selection of SLIP mechanisms from data is consistent with common template walking models and suggests that elastic legs are important mechanisms for describing COM accelerations during walking across individuals [71, 76, 161, 164, 165]. Our observation that rotary mechanisms were not critical to reconstructing COM accelerations for all individuals aligns with their less frequent application in template walking models [32, 163]. Note that each template signature mechanism describes characteristic coordination patterns between leg

kinematics and COM accelerations. It is possible SLIP mechanisms describe coordination patterns necessary for efficient walking, while rotary mechanisms describe coordination patterns that have smaller, more individualized impacts on gait. Determining if these characteristic patterns are associated with biological control and exoskeleton responses represent important areas of future research.

Parameterizing whole-limb COM dynamics using template signatures also revealed compensation strategies post-stroke. Consistent with template-based studies in children with cerebral palsy, the stroke participant's paretic limb was stiffer than the nonparetic limb in single- and second double-limb support [88, 169]. Increased paretic leg stiffness may reflect a more pendular gait post-stroke and increased co-contraction [64]. In first double-limb support, sagittal-plane rotary stiffness and damping mechanisms suggest altered braking during loading response, consistent with experimental observations that the paretic-limb does greater negative work than the non-paretic limb during loading response in individuals post-stroke [36]. These results serve to highlight the functional interpretation of template signatures during walking and the importance of personalized parameterizations of whole-limb COM dynamics.

5.4.3 *Innovation & insights of Hybrid-SINDy for human walking*

Our use of the Hybrid-SINDy algorithm ([23]) provides two primary contributions to locomotion research. First, by automatically identifying and comparing different representations of COM dynamics, our approach rapidly compares many competing hypotheses about human locomotion. To our knowledge, only one other study in bipedal locomotion has taken a similar approach [31]. The authors performed a multi-layer optimization to select human-like template dynamics for

walking robot controllers. Our approach extends their work by permitting many plausible representations of walking to be analyzed for an individual. This approach acknowledges uncertainty and redundancy in human locomotion, and the existence of multiple plausible template signatures may inform future experimental designs to better distinguish between candidate mechanisms describing gait. Second, our use of information criteria to select *plausible* template signatures may be particularly beneficial when studying mechanisms contributing to locomotion. By favoring parsimonious representations of gait, the AICc selected SLIP mechanisms to describe gait across individuals and rotary stiffness as individual-specific descriptions of walking [171, 173]. If applied to higher-dimensional physiologically-detailed dynamics, both Hybrid-SINDy and information criteria alone may, for example, be useful in ranking candidate biological mechanisms explaining pathological gait [22, 83].

Since data-driven models may be sensitive to measurement noise and (inevitably) incorrect model dynamics, we used a simulated SLIP to evaluate the extent to which Hybrid-SINDy correctly identified template signatures during walking. The Hybrid-SINDy algorithm performed as expected in the noise-free condition, accurately identifying single-limb support and swing dynamics, with the exception of small damping terms. Terms with small contributions to system behavior, such as damping in this study, may be omitted by the AICc in favor of parsimony [171, 173]. A theoretical implication exemplified by this result is that the Hybrid-SINDy algorithm will not always select the true system dynamics but will select terms critical to describing salient behavior. Therefore, sound experimental design in is critical to identifying walking mechanisms from data. For example, alternative gait patterns that induce large leg velocities may result in damping terms being correctly selected by Hybrid-SINDy. Poor signature predictions during

double limb support highlight the importance of selecting cluster sizes smaller than the smallest hybrid regime, consistent with conclusions from Mangan and colleagues[23]. For human walking, we ensured that the cluster size (800 samples; 7.4% of training samples) was smaller than the amount training data in double-limb support (~10-12% of training samples). When measurement noise was approximately equal to that observed in motion capture ($\eta = 1\,mm$), simulated SLIP template signatures during single-limb support and swing were within 29% of ground truth values, though error was less than 3% in most terms. Based on the simulated SLIP's robustness to noise during single-limb support, we expect that the structure and coefficients of template signatures identified by Hybrid-SINDy for human walking likely encode meaningful information about COM dynamics. This expectation is supported by low variability in the bootstrapped dynamics of human template signatures, indicating their robustness to stride-to-stride variations in the measurements.

5.4.4 *Challenges and limitations*

This study has a number of limitations that motivate future data-driven modeling studies in human locomotion. First, human gait dynamics are continuously phase-varying rather than hybrid, such that template signature parameters varied between clusters within a single hybrid regime. To address this challenge, we modified the model selection procedure to evaluate models within pre-defined hybrid regimes, making it more consistent with hybrid template models of human walking [23, 76, 163, 164]. Second, we evaluated only a subset of mechanisms describing whole-limb COM dynamics, which may not encode all important features of human gait. However, we chose a broad class of physically-meaningful mechanisms from literature ([75, 76, 163-165, 170]) that should motivate future studies using larger mechanism libraries describing COM dynamics. For example, our approach may be extended to include elements describing assistive devices or joint-level mechanisms [85]. Finally, we had a limited sample size in

unimpaired adults, which may have masked exoskeleton impacts on unimpaired gait. Particularly, rotary stiffness appeared to increase slightly with exoskeletons but did not reach significance. Similarly, our post-stroke case study only provides a proof of concept highlighting the potential of ankle exoskeletons to elicit changes in COM dynamics. Evaluating template signatures on larger unimpaired and post-stroke cohorts may provide additional insight into how whole-limb COM dynamics change with ankle exoskeletons.

5.4.5 *Extensions and applications*

Integrating principles from biomechanics and neuromechanics with state-of-the-art *interpretable* data-driven modeling techniques may accelerate discovery in mechanisms underlying diverse movement patterns in human locomotion and opens exciting new research avenues. Broadly, these methods may be applied to any intervention or walking condition and may inform the design of prosthetic limbs and other assistive devices. A natural extension of this work is to investigate the impacts of powered exoskeletons on whole-limb COM dynamics. Changes in gait kinematics and kinetics with our passive ankle exoskeletons were small compared to changes in elicited by powered exoskeletons and individuals may exhibit larger changes in COM dynamics in response to different exoskeleton control strategies [18, 45, 172]. As powered exoskeleton research transitions focus from reducing metabolic demand to assisting other locomotion objectives, such as stability or agility, understanding changes in whole-limb control with exoskeletons may provide insight into how individuals use exoskeletons to achieve these task-level goals [2]. Further, quantifying changes in whole-limb COM dynamics with exoskeletons may improve our understanding of the diverse responses to exoskeletons observed in individuals with motor impairments [4, 20, 29]. For example, McCain and colleagues (2019) identified limb orientation

as a potential mechanism impacting the conversion of exoskeleton torque to forward propulsion post-stroke [20]. Our results suggest that characterizing altered coordination between leg orientation and ground reaction forces (*e.g.*, using template signature mechanisms) with exoskeletons may unveil sub-classes of responses to exoskeletons, enabling the identification of device control strategies to assist individuals in each sub-class. Finally, *anchoring* template signatures in physiological detail may reveal biological mechanisms that characterize responses to exoskeletons or other assistive devices [33]. Template models of human walking are rarely anchored in physiological detail [32] and doing so represents an exciting area of future research.

5.5 CONCLUSIONS

We quantified changes in subject-specific whole-limb COM dynamics in response to passive ankle exoskeletons using a novel physics-informed data-driven modeling framework, Hybrid-SINDy. Hybrid-SINDy successfully constructed characteristic template signatures during walking by identifying salient mechanisms describing an individual's COM accelerations. Unimpaired adults maintained nearly invariant COM dynamics with ankle exoskeletons, while exoskeletons altered COM dynamics in an individual post-stroke. These findings provide insight into task-level control of walking with ankle exoskeletons and extend a powerful data-driven modeling tool to human locomotion.

Chapter 6. CONCLUSION

6.1 SUMMARY

The goal of this dissertation was to improve our understanding of responses to ankle exoskeletons. This dissertation was the first to use subject-specific physiologically-detailed models to study ankle exoskeleton impacts on gait in children with cerebral palsy and to use phase-varying and sparse hybrid dynamics modeling frameworks to predict and study subject-specific responses to ankle exoskeletons. Moreover, this work was the first to study changes in task-level control of walking with ankle exoskeletons using physics-informed data-driven models that automatically compared competing hypotheses about control with ankle exoskeletons. The results of this work *contributed to our knowledge* of how gait mechanics alter ankle exoskeleton impacts on gait, and how individuals adapt their mechanics and task-level control in response to ankle exoskeletons. Additionally, this work *contributed to our understanding* of how data-driven models of locomotion may be applied to study and predict gait with ankle exoskeletons, which may be extended to other assistive devices, such as prostheses. The data and code from this work were made freely available. The work from Chapter 3 contributed additional analyses and simulations to an existing repository of crouch gait simulations, available at (https://simtk.org/projects/crouchgait). The data and code from Chapter 4, used to generate phase-varying models of walking with ankle exoskeletons is available at (https://simtk.org/projects/ankleexopred). By extending state-of-the-art data-driven modeling techniques to study gait with ankle exoskeletons, this work provides a foundation for future research into the mechanisms influencing heterogeneous responses to ankle exoskeletons, informing device design and prescription.

The first objective of this work used musculoskeletal simulation to predict subject-specific changes in muscle demand with passive and powered ankle exoskeletons (Chapter 3). This work showed that powered ankle exoskeletons had the potential to reduce muscle demand more than optimized passive ankle exoskeletons in children with cerebral palsy and that knee flexion moments were associated with reductions in demand on the biarticular plantarflexor muscles. However, small reductions in muscle demand with powered ankle exoskeletons compared to passive ankle exoskeletons for some individuals highlighted the importance of identifying individuals for whom powered ankle exoskeletons are likely to benefit over less-expensive passive exoskeletons.

The second objective of this dissertation was to develop predictive data-driven models of responses to ankle exoskeletons. In Chapter 4, we showed that subject-specific linear and nonlinear phase-varying models could predict kinematic responses to exoskeleton torque without knowledge or assumptions about the individual's physiology or control. We also identified prediction horizons beyond which kinematic posture could not predict stride-specific responses to exoskeleton torque, potentially informing control policies for powered exoskeletons. However, predicting cycle-to-cycle variability in myoelectric responses to torque was more challenging, suggesting that measurements beyond kinematics and myoelectric signals may be needed to predict myoelectric responses to torque.

The final objective of this dissertation was to quantify changes in COM dynamics in response to ankle exoskeletons. In Chapter 5, we extended the Hybrid-SINDy algorithm to show that low-dimensional template signatures of COM dynamics were consistent across unimpaired adults and reflected asymmetrical contributions of a stroke survivor's paretic and non-paretic legs to COM

acceleration. While unimpaired template signatures were robust to passive exoskeleton stiffness, the stroke survivor's signatures changed with ankle exoskeleton stiffness, suggesting that individuals post-stroke may alter their whole-limb strategy for walking with ankle exoskeletons.

By evaluating and predicting ankle exoskeleton impacts using physiological, data-driven, and physics-based modeling frameworks, the research in this dissertation provided insight into muscle-, joint-, and task (COM)-level features of gait with exoskeletons. Specifically, this research contributed to our understanding of (1) how gait mechanics may alter ankle exoskeleton impacts on muscle demand, (2) the potential of subject-specific responses to ankle exoskeletons to be quantified using tools grounded in dynamical systems theory, and (3) how individuals alter task-level control of walking in response to ankle exoskeletons. In a short, this work tells the story:

> *While ankle exoskeleton impacts on muscle demand are likely altered by gait mechanics, changes in muscle activity remain challenging to predict from kinematic and myoelectric measurements. Changes in task-level control with passive exoskeletons are unlikely to contribute to variable myoelectric responses in unimpaired adults but may help explain characteristic responses in individuals with motor impairments.*

Further, this research introduced novel data-driven modeling tools to ankle exoskeleton research. The knowledge and tools that this work contributes to the biomechanics and ankle exoskeleton research communities provide a foundation for future studies aiming to identify mechanisms driving diverse responses to exoskeletons or other assistive devices in individuals with neurological injuries.

6.2 FUTURE WORK

The work constituting this dissertation created a foundation for the application of data-driven models to predict and understanding diverse responses to ankle exoskeletons and other

interventions. The results of these studies suggest exciting future research directions in human movement, combining first-principles in biomechanics and neuromechanics, data-driven modeling, and experimental design to understand gait pathology and assistive device use. The following sections outline important avenues of future work that may expand our understanding of the mechanisms driving responses to assistive devices and inform innovations in assistive or rehabilitative device design:

Understanding pathological task-level control and responses to ankle exoskeletons

Identifying sub-classes of task-level control and their relationship to impaired muscle coordination may help identify candidates for ankle exoskeleton interventions and provide targets of rehabilitation treatments.

- **Are template signatures associated with functional impairments in individuals with motor impairments?**

As we showed in Chapter 5, parameterizing whole-limb control of COM motion may elucidate differences in task-level control of walking without requiring knowledge of an individual's unique physiology. Our post-stroke case study in which we showed that template signatures may reflected altered paretic limb contributions to COM accelerations post-stroke. If and how these signatures vary between individuals remains unclear. The methodology from Chapter 5 may be extended to individuals post-stroke with different levels of walking function. If template signatures are associated with post-stroke walking function, the signatures may serve as intervention targets or help stratify individuals (*e.g.* into responder and non-responder groups for a particular treatment).

- **Do individuals with similar template signatures exhibit similar responses to ankle exoskeletons?**

Identifying whole-limb mechanisms associated with characteristic responses to ankle exoskeletons could enable the prediction of intervention responses based only on baseline (*i.e.,* no exoskeleton) walking data. Extending the methodology from Chapter 5 to datasets with larger perturbations, such as powered exoskeletons or passive exoskeletons with larger differences in mechanical properties, may enable diverse kinematic, kinetic, or myoelectric responses to ankle exoskeletons to be associated with features of baseline template signatures. Identifying template signature features that are highly predictive of exoskeleton responses provide whole-limb targets that could be anchored in physiological detail to identify biological mechanisms driving exoskeleton responses.

- **Does altered motor control predict whole-limb COM dynamics in individuals with motor impairments?**

Understanding the relationships between mechanisms describing COM dynamics and muscle coordination – a primary impairment in stroke and cerebral palsy – could provide a principled foundation for novel interventions, such as biofeedback training, to target muscle coordination. Identifying sub-features of interpretable data-driven models of COM dynamics that are associated with muscle coordination post-stroke or in CP may suggest whole-limb mechanisms that, when altered by intervention may also alter motor control.

Advancing data-driven modeling in human biomechanics

Data-driven models have the potential to accelerate the rate of discovery in biomechanics but must operate within the constraints of experimental measurements and protocols.

- **Can we combine experimental design and data-driven models to rapidly test hypotheses about mechanisms driving heterogeneous responses to ankle exoskeletons?**

Testing hypotheses about mechanisms influencing intervention responses in biomechanics is a slow and expensive process, and single experimental protocols may lack sufficient information to identify one hypothesis as more plausible than all others. Automatically designing experimental protocols that compare competing hypotheses about mechanisms driving intervention responses may accelerate the rate of discovery in biomechanics. For example, information theory can be used to compared data-driven models – each encoding a mechanistic hypothesis – and identify experimental conditions that may better distinguish between competing models [179]. The perturbations could then be applied by a real-time experimental framework, such as biofeedback.

- **What data are needed to encode responses to ankle exoskeletons?**

As we showed in Chapter 4, the available measurements may be insufficient to capture the dynamics of response using data-driven models, such as those explaining stride-to-stride variability in myoelectric responses. Identifying measurement sets that improve predictions of kinematic, kinetic, and myoelectric responses to ankle exoskeletons may guide further investigation into non-biomechanical factors influencing ankle exoskeleton responses and inform measurement selection for real-time control of robotic exoskeletons. A dataset with many different measurement modalities expected to encode responses (*e.g.* motion capture, muscle activity, ultrasound, heart rate) could be used in combination with sparse regression and model selection, such as that employed in Chapter 5, to identify plausible low-dimensional measurement sets that predict responses to ankle exoskeletons.

Bringing ankle exoskeleton optimization research back to the real world

Laboratory-based ankle exoskeleton optimization may be sub-optimal for use in daily life. Rethinking our definition of optimality may improve the effectiveness of ankle exoskeleton assistance.

- **How sub-optimal is an optimized ankle exoskeleton in real life? *i.e.*, Over what range of gait patterns are optimal ankle exoskeleton properties actually optimal?**

Ankle exoskeleton properties are typically tuned at a single walking speed, while humans – children especially – move over a range of speeds and with varying kinematics. Ankle exoskeletons optimized at a fixed speed may, therefore, be sub-optimal at faster or slower speeds. Predictive neuromusculoskeletal models could be used to simulate walking with ankle exoskeletons at different speeds to estimate the increase in the energetic cost of transport for walking at speeds above or below the cost-minimizing speed. Large increases in energetic costs at speeds that are sub-optimal for the ankle exoskeletons would suggest that "optimized" ankle exoskeletons may discourage diversity in movement patterns in daily activity.

- **Do responses to ankle exoskeletons differ during transient events (*e.g.* accelerating, turning, stopping) compared to steady-state walking?**

Ankle exoskeleton properties are typically tuned and studied at a steady walking speed. However, much of walking is transient: individuals start, stop, and turn frequently throughout the day. Along with the data collected in Chapter 4, we collected overground steady walking and accelerations from quiet standing. Investigating differences in the impacts of ankle exoskeleton stiffness on kinematics, muscle activity, and gait energetics between steady walking and accelerations may indicate if ankle exoskeletons optimized for steady walking should be expected to have similar impacts on gait across tasks of daily living.

The long-term goal of this dissertation and the future work described above is to improve exoskeletons' ability to enhance mobility for individuals with motor impairments. The coming decades of biomechanics and exoskeleton research will see the integration of data-driven modeling techniques and advanced experimental methods, with state-of-the-art exoskeletons gaining ubiquity and emerging from the gait lab into the real world. The proposed research avenues represent exciting opportunities to accelerate researchers towards this promising future, connecting models to experiments to daily life. Enhancing mobility can change an individual's life, and embracing state-of-the-art computational and experimental tools can help enhance mobility for individuals with diverse physiology and locomotor capacity.

REFERENCES

[1] Herr, H., Whiteley, G.P. & Childress, D. 2003 Cyborg technology--biomimetic orthotic and prosthetic technology. (pp. 103-143, SPIE Press, Bellingham, Washington.

[2] Sawicki, G.S., Beck, O.N., Kang, I. & Young, A.J. 2020 The exoskeleton expansion: improving walking and running economy. *Journal of NeuroEngineering and Rehabilitation* **17**, 25. (doi:10.1186/s12984-020-00663-9).

[3] Dollar, A.M. & Herr, H. 2008 Lower Extremity Exoskeletons and Active Orthoses: Challenges and State-of-the-Art. *Trans. Rob.* **24**, 144-158. (doi:10.1109/tro.2008.915453).

[4] Ries, A.J., Novacheck, T.F. & Schwartz, M.H. 2015 The efficacy of ankle-foot orthoses on improving the gait of children with diplegic cerebral palsy: a multiple outcome analysis. *PM&R* **7**, 922-929.

[5] Jezernik, S., Colombo, G., Keller, T., Frueh, H. & Morari, M. 2003 Robotic orthosis lokomat: A rehabilitation and research tool. *Neuromodulation: Technology at the neural interface* **6**, 108-115.

[6] Gilbert, K. 1967 Exoskeleton prototype project: Final report on phase I. *General Electric Company, Schenectady, NY, GE Tech. Rep. S-67-1011*.

[7] Zaroodny, S.J. 1963 BUMPUSHER-A POWERED AID TO LOCOMOTION. (BALLISTIC RESEARCH LABS ABERDEEN PROVING GROUND MD.

[8] Zoss, A.B., Kazerooni, H. & Chu, A. 2006 Biomechanical design of the Berkeley lower extremity exoskeleton (BLEEX). *IEEE/ASME Transactions on mechatronics* **11**, 128-138.

[9] Collins, S.H., Wiggin, M.B. & Sawicki, G.S. 2015 Reducing the energy cost of human walking using an unpowered exoskeleton. *Nature* **522**, 212-215.

[10] Wingstrand, M., Hägglund, G. & Rodby-Bousquet, E. 2014 Ankle-foot orthoses in children with cerebral palsy: a cross sectional population based study of 2200 children. *BMC musculoskeletal disorders* **15**, 327.

[11] Ferreira, L.A.B., Neto, H.P., Christovão, T.C.L., Duarte, N.A., Lazzari, R.D., Galli, M. & Oliveira, C.S. 2013 Effect of ankle-foot orthosis on gait velocity and cadence of stroke patients: a systematic review. *Journal of physical therapy science* **25**, 1503-1508.

[12] Rinaldi, L., Yeung, L.-F., Lam, P.C.-H., Pang, M.Y., Tong, R.K.-Y. & Cheung, V.C. 2020 Adapting to the Mechanical Properties and Active Force of an Exoskeleton by Altering Muscle Synergies in Chronic Stroke Survivors. *IEEE Transactions on Neural Systems and Rehabilitation Engineering* **28**, 2203-2213.

[13] Ferris, D.P. 2009 The exoskeletons are here. *Journal of neuroEngineering and rehabilitation* **6**, 1-3.

[14] Conner, B.C., Luque, J. & Lerner, Z.F. 2020 Adaptive ankle resistance from a wearable robotic device to improve muscle recruitment in cerebral palsy. *Annals of biomedical engineering* **48**, 1309-1321.

[15] Orekhov, G., Fang, Y., Luque, J. & Lerner, Z.F. 2020 Ankle exoskeleton assistance can improve over-ground walking economy in individuals with cerebral palsy. *IEEE Transactions on Neural Systems and Rehabilitation Engineering* **28**, 461-467.

[16] Koller, J.R., Jacobs, D.A., Ferris, D.P. & Remy, C.D. 2015 Learning to walk with an adaptive gain proportional myoelectric controller for a robotic ankle exoskeleton. *Journal of neuroengineering and rehabilitation* **12**, 97.

[17] Malcolm, P., Derave, W., Galle, S. & De Clercq, D. 2013 A simple exoskeleton that assists plantarflexion can reduce the metabolic cost of human walking. *PloS one* **8**, e56137.

[18] Mooney, L.M. & Herr, H.M. 2016 Biomechanical walking mechanisms underlying the metabolic reduction caused by an autonomous exoskeleton. *Journal of neuroengineering and rehabilitation* **13**, 4.

[19] Zhang, J., Fiers, P., Witte, K.A., Jackson, R.W., Poggensee, K.L., Atkeson, C.G. & Collins, S.H. 2017 Human-in-the-loop optimization of exoskeleton assistance during walking. *Science* **356**, 1280-1284.

[20] McCain, E.M., Dick, T.J., Giest, T.N., Nuckols, R.W., Lewek, M.D., Saul, K.R. & Sawicki, G.S. 2019 Mechanics and energetics of post-stroke walking aided by a powered ankle exoskeleton with speed-adaptive myoelectric control. *Journal of neuroengineering and rehabilitation* **16**, 1-12.

[21] Halilaj, E., Rajagopal, A., Fiterau, M., Hicks, J.L., Hastie, T.J. & Delp, S.L. 2018 Machine learning in human movement biomechanics: best practices, common pitfalls, and new opportunities. *Journal of biomechanics* **81**, 1-11.

[22] Pitto, L., Kainz, H., Falisse, A., Wesseling, M., Van Rossom, S., Hoang, H., Papageorgiou, E., Hallemans, A., Desloovere, K. & Molenaers, G. 2019 SimCP: a simulation platform to predict gait performance following orthopedic intervention in children with Cerebral Palsy. *Frontiers in neurorobotics* **13**, 54.

[23] Mangan, N.M., Askham, T., Brunton, S.L., Kutz, J.N. & Proctor, J.L. 2019 Model selection for hybrid dynamical systems via sparse regression. *Proceedings of the Royal Society A* **475**, 20180534.

[24] Steele, K.M., Rozumalski, A. & Schwartz, M.H. 2015 Muscle synergies and complexity of neuromuscular control during gait in cerebral palsy. *Developmental Medicine & Child Neurology* **57**, 1176-1182.

[25] Uchida, T.K., Seth, A., Pouya, S., Dembia, C.L., Hicks, J.L. & Delp, S.L. 2016 Simulating Ideal Assistive Devices to Reduce the Metabolic Cost of Running. *PloS one* **11**, e0163417.

[26] Ries, A.J., Novacheck, T.F. & Schwartz, M.H. 2014 A data driven model for optimal orthosis selection in children with cerebral palsy. *Gait & posture* **40**, 539-544.

[27] Maus, H.-M., Revzen, S., Guckenheimer, J., Ludwig, C., Reger, J. & Seyfarth, A. 2015 Constructing predictive models of human running. *Journal of The Royal Society Interface* **12**, 20140899.

[28] Wang, W.-X., Lai, Y.-C. & Grebogi, C. 2016 Data based identification and prediction of nonlinear and complex dynamical systems. *Physics Reports* **644**, 1-76.

[29] Kerkum, Y.L., Buizer, A.I., van den Noort, J.C., Becher, J.G., Harlaar, J. & Brehm, M.-A. 2015 The effects of varying ankle foot orthosis stiffness on gait in children with spastic cerebral palsy who walk with excessive knee flexion. *PloS one* **10**, e0142878.

[30] Clever, D. & Mombaur, K. 2014 A new template model for optimization studies of human walking on different terrains. In *2014 IEEE-RAS International Conference on Humanoid Robots* (pp. 500-505, IEEE.

[31] Chen, Y.-M. & Posa, M. 2020 Optimal reduced-order modeling of bipedal locomotion. In *2020 IEEE International Conference on Robotics and Automation (ICRA)* (pp. 8753-8760, IEEE.

[32] Davoodi, A., Mohseni, O., Seyfarth, A. & Sharbafi, M.A. 2019 From template to anchors: transfer of virtual pendulum posture control balance template to adaptive neuromuscular gait model increases walking stability. *Royal Society open science* **6**, 181911.

[33] Full, R.J. & Koditschek, D.E. 1999 Templates and anchors: neuromechanical hypotheses of legged locomotion on land. *Journal of experimental biology* **202**, 3325-3332.

[34] McGeer, T. 1990 Passive dynamic walking. *I. J. Robotic Res.* **9**, 62-82.

[35] Sawicki, G.S. & Ferris, D.P. 2008 Mechanics and energetics of level walking with powered ankle exoskeletons. *Journal of Experimental Biology* **211**, 1402-1413.

[36] Farris, D.J., Hampton, A., Lewek, M.D. & Sawicki, G.S. 2015 Revisiting the mechanics and energetics of walking in individuals with chronic hemiparesis following stroke: from individual limbs to lower limb joints. *Journal of neuroengineering and rehabilitation* **12**, 1-12.

[37] Sawicki, G.S. & Khan, N.S. 2016 A Simple Model to Estimate Plantarflexor Muscle–Tendon Mechanics and Energetics During Walking With Elastic Ankle Exoskeletons. *IEEE Transactions on Biomedical Engineering* **63**, 914-923.

[38] Steele, K.M., Jackson, R.W., Shuman, B.R. & Collins, S.H. 2017 Muscle recruitment and coordination with an ankle exoskeleton. *Journal of biomechanics* **59**, 50-58.

[39] Owen, E. 2010 The importance of being earnest about shank and thigh kinematics especially when using ankle-foot orthoses. *Prosthetics and orthotics international* **34**, 254-269.

[40] Hegarty, A.K., Petrella, A.J., Kurz, M.J. & Silverman, A.K. 2016 Evaluating the Effects of Ankle Foot Orthosis Mechanical Property Assumptions on Gait Simulation Muscle Force Results. *Journal of Biomechanical Engineering*.

[41] Brunner, R., Meier, G. & Ruepp, T. 1998 Comparison of a stiff and a spring-type ankle-foot orthosis to improve gait in spastic hemiplegic children. *Journal of Pediatric Orthopaedics* **18**, 719-726.

[42] Choi, H., Peters, K.M., MacConnell, M.B., Ly, K.K., Eckert, E.S. & Steele, K.M. 2017 Impact of ankle foot orthosis stiffness on Achilles tendon and gastrocnemius function during unimpaired gait. *Journal of biomechanics* **64**, 145-152.

[43] Harper, N.G., Esposito, E.R., Wilken, J.M. & Neptune, R.R. 2014 The influence of ankle-foot orthosis stiffness on walking performance in individuals with lower-limb impairments. *Clinical Biomechanics* **29**, 877-884.

[44] Waterval, N.F., Nollet, F., Harlaar, J. & Brehm, M.-A. 2019 Modifying ankle foot orthosis stiffness in patients with calf muscle weakness: gait responses on group and individual level. *Journal of NeuroEngineering and Rehabilitation* **16**, 1-9.

[45] Jackson, R.W. & Collins, S.H. 2015 An experimental comparison of the relative benefits of work and torque assistance in ankle exoskeletons. *Journal of applied physiology* **119**, 541-557.

[46] Jacobs, D.A., Koller, J.R., Steele, K.M. & Ferris, D.P. 2018 Motor modules during adaptation to walking in a powered ankle exoskeleton. *Journal of neuroengineering and rehabilitation* **15**, 2.

[47] Koller, J.R., Remy, C.D. & Ferris, D.P. 2018 Biomechanics and energetics of walking in powered ankle exoskeletons using myoelectric control versus mechanically intrinsic control. *Journal of neuroengineering and rehabilitation* **15**, 42.

[48] Brehm, M.-A., Harlaar, J. & Schwartz, M. 2008 Effect of ankle-foot orthoses on walking efficiency and gait in children with cerebral palsy. *Journal of rehabilitation medicine* **40**, 529-534.

[49] Christensen, D., Van Naarden Braun, K., Doernberg, N.S., Maenner, M.J., Arneson, C.L., Durkin, M.S., Benedict, R.E., Kirby, R.S., Wingate, M.S. & Fitzgerald, R. 2014 Prevalence of cerebral palsy, co-occurring autism spectrum disorders, and motor functioning–A utism and D evelopmental D isabilities M onitoring N etwork, USA, 2008. *Developmental Medicine & Child Neurology* **56**, 59-65.

[50] Figueiredo, E.M., Ferreira, G.B., Moreira, R.C.M., Kirkwood, R.N. & Fetters, L. 2008 Efficacy of ankle-foot orthoses on gait of children with cerebral palsy: systematic review of literature. *Pediatric Physical Therapy* **20**, 207-223.

[51] Totah, D., Menon, M., Jones-Hershinow, C., Barton, K. & Gates, D.H. 2019 The impact of ankle-foot orthosis stiffness on gait: A systematic literature review. *Gait & posture*.

[52] Graham, H.K., Rosenbaum, P., Paneth, N., Dan, B., Lin, J.-P., Damiano, D.L., Becher, J.G., Gaebler-Spira, D., Colver, A., Reddihough, D.S., et al. 2016 Cerebral palsy. *Nature Reviews Disease Primers* **2**, 15082. (doi:10.1038/nrdp.2015.82).

[53] Waters, R.L. & Mulroy, S. 1999 The energy expenditure of normal and pathologic gait. *Gait & posture* **9**, 207-231.

[54] Wren, T.A., Rethlefsen, S. & Kay, R.M. 2005 Prevalence of specific gait abnormalities in children with cerebral palsy: influence of cerebral palsy subtype, age, and previous surgery. *Journal of Pediatric Orthopaedics* **25**, 79-83.

[55] Lerner, Z.F., Harvey, T.A. & Lawson, J.L. 2019 A Battery-Powered Ankle Exoskeleton Improves Gait Mechanics in a Feasibility Study of Individuals with Cerebral Palsy. *Annals of biomedical engineering* **47**, 1345-1356.

[56] Mooney, L.M., Rouse, E.J. & Herr, H.M. 2014 Autonomous exoskeleton reduces metabolic cost of human walking during load carriage. *Journal of neuroengineering and rehabilitation* **11**, 80.

[57] Faraji, S., Wu, A.R. & Ijspeert, A.J. 2018 A simple model of mechanical effects to estimate metabolic cost of human walking. *Scientific reports* **8**, 1-12.

[58] Bauby, C.E. & Kuo, A.D. 2000 Active control of lateral balance in human walking. *Journal of biomechanics* **33**, 1433-1440.

[59] Donelan, J.M., Kram, R. & Kuo, A.D. 2002 Mechanical work for step-to-step transitions is a major determinant of the metabolic cost of human walking. *Journal of Experimental Biology* **205**, 3717-3727.

[60] Dean, J.C., Alexander, N.B. & Kuo, A.D. 2007 The effect of lateral stabilization on walking in young and old adults. *IEEE Transactions on Biomedical Engineering* **54**, 1919-1926.

[61] Hof, A., Gazendam, M. & Sinke, W. 2005 The condition for dynamic stability. *Journal of biomechanics* **38**, 1-8.

[62] Zajac, F.E., Neptune, R.R. & Kautz, S.A. 2002 Biomechanics and muscle coordination of human walking: Part I: Introduction to concepts, power transfer, dynamics and simulations. *Gait & posture* **16**, 215-232.

[63] Neptune, R.R., Clark, D.J. & Kautz, S.A. 2009 Modular control of human walking: a simulation study. *Journal of biomechanics* **42**, 1282-1287.

[64] Clark, D.J., Ting, L.H., Zajac, F.E., Neptune, R.R. & Kautz, S.A. 2010 Merging of Healthy Motor Modules Predicts Reduced Locomotor Performance and Muscle Coordination Complexity Post-Stroke. *Journal of Neurophysiology* **103**, 844-857. (doi:10.1152/jn.00825.2009).

[65] Umberger, B.R., Gerritsen, K.G. & Martin, P.E. 2003 A model of human muscle energy expenditure. *Computer methods in biomechanics and biomedical engineering* **6**, 99-111.

[66] Ackermann, M. & van den Bogert, A.J. 2010 Optimality principles for model-based prediction of human gait. *Journal of biomechanics* **43**, 1055-1060.

[67] Handsfield, G.G., Meyer, C.H., Abel, M.F. & Blemker, S.S. 2016 Heterogeneity of muscle sizes in the lower limbs of children with cerebral palsy. *Muscle & nerve* **53**, 933-945.

[68] Samadi, B., Achiche, S., Parent, A., Ballaz, L., Chouinard, U. & Raison, M. 2016 Custom sizing of lower limb exoskeleton actuators using gait dynamic modelling of children with cerebral palsy. *Computer methods in biomechanics and biomedical engineering* **19**, 1519-1524.

[69] Mehrabi, N., Schwartz, M.H. & Steele, K.M. 2019 Can altered muscle synergies control unimpaired gait? *Journal of biomechanics* **90**, 84-91.

[70] Delp, S.L., Anderson, F.C., Arnold, A.S., Loan, P., Habib, A., John, C.T., Guendelman, E. & Thelen, D.G. 2007 OpenSim: open-source software to create and analyze dynamic simulations of movement. *IEEE transactions on biomedical engineering* **54**, 1940-1950.

[71] Alexander, R.M. 1995 Simple models of human movement.

[72] Kuo, A.D. 2007 The six determinants of gait and the inverted pendulum analogy: A dynamic walking perspective. *Human movement science* **26**, 617-656.

[73] Kuo, A.D. 2002 Energetics of actively powered locomotion using the simplest walking model. *Journal of biomechanical engineering* **124**, 113-120.

[74] Srinivasan, M. & Ruina, A. 2006 Computer optimization of a minimal biped model discovers walking and running. *Nature* **439**, 72.

[75] Holmes, P., Full, R.J., Koditschek, D. & Guckenheimer, J. 2006 The dynamics of legged locomotion: Models, analyses, and challenges. *SIAM review* **48**, 207-304.

[76] Geyer, H., Seyfarth, A. & Blickhan, R. 2006 Compliant leg behaviour explains basic dynamics of walking and running. *Proceedings of the Royal Society B: Biological Sciences* **273**, 2861-2867.

[77] Anand, M., Seipel, J. & Rietdyk, S. 2017 A modelling approach to the dynamics of gait initiation. *Journal of The Royal Society Interface* **14**, 20170043.

[78] Guckenheimer, J. & Holmes, P. 2013 *Nonlinear Oscillations, Dynamical Systems, and Bifurcations of Vector Fields*, Springer New York.

[79] Wang, Y. & Srinivasan, M. System identification and stability analyses of steady human locomotion. *Foot* **300**, 600.

[80] Ankaralı, M.M., Sefati, S., Madhav, M.S., Long, A., Bastian, A.J. & Cowan, N.J. 2015 Walking dynamics are symmetric (enough). *Journal of the Royal Society Interface* **12**, 20150209.

[81] Bernstein, N. 1966 The co-ordination and regulation of movements. *The co-ordination and regulation of movements*.

[82] Cavagna, G.A., Thys, H. & Zamboni, A. 1976 The sources of external work in level walking and running. *The Journal of physiology* **262**, 639-657.

[83] Falisse, A., Serrancolí, G., Dembia, C.L., Gillis, J., Jonkers, I. & De Groote, F. 2019 Rapid predictive simulations with complex musculoskeletal models suggest that diverse healthy and pathological human gaits can emerge from similar control strategies. *Journal of the Royal Society Interface* **16**, 20190402.

[84] Inman, V.T. & Eberhart, H.D. 1953 The major determinants in normal and pathological gait. *JBJS* **35**, 543-558.

[85] Bregman, D., Van der Krogt, M., De Groot, V., Harlaar, J., Wisse, M. & Collins, S. 2011 The effect of ankle foot orthosis stiffness on the energy cost of walking: a simulation study. *Clinical Biomechanics* **26**, 955-961.

[86] Meyer, A.J., Patten, C. & Fregly, B.J. 2017 Lower extremity EMG-driven modeling of walking with automated adjustment of musculoskeletal geometry. *PloS one* **12**, e0179698.

[87] Garcia, M., Chatterjee, A., Ruina, A. & Coleman, M. 1998 The simplest walking model: stability, complexity, and scaling.

[88] Holt, K.G., Fonseca, S.T. & LaFiandra, M.E. 2000 The dynamics of gait in children with spastic hemiplegic cerebral palsy: theoretical and clinical implications. *Human Movement Science* **19**, 375-405.

[89] Holt, K.G., Hamill, J. & Andres, R.O. 1990 The force-driven harmonic oscillator as a model for human locomotion. *Human Movement Science* **9**, 55-68.

[90] Chau, T. 2001 A review of analytical techniques for gait data. Part 2: neural network and wavelet methods. *Gait & posture* **13**, 102-120.

[91] Floquet, G. 1883 Sur les équations différentielles linéaires à coefficients périodiques. In *Annales scientifiques de l'École normale supérieure* (pp. 47-88.

[92] Revzen, S. & Kvalheim, M. 2015 *Data driven models of legged locomotion*, SPIE.

[93] Brunton, S.L. & Kutz, J.N. 2019 *Data-driven science and engineering: Machine learning, dynamical systems, and control*, Cambridge University Press.

[94] Hartman, P. 2002 *Ordinary differential equations*. 2nd ed. ed. Philadelphia, Philadelphia : Society for Industrial and Applied Mathematics.

[95] Drnach, L., Allen, J.L., Essa, I. & Ting, L.H. 2019 A Data-Driven Predictive Model of Individual-Specific Effects of FES on Human Gait Dynamics. In *2019 International Conference on Robotics and Automation (ICRA)* (pp. 5090-5096, IEEE.

[96] Burden, S.A., Revzen, S. & Sastry, S.S. 2015 Model reduction near periodic orbits of hybrid dynamical systems. *IEEE Transactions on Automatic Control* **60**, 2626-2639.

[97] Revzen, S. & Guckenheimer, J.M. 2011 Finding the dimension of slow dynamics in a rhythmic system. *Journal of The Royal Society Interface* **9**, 957-971.

[98] Kutz, J.N., Brunton, S.L., Brunton, B.W. & Proctor, J.L. 2016 *Dynamic mode decomposition: data-driven modeling of complex systems*, SIAM.

[99] Proctor, J.L., Brunton, S.L. & Kutz, J.N. 2016 Dynamic mode decomposition with control. *SIAM Journal on Applied Dynamical Systems* **15**, 142-161.

[100] Lee, D.D. & Seung, H.S. 1999 Learning the parts of objects by non-negative matrix factorization. *Nature* **401**, 788.

[101] Ting, L.H., Chiel, H.J., Trumbower, R.D., Allen, J.L., McKay, J.L., Hackney, M.E. & Kesar, T.M. 2015 Neuromechanical principles underlying movement modularity and their implications for rehabilitation. *Neuron* **86**, 38-54.

[102] Schwartz, M.H. & Rozumalski, A. 2008 The Gait Deviation Index: a new comprehensive index of gait pathology. *Gait & posture* **28**, 351-357.

[103] Rose, J., Gamble, J.G., Medeiros, J., Burgos, A. & Haskell, W.L. 1989 Energy cost of walking in normal children and in those with cerebral palsy: comparison of heart rate and oxygen uptake. *Journal of Pediatric Orthopaedics* **9**, 276-279.

[104] Hicks, J.L., Schwartz, M.H., Arnold, A.S. & Delp, S.L. 2008 Crouched postures reduce the capacity of muscles to extend the hip and knee during the single-limb stance phase of gait. *Journal of biomechanics* **41**, 960-967.

[105] Perry, J., Antonelli, D. & Ford, W. 1975 Analysis of knee-joint forces during flexed-knee stance. *J Bone Joint surg am* **57**, 961-967.

[106] Steele, K.M., Seth, A., Hicks, J.L., Schwartz, M.H. & Delp, S.L. 2013 Muscle contributions to vertical and fore-aft accelerations are altered in subjects with crouch gait. *Gait & posture* **38**, 86-91.

[107] Bregman, D., Rozumalski, A., Koops, D., De Groot, V., Schwartz, M. & Harlaar, J. 2009 A new method for evaluating ankle foot orthosis characteristics: BRUCE. *Gait & posture* **30**, 144-149.

[108] Harrington, E.D., Lin, R.S. & Gage, J. 1984 Use of the anterior floor reaction orthosis in patients with cerebral palsy. *Ortho Prosthet* **37**, 34-42.3734.

[109] Wren, T.A., Dryden, J.W., Mueske, N.M., Dennis, S.W., Healy, B.S. & Rethlefsen, S.A. 2015 Comparison of 2 orthotic approaches in children with cerebral palsy. *Pediatric Physical Therapy* **27**, 218-226.

[110] Maltais, D., Bar-Or, O., Galea, V. & Pierrynowski, M. 2001 Use of orthoses lowers the O (2) cost of walking in children with spastic cerebral palsy. *Medicine and science in sports and exercise* **33**, 320-325.

[111] Schwartz, M.H., Viehweger, E., Stout, J., Novacheck, T.F. & Gage, J.R. 2004 Comprehensive treatment of ambulatory children with cerebral palsy: an outcome assessment. *Journal of Pediatric Orthopaedics* **24**, 45-53.

[112] Browning, R.C., Modica, J.R., Kram, R. & Goswami, A. 2007 The effects of adding mass to the legs on the energetics and biomechanics of walking. *Medicine and science in sports and exercise* **39**, 515.

[113] Lamarra, N., Whipp, B.J., Ward, S.A. & Wasserman, K. 1987 Effect of interbreath fluctuations on characterizing exercise gas exchange kinetics. *Journal of Applied Physiology* **62**, 2003-2012.

[114] Turner, D.L. 1991 Cardiovascular and respiratory control mechanisms during exercise: an integrated view. *Journal of Experimental Biology* **160**, 309-340.

[115] Steele, K.M., Seth, A., Hicks, J.L., Schwartz, M.S. & Delp, S.L. 2010 Muscle contributions to support and progression during single-limb stance in crouch gait. *Journal of biomechanics* **43**, 2099-2105.

[116] Liu, M.Q., Anderson, F.C., Schwartz, M.H. & Delp, S.L. 2008 Muscle contributions to support and progression over a range of walking speeds. *Journal of biomechanics* **41**, 3243-3252.

[117] Steele, K.M., DeMers, M.S., Schwartz, M.H. & Delp, S.L. 2012 Compressive tibiofemoral force during crouch gait. *Gait & posture* **35**, 556-560.

[118] Delp, S.L., Loan, J.P., Hoy, M.G., Zajac, F.E., Topp, E.L. & Rosen, J.M. 1990 An interactive graphics-based model of the lower extremity to study orthopaedic surgical procedures. *IEEE Transactions on Biomedical engineering* **37**, 757-767.

[119] Hicks, J.L., Uchida, T.K., Seth, A., Rajagopal, A. & Delp, S.L. 2015 Is my model good enough? Best practices for verification and validation of musculoskeletal models and simulations of movement. *Journal of biomechanical engineering* **137**, 020905.

[120] Thelen, D.G. & Anderson, F.C. 2006 Using computed muscle control to generate forward dynamic simulations of human walking from experimental data. *Journal of biomechanics* **39**, 1107-1115.

[121] Summa, A., Vannozzi, G., Bergamini, E., Iosa, M., Morelli, D. & Cappozzo, A. 2016 Multilevel Upper Body Movement Control during Gait in Children with Cerebral Palsy. *PloS one* **11**, e0151792.

[122] Meyns, P., Molenaers, G., Duysens, J. & Jonkers, I. 2017 The Differential Effect of Arm Movements during Gait on the Forward Acceleration of the Centre of Mass in Children with Cerebral Palsy and Typically Developing Children. *Frontiers in Human Neuroscience* **11**.

[123] Griffin, T.M., Roberts, T.J. & Kram, R. 2003 Metabolic cost of generating muscular force in human walking: insights from load-carrying and speed experiments. *Journal of Applied Physiology* **95**, 172-183.

[124] Hof, A.L. 1996 Scaling gait data to body size. *Gait & posture* **3**, 222-223.

[125] Crowninshield, R.D. & Brand, R.A. 1981 A physiologically based criterion of muscle force prediction in locomotion. *Journal of biomechanics* **14**, 793-801.

[126] Silder, A., Besier, T. & Delp, S.L. 2012 Predicting the metabolic cost of incline walking from muscle activity and walking mechanics. *Journal of biomechanics* **45**, 1842-1849.

[127] Kerkum, Y.L., Harlaar, J., Buizer, A.I., van den Noort, J.C., Becher, J.G. & Brehm, M.-A. 2016 An individual approach for optimizing ankle-foot orthoses to improve mobility in children with spastic cerebral palsy walking with excessive knee flexion. *Gait & posture* **46**, 104-111.

[128] Harlaar, J., Brehm, M., Becher, J.G., Bregman, D.J., Buurke, J., Holtkamp, F., De Groot, V. & Nollet, F. 2010 Studies examining the efficacy of ankle foot orthoses should report activity level and mechanical evidence. *Prosthetics and orthotics international* **34**, 327-335.

[129] Royer, T.D. & Martin, P.E. 2005 Manipulations of leg mass and moment of inertia: effects on energy cost of walking. *Medicine and science in sports and exercise* **37**, 649-656.

[130] Fowler, E.G., Staudt, L.A. & Greenberg, M.B. 2010 Lower-extremity selective voluntary motor control in patients with spastic cerebral palsy: increased distal motor impairment. *Developmental Medicine & Child Neurology* **52**, 264-269.

[131] Hsu, A.-T., Perry, J., Gronley, J.K. & Hislop, H.J. 1993 Quadriceps force and myoelectric activity during flexed knee stance. *Clinical orthopaedics and related research* **288**, 254-262.

[132] Hicks, J.L., Delp, S.L. & Schwartz, M.H. 2011 Can biomechanical variables predict improvement in crouch gait? *Gait & posture* **34**, 197-201.

[133] Hoang, H.X. & Reinbolt, J.A. 2012 Crouched posture maximizes ground reaction forces generated by muscles. *Gait & posture* **36**, 405-408.

[134] Arnold, A.S., Liu, M.Q., Schwartz, M.H., Õunpuu, S., Dias, L.S. & Delp, S.L. 2006 Do the hamstrings operate at increased muscle–tendon lengths and velocities after surgical lengthening? *Journal of biomechanics* **39**, 1498-1506.

[135] Gordon, K.E. & Ferris, D.P. 2007 Learning to walk with a robotic ankle exoskeleton. *Journal of biomechanics* **40**, 2636-2644.

[136] Arnold, E.M., Hamner, S.R., Seth, A., Millard, M. & Delp, S.L. 2013 How muscle fiber lengths and velocities affect muscle force generation as humans walk and run at different speeds. *The Journal of Experimental Biology* **216**, 2150-2160. (doi:10.1242/jeb.075697).

[137] Hicks, J., Arnold, A., Anderson, F., Schwartz, M. & Delp, S. 2006 Tibial torsion reduces the capacity of muscles to extend the hip and knee during single limb stance. *Gait & Posture* **24**, S99-S101.

[138] Ding, Y., Kim, M., Kuindersma, S. & Walsh, C.J. 2018 Human-in-the-loop optimization of hip assistance with a soft exosuit during walking. *Science Robotics* **3**, eaar5438.

[139] Åström, K.J. & Murray, R.M. 2010 *Feedback systems: an introduction for scientists and engineers*, Princeton university press.

[140] Rosenberg, M. & Steele, K.M. 2017 Simulated impacts of ankle foot orthoses on muscle demand and recruitment in typically-developing children and children with cerebral palsy and crouch gait. *PloS one* **12**, e0180219.

[141] Selinger, J.C., Wong, J.D., Simha, S.N. & Donelan, J.M. 2019 How humans initiate energy optimization and converge on their optimal gaits. *Journal of Experimental Biology* **222**, jeb198234.

[142] Chisholm, A.E. & Perry, S.D. 2012 Ankle-foot orthotic management in neuromuscular disorders: recommendations for future research. *Disability and Rehabilitation: Assistive Technology* **7**, 437-449.

[143] Jackson, R.W., Dembia, C.L., Delp, S.L. & Collins, S.H. 2017 Muscle–tendon mechanics explain unexpected effects of exoskeleton assistance on metabolic rate during walking. *Journal of Experimental Biology* **220**, 2082-2095.

[144] Revzen, S. & Guckenheimer, J.M. 2008 Estimating the phase of synchronized oscillators. *Physical Review E* **78**, 051907.

[145] Wong, J.D., Selinger, J.C. & Donelan, J.M. 2019 Is natural variability in gait sufficient to initiate spontaneous energy optimization in human walking? *Journal of neurophysiology* **121**, 1848-1855.

[146] Kadaba, M.P., Ramakrishnan, H. & Wootten, M. 1990 Measurement of lower extremity kinematics during level walking. *Journal of orthopaedic research* **8**, 383-392.

[147] Hermens, H.J., Freriks, B., Merletti, R., Stegeman, D., Blok, J., Rau, G., Disselhorst-Klug, C. & Hägg, G. 1999 European recommendations for surface electromyography. *Roessingh research and development* **8**, 13-54.

[148] Rajagopal, A., Dembia, C.L., DeMers, M.S., Delp, D.D., Hicks, J.L. & Delp, S.L. 2016 Full-body musculoskeletal model for muscle-driven simulation of human gait. *IEEE transactions on biomedical engineering* **63**, 2068-2079.

[149] Villarreal, D.J., Poonawala, H.A. & Gregg, R.D. 2016 A robust parameterization of human gait patterns across phase-shifting perturbations. *IEEE Transactions on Neural Systems and Rehabilitation Engineering* **25**, 265-278.

[150] Revzen, S. 2020 BIRDS Lab mathmisc. (GitHub).

[151] Glorot, X. & Bengio, Y. 2010 Understanding the difficulty of training deep feedforward neural networks. In *Proceedings of the thirteenth international conference on artificial intelligence and statistics* (pp. 249-256.

[152] LeCun, Y., Bengio, Y. & Hinton, G. 2015 Deep learning. *nature* **521**, 436-444.

[153] Zajac, F.E. 1989 Muscle and tendon: properties, models, scaling, and application to biomechanics and motor control. *Critical reviews in biomedical engineering* **17**, 359-411.

[154] Carter, G.C. 1987 Coherence and time delay estimation. *Proceedings of the IEEE* **75**, 236-255.

[155] Glantz, S. 2012 Primer of Biostatistics, 7th edn, pp. 65–67. (New York: McGraw-Hill.

[156] Martelli, S., Calvetti, D., Somersalo, E. & Viceconti, M. 2015 Stochastic modelling of muscle recruitment during activity. *Interface focus* **5**, 20140094.

[157] Brunton, S.L., Proctor, J.L. & Kutz, J.N. 2016 Discovering governing equations from data by sparse identification of nonlinear dynamical systems. *Proceedings of the National Academy of Sciences* **113**, 3932-3937.

[158] Allen, J.L. & Ting, L.H. 2016 Why is neuromechanical modeling of balance and locomotion so hard? In *Neuromechanical Modeling of Posture and Locomotion* (pp. 197-223, Springer.

[159] Veerkamp, K., Schallig, W., Harlaar, J., Pizzolato, C., Carty, C.P., Lloyd, D.G. & van der Krogt, M.M. 2019 The effects of electromyography-assisted modelling in estimating musculotendon forces during gait in children with cerebral palsy. *Journal of biomechanics* **92**, 45-53.

[160] Cavagna, G.A., Heglund, N.C. & Taylor, C.R. 1977 Mechanical work in terrestrial locomotion: two basic mechanisms for minimizing energy expenditure. *American Journal of Physiology-Regulatory, Integrative and Comparative Physiology* **233**, R243-R261.

[161] Mochon, S. & McMahon, T.A. 1980 Ballistic walking. *Journal of biomechanics* **13**, 49-57.

[162] Kuo, A.D. 1999 Stabilization of Lateral Motion in Passive Dynamic Walking. *The International Journal of Robotics Research* **18**, 917-930. (doi:10.1177/02783649922066655).

[163] Antoniak, G., Biswas, T., Cortes, N., Sikdar, S., Chun, C. & Bhandawat, V. 2019 Spring-loaded inverted pendulum goes through two contraction-extension cycles during the single-support phase of walking. *Biology open* **8**.

[164] Lipfert, S.W., Günther, M., Renjewski, D., Grimmer, S. & Seyfarth, A. 2012 A model-experiment comparison of system dynamics for human walking and running. *Journal of theoretical biology* **292**, 11-17.

[165] Maus, H.-M., Lipfert, S., Gross, M., Rummel, J. & Seyfarth, A. 2010 Upright human gait did not provide a major mechanical challenge for our ancestors. *Nature communications* **1**, 1-6.

[166] Buczek, F.L., Cooney, K.M., Walker, M.R., Rainbow, M.J., Concha, M.C. & Sanders, J.O. 2006 Performance of an inverted pendulum model directly applied to normal human gait. *Clinical Biomechanics* **21**, 288-296.

[167] Donelan, J.M., Shipman, D.W., Kram, R. & Kuo, A.D. 2004 Mechanical and metabolic requirements for active lateral stabilization in human walking. *Journal of biomechanics* **37**, 827-835.

[168] Dingwell, J.B. & Cusumano, J.P. 2019 Humans use multi-objective control to regulate lateral foot placement when walking. *PLoS computational biology* **15**, e1006850.

[169] Fonseca, S.r.T., Holt, K.G., Fetters, L. & Saltzman, E. 2004 Dynamic resources used in ambulation by children with spastic hemiplegic cerebral palsy: relationship to kinematics, energetics, and asymmetries. *Physical Therapy* **84**, 344-354.

[170] Kim, S. & Park, S. 2011 Leg stiffness increases with speed to modulate gait frequency and propulsion energy. *Journal of Biomechanics* **44**, 1253-1258. (doi:https://doi.org/10.1016/j.jbiomech.2011.02.072).

[171] Anderson, D. & Burnham, K. 2004 Model selection and multi-model inference. *Second. NY: Springer-Verlag* **63**.

[172] Rosenberg, M.C., Banjanin, B.S., Burden, S.A. & Steele, K.M. 2020 Predicting walking response to ankle exoskeletons using data-driven models. *Journal of the Royal Society Interface* **17**, 20200487.

[173] Akaike, H. 1974 A new look at the statistical model identification. In *Selected Papers of Hirotugu Akaike* (pp. 215-222, Springer.

[174] Donelan, J.M., Kram, R. & Kuo, A.D. 2002 Simultaneous positive and negative external mechanical work in human walking. *Journal of biomechanics* **35**, 117-124.

[175] Lee, C.R. & Farley, C.T. 1998 Determinants of the center of mass trajectory in human walking and running. *Journal of experimental biology* **201**, 2935-2944.

[176] Farris, D.J. & Sawicki, G.S. 2012 The mechanics and energetics of human walking and running: a joint level perspective. *Journal of The Royal Society Interface* **9**, 110-118.

[177] Pandy, M.G., Lin, Y.-C. & Kim, H.J. 2010 Muscle coordination of mediolateral balance in normal walking. *Journal of Biomechanics* **43**, 2055-2064. (doi:http://dx.doi.org/10.1016/j.jbiomech.2010.04.010).

[178] Kim, M. & Collins, S.H. 2013 Stabilization of a three-dimensional limit cycle walking model through step-to-step ankle control. In *Rehabilitation Robotics (ICORR), 2013 IEEE International Conference on* (pp. 1-6, IEEE.

[179] Liepe, J., Filippi, S., Komorowski, M. & Stumpf, M.P. 2013 Maximizing the information content of experiments in systems biology. *PLoS Comput Biol* **9**, e1002888.

[180] Cybenko, G. 1989 Approximation by superpositions of a sigmoidal function. *Mathematics of control, signals and systems* **2**, 303-314.

[181] Hespanha, J.P. 2018 *Linear systems theory*, Princeton university press.

[182] Kelley, K. & Preacher, K.J. 2012 On effect size. *Psychological methods* **17**, 137.

APPENDIX A: CHAPTER 4 SUPPLEMENTARY MATERIAL

A1. **SUPPLEMENTAL S1** – EXPERIMENTAL PROTOCOL AND METHODOLOGICAL DETAILS

This document provides additional details of the experimental setup and additional information to facilitate replication of our work. The following sections discuss:

I. Experimental setup

II. Computing joint kinematics, and estimating exoskeleton torque

III. Model algorithms and explanations of the processing pipeline

IV. Additional information on prediction accuracy evaluation

A1.1 Experimental setup

A1.1.1 Marker and electromyography recordings

We used a modified Helen Hayes marker set for motion capture and placed electromyography (EMG) sensors (Delsys Inc, Natick USA) according to SENIAM guidelines [146, 147]. The EMG sensors were placed bilaterally on the gluteus medius, rectus femoris, vastus medialis, biceps femoris, medial gastrocnemius, soleus, and tibialis anterior. Marker trajectories were collected using a 10-camera infrared motion capture system (Qualisys AB, Göteborg, SE). Participants walked on an instrumented split-belt treadmill (Bertec Inc, Columbus OH) and were instructed to walk naturally. Marker trajectories were sampled at 120Hz and EMG data were sampled at 2000Hz. All data were downsampled to 120Hz before exporting for processing and analysis.

A1.2 Data preprocessing

A1.2.1 Computing joint kinematics

Marker trajectories were low-pass filtered at 6 Hz using a fourth-order zero-lag Butterworth filter. We converted marker trajectories to joint kinematics using OpenSim 3.3 [70]. First, we scaled a generic 29 degree-of-freedom skeletal model to each participant's skeletal geometry [148]. The subtalar, metatarsophalangeal, wrist flexion, and wrist deviation degrees of freedom were locked. We ensured that root-mean-squared marker errors were less than 1 cm and maximum marker errors were less than 2 cm. Joint kinematics were then computed using OpenSim's inverse kinematics algorithm. The inverse kinematics algorithm identifies joint angle trajectories to minimize error between model markers, which are fixed on rigid body segments of the model, and the experimental marker trajectories. The knee joint range of motion was increased to permit up to five degrees of hyperextension for participants who appeared to hyperextend their knee during

walking. We evaluated model quality using experimental marker errors, in line with best-practices [119]. Root-mean-squared marker errors were less than 2 cm and maximum marker errors were less than 4 cm for each trial.

A1.2.2 Estimating exoskeleton torque profiles

For a passive exoskeleton, the torque, τ_{exo}, depended approximately linearly on the user's ankle kinematics, θ_{ankle}, exoskeleton equilibrium angle, θ_{eq}, and exoskeleton's rotational stiffness, k_{exo} (equation A1.1) as:

$$\tau_{\mathrm{exo}}(\mathrm{t}) = \begin{cases} -\mathrm{k}_{\mathrm{exo}}\left(\theta_{ankle}(t) - \theta_{eq}\right), & \theta_{ankle} \geq \theta_{eq} \\ 0 & \theta_{ankle} < \theta_{eq} \end{cases} \quad \text{(A1.1)}$$

Unlike many clinical exoskeletons, whose torque profiles are smooth functions of ankle angle, torque in the exoskeletons used in this work were piecewise-smooth functions of ankle angle, providing plantarflexion assistance similar to other experimental devices (Figure 4.2) [9, 39].

The linear approximation in Eqn A1.2 was deemed sufficient based on calibration trials with pilot datasets, during which tension load cells (Omega Engineering, Norwalk, CT) were attached in series to each exoskeleton spring (equation A1.2). The measured torque from the load cell, τ_{exo}, was,

$$\tau_{\mathrm{exo}}(\mathrm{t}) = \vec{r}_{\mathrm{ma}}(\mathrm{t}) \times \left[-k_{sp}\left(\vec{l}_{pd}(t) - l_{eq}\right)\right], \quad \text{(A1.2)}$$

where l_{pd} is the distance the proximal and distal spring attachment points, and l_{eq} is the equilibrium length of the spring cable, which we estimated by having the subject dorsiflex until they felt the spring engage with the exoskeleton raised off the ground. The spring stiffness is denoted by k_{sp}. The cross product of the spring force vector and the vector between the moment arm at the distal end of the spring cable and the exoskeleton ankle joint, r_{ma}, defined the exoskeleton torque. Preliminary analyses showed small differences between torque profiles estimated from the nonlinear torque-ankle angle relationship (equation A1.2) and the linear relationship (equation A1.1) that we employed in our analysis.

A1.3 Phase-varying model algorithms

We used hip flexion angles of the right and left limbs as phase variable inputs to the Phaser algorithm [144], which is similar to [149]. Phase estimates were used as the variable in the Fourier series representation of the phase-varying (PV) and linear phase-varying (LPV) models to cluster subsets of the time series data when fitting the LPV model and as inputs to the nonlinear phase-varying (NPV) model. We denoted phase as $\phi \in \mathbb{R}^{T}$, where T denotes the number of samples in the training set. Each model had N = 20 outputs. The LPV and NPV models used the same M = 80 inputs, though the NPV model also took phase as an input.

A1.3.1 Phase-varying model

The PV model, F_{pv}^{w}, is purely a function of phase and was represented in this work using a Fourier Series of order H=7 (equation. A1.3). The Fourier Series was parameterized by matrix coefficients $w_j, j \in \{1,2,\ldots,2H\}$, which were fit using a least-squares approximation of each trajectory.

$$F_{pv}^{w} = \frac{1}{2}w_0 + \sum_{h=1}^{H} w_{2h-1}\cos(h\phi) + \sum_{h=1}^{H} w_{2h}\sin(h\phi) \quad \text{(A1.3)}$$

A1.3.2 Linear phase-varying model

The LPV model is linear with respect to the inputs, $X(\phi)$, but nonlinear with respect to phase and has the form $X(\phi + \Delta) = A_{\phi,\Delta}X(\phi)$, where Δ denotes the lookahead window length. The LPV takes in a phase, ϕ, and returns affine matrices $A_{\phi,\Delta} \in \mathbb{R}^{N\times M+1}$. For 64 phases over the cycle, we fit discrete maps $A_{\phi_l,\Delta}: X(\phi_l) \rightarrow X(\phi_l + \Delta)$ using a weighted least-squares regression with a Gaussian weighting scheme to penalize samples based on proximity to the phase ϕ_l. To generate a continuous representation of the 64 discrete maps, $F_{LPV,\Delta}^{w}$, we parameterized each element of the maps using a seventh-order Fourier Series as a function of phase (equation. A1.3). We used the same least-squares approximation as with the PV model. This fitting procedure was repeated independently for each lookahead window.

A1.3.3 Nonlinear phase-varying model

The NPV model used a fully-connected three-layer feedforward neural network to represent the response to torque. The model's hidden layer was 128 units wide – greater than the number of inputs to avoid enforcing a reduced-order representation of the input-output relationships – and used a softsign activation function [151, 180]. The NPV took the 80 inputs plus phase to predict the same 20 outputs as the PV and LPV models. We implemented the NPV model in the Keras Python framework, using RMSprop gradient descent. The NPV model's hyperparameters included interconnection weights and biases.

A1.4 Evaluating model prediction accuracy

A1.4.1 Relative Remaining Variance

The Relative Remaining Variance (RRV) outcome used in this study is defined as

$$RRV = \frac{var\left(Y - \hat{Y}\right)}{var(Y)}, \tag{A1.4}$$

$$0 < RRV < \infty \tag{A1.5}$$

where *var* denotes the variance in the each output, Y denotes the test data, and $\hat{Y}$ denotes the predicted outputs. In this work $Y, \hat{Y} \in \mathbb{R}^{T \times 20}$, with ten outputs for each leg. We bootstrapped RRV values 200 times for each output and reported the average RRV values for each output.

A2. **SUPPLEMENTAL S2** – PREDICTING WALKING RESPONSE TO ANKLE EXOSKELETONS USING DATA-DRIVEN MODELS

This document provides additional theory and results supporting modeling decisions. The following sections discuss:

V. Exoskeleton stiffness and torque profiles as inputs to the phase-varying models

VI. Ground reaction force data and predicting joint dynamics

VII. Individual responses to varying prediction horizon

A2.1 Exoskeleton stiffness and torque profiles as inputs to phase-varying models

We used passive exoskeleton torque profiles, rather than stiffness as inputs to our linear and nonlinear phase-varying models. We discretized torque profiles between the initial and final phases (10 samples per leg) as inputs to the model. However, based on our fitting procedure – using multiple exoskeleton conditions to fit a single model – the models do not simply predict ankle angle purely as a function of torque.

As noted in the main manuscript, using stiffness rather than torque as a model input is possible, but lacks physical or theoretical basis, whereas torque represents the mechanical interaction between the exoskeleton and the user. Our decision to use exoskeleton torque samples was driven by the theoretical support that the future state of a discrete-time linear model, such as the linear phase-varying (LPV) model, is a linear function of the initial state and the entire input history between initial and final times [181]. Similar theory supports stiffness being insufficient as an input variable to the LPV model: While torque is a linear function of stiffness and ankle kinematics, ankle kinematics are a nonlinear function of phase, indicating that using stiffness as a model input is not equivalent to using torque as an input. However, since the nonlinear phase-varying (NPV) model may use nonlinear functions of stiffness, it is possible that using stiffness as an input would generate similarly accurate predictions to the torque-based NPV model.

We compared the prediction accuracy of stiffness-based LPV and NPV models to torque-based models using the K_2 validation condition. The torque inputs used ten time-history samples per leg, while the stiffness condition used a single constant stiffness value per exoskeleton condition as an input. We expected prediction accuracies to be lower in the stiffness-based models, due to

theoretical support against stiffness as an input and the added information in the torque samples. Indeed, The LPV model's predictions using the stiffness input were 0.16 ± 0.13 RRV points worse than with torque inputs at the ankle ($p < 0.001$) according to paired t-tests with Holm-Sidak correction for multiple comparisons at a significance level of $\alpha = 0.05$ (Figure A2.1) [155]. The NPV model was more sensitive to input type than the LPV model and its predictions were worse at the hip (0.19 ± 0.19 RRV points), knee (0.37 ± 0.21 RRV points), and ankle (0.41 ± 0.16 RRV points) when using stiffness as an input (all $p < 0.001$), compared to using torque inputs. The reduced prediction accuracy in the stiffness-based LPV and NPVs model does not support the use of stiffness as an input variable to phase-varying models.

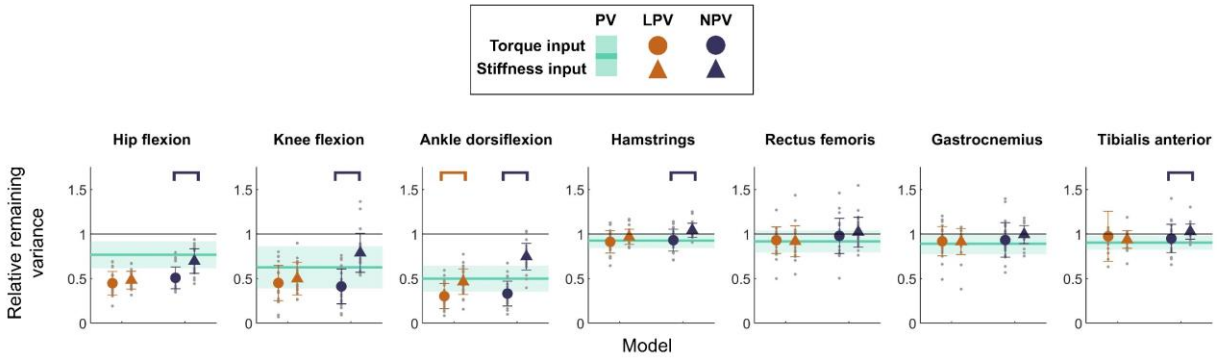

Figure A2.1. A comparison of prediction accuracies for stiffness (triangles) and torque (circles) inputs in the K_2 validation condition. Averages (±1SD) are shown for the LPV and NPV models. The PV model shows the average (±1SD) as a solid line (shaded region). The PV (green) model was agnostic to inputs and was constant across input conditions. Brackets denote significant differences between torque and stiffness prediction accuracies according to paired t-tests with Holm-Sidak correction for multiple comparisons at a significance level of $\alpha = 0.05$.

A2.2 Ground reaction force data and predicting joint dynamics

Data-driven phase-varying models can accept arbitrary input and output variables, which makes predicting GRFs or joint moments an interesting area of future research. Our dataset was inappropriate for predicting dynamic variables for two reasons:

1. Some participants frequently stepped on both belts of the split-belt treadmill with one foot, causing incorrect estimates of the center of pressure and GRFs corresponding to each leg. Sporadic inaccuracies in the GRF and center of pressure data may result in model fits and predictions being highly sensitive to which gait cycles are included in the training and validation datasets.

2. Changes in GRFs between exoskeleton conditions were small (Figure A2.2). Although we observed statistical differences ($p < 0.05$; paired t-tests) for the anterior-posterior and vertical GRFs, the differences between conditions were small: (Cohen's $d < 0.20$) for all GRF directions, and frequently less than 0.05 [182]. Moreover, the zero-stiffness baseline exoskeleton condition accounted for 99% [97.5%, 99.4%] (median [IQR]) of the variance across all GRF signals. Consequently, the LPV or NPV models' predictions would at most account for an additional three percent of the variance in the GRF data.

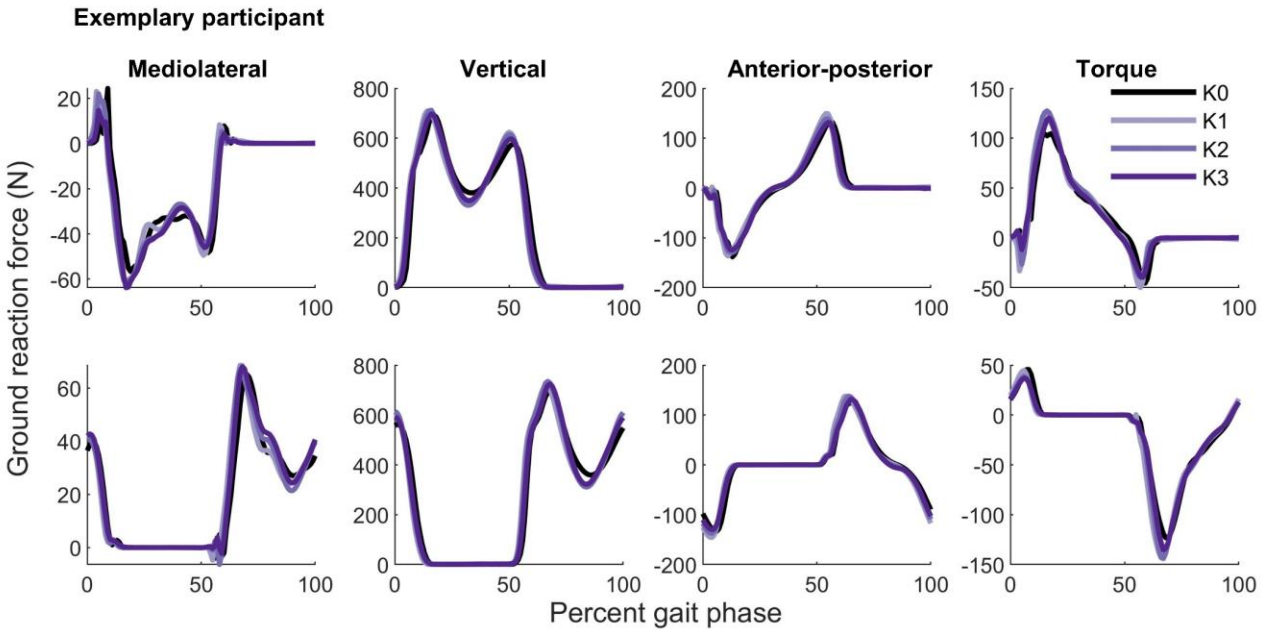

Figure A2.2. Exemplary average ground reaction force across the four exoskeleton conditions data for one participant (P03) that exhibited a large kinematic response to ankle exoskeletons. The signals represent the data averaged over all gait cycles of each condition. Other participants' ground reaction force data exhibited similar or smaller changes between exoskeleton conditions.

A2.3 Individual responses to varying prediction horizon

While average model predictions approached those of the PV model at large prediction horizons, the LPV and NPV models explained some of the variance in participants' gait kinematics (Figure A2.3) and muscle activity (Figure A2.4) or prediction horizons spanning the entire gait cycle.

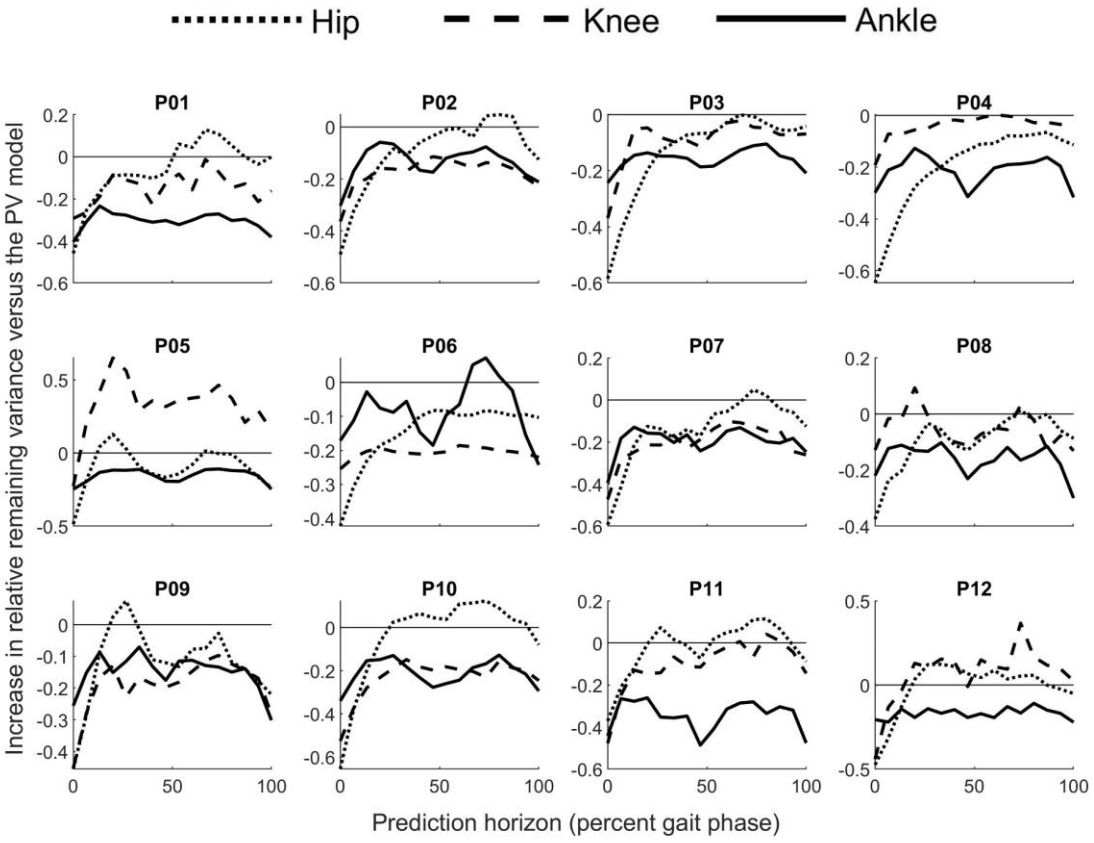

Figure A2.3. Change in relative remaining variance (RRV) of the LPV model compared to the PV model across prediction horizons for each participant's kinematic responses to torque in the K_2 validation condition. The RRV values were averaged across legs. An RRV value < 0 implies that the prediction is better than guessing the average response at each gait phase (*i.e.* the PV model).

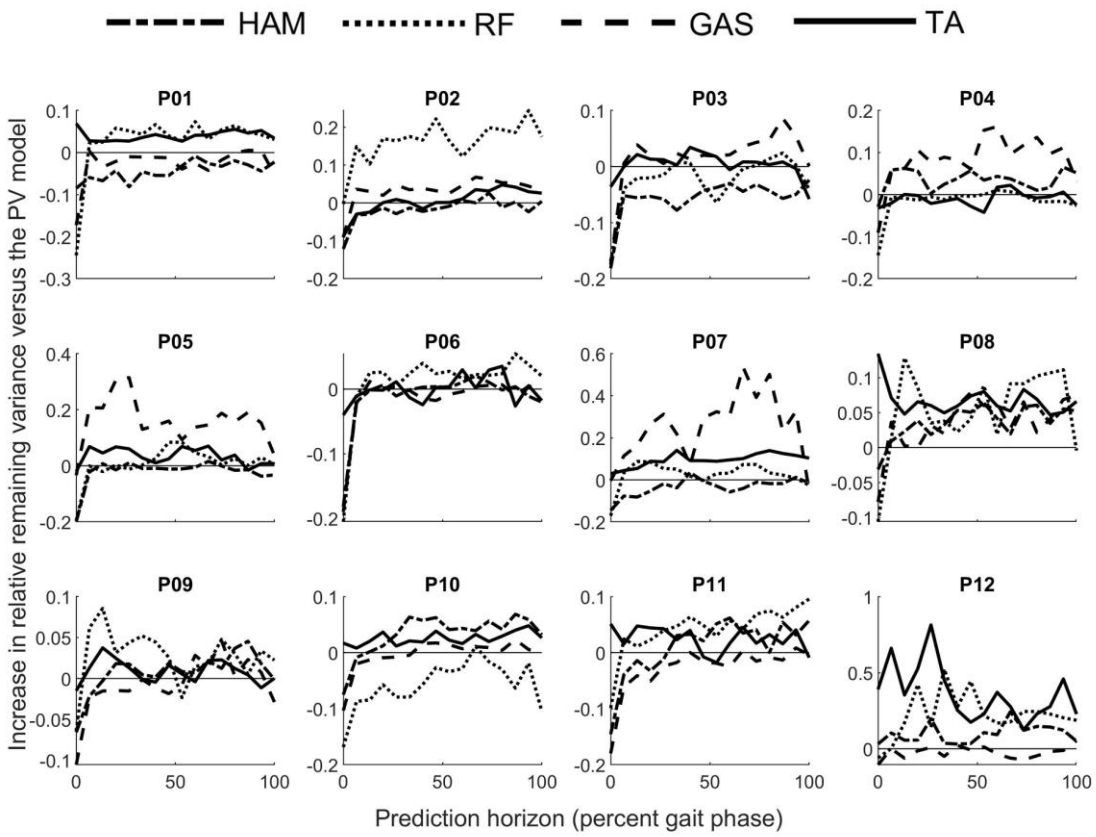

Figure A2.4. Change in relative remaining variance (RRV) of the LPV model compared to the PV model across prediction horizons for each participant's myoelectric responses to torque in the K_2 validation condition. The RRV values were averaged across legs. An RRV value < 0 implies that the prediction is better than guessing the average response at each gait phase (*i.e.* the PV model).